Numerical modelling of Tropical Cyclone Dineo and its rainfall impacts over north-eastern South Africa

by

Sbongile Meyiwa

Supervisor:

Prof. Chris Reason

A dissertation submitted to the Faculity of Science in fulfilment of the requirements for the Degree in Master of Science

Department of Oceanography, University of Cape Town, May 2019

Plagiarism Declaration

I, Sbongile Meyiwa, know the meaning of plagiarism and declare that all the work in this dissertation is my own, except for that which is acknowledged. The thesis has not previously been submitted for academic examination towards qualification in any university.

Signature: Signed by candidate

Date: May 2019

Acknowledgments

I am most grateful to my supervisor, Prof. Chris Reason for his invaluable input, advice and support from when I chose the research topic and through to its completion. I am thankful for his constant availability, assistance, prompt responses and patience. Many thanks go to Dr Raymond Roman, for assisting with WRF model set up and all other technical related matters. Big thanks to Ramontsheng Rapolaki and Dedricks Morake for Matlab assistance and advice on my research. I would like to appreciate my family for their support and constant encouragements. I am grateful to National Research Foundation (NRF) and UCT Postgraduate Funding for financial support.

Abstract

Widespread flooding over parts of Mozambique, Zimbabwe, Malawi, Botswana as well as north-eastern South Africa was experienced in February 2017. The flooding was associated with Tropical Cyclone Dineo that was generated in the Mozambique Channel on 12 February 2017 and made landfall over the south-central coast of Mozambique on 15 February. This study investigates the atmospheric circulation and potential mechanisms responsible for the heavy rainfall that occurred during the passage of ex-Tropical Cyclone Dineo inland from the Mozambican coast with focus on the rainfall patterns over north-eastern South Africa. Output from the Weather Research and Forecasting (WRF) model, the Climate Forecast System Reanalyses version 2 (CFSv2) atmospheric reanalysis, satellite derived rainfall and wind data, and station rainfall data are used for this purpose.

Tropical Rainfall Measuring Mission (TRMM) rainfall estimates, WRF model rainfall and rainfall station data indicated that many parts of north-eastern South Africa experienced large amounts of rainfall during the final stages of Dineo (16-17 February 2017) while Mozambique experienced heavy rainfall soon after the cyclone made landfall. An inland trough ahead of Dineo led to substantial rainfall at this time over Malawi and Botswana. Furthermore, analysis of the station data revealed that in north-eastern South Africa some stations recorded about 80 % of their total monthly rainfall from this event. The WRF model run indicated low level monsoonal north-easterly moisture fluxes feeding into Dineo in the Mozambique Channel. Subsequent convergence over south-eastern Africa between this flow and the south-easterly cyclonic flux associated with Dineo led to substantial rainfall over Mozambique, Zimbabwe, Botswana and north-eastern South Africa. Although the 2016/17 tropical cyclone season recorded below average numbers of storms, it is suggested that the conditions prior to the storm

formation were favourable for the track of Tropical Cyclone Dineo and landfall on the south-central Mozambican coast.

Table of contents

Figure captions and tables:

List of Acronyms and Abbreviations:

ARW Advanced Research WRF

ASCAT Advanced Scatterometer

EUMETSAT European Organisation for the Exploitation of Meteorological Satellites

GDAS Global Data Assimilation System

GESDISC Goddard Earth Science Data and Information Services Centre

CFSv2 Climate Forecasting System version 2

ITCZ Inter-tropical Convergence Zone

JFM January February March

MCCs Mesoscale Convective Complexes

NCAR National Centre for Atmospheric Research

NCEP National Centers for Environmental Prediction

NWP Numerical Weather Prediction

RDA Research Data Archive

SAWS South African Weather Service

SIOD South Indian Ocean Dipole

SWIO South West Indian Ocean

SST Sea Surface Temperature

TTTs Tropical Temperate -Troughs

TC Tropical Cyclone

TD Tropical Depression

TS Tropical Storm

TE Tropical-Extratropical

TMI TRMM Microwave Imager

TRMM Tropical Rainfall Measuring Mission

UTC Coordinated Universal Time

WRF Weather Research and Forecasting

WSM-6 WRF Single-Moment-6 Class

YSU Yonsei University

Chapter 1

1. Introduction

In February 2017, a few regions in the north-east of South Africa experienced severe floods that were associated with Tropical Cyclone Dineo which made landfall near Inhambane, south-central coast of Mozambique, on the 15th of that month. Dineo developed from a tropical disturbance that formed in the Mozambique Channel on February 12. In addition to causing widespread flooding in eastern / south-eastern Zimbabwe, and southern Mozambique, Dineo strongly impacted north-eastern South Africa. Several rainfall stations located in Limpopo and Mpumalanga Province, received from 40 – 80% of their total February rainfall following landfall of tropical cyclone Dineo.

As reported by the World Bank, Dineo led to the deaths of 7 people, cutting telephone communications and electricity supplies in Mozambique as well as damaging other infrastructure. The south-eastern African regions impacted by tropical cyclones, and particularly Mozambique and Madagascar, are generally underdeveloped with poor communication channels, insufficient emergency response capabilities, not well-established economies and little proper infrastructure. Such factors make these regions more vulnerable to the impacts of severe weather, commonly leading to displacement of thousands of people and significant loss of human life, as occurred during Dineo. Furthermore, although such flooding events are short-lived (lingering for several hours to days), their impact can significantly hamper economic and agricultural development, as some cropping areas can take much longer to recover from the impacts of floods.

Over north-eastern South Africa, Mozambique and Zimbabwe, most flooding originates from tropical storms (sometimes resulting from land-falling tropical cyclones), mesoscale convective complexes and tropical extratropical cloud bands or tropical temperate troughs (TTTs) (Rapolaki et al., 2019). Some of the most prominent storms that have occurred include Tropical Cyclone Eline in February 2000 which contributed about 25% of the seasonal rainfall (January-February-March) over Namibia, some days after landfall on the central Mozambique coast near Beira (Reason & Keibel, 2004) and most recently Tropical Cyclone Idai (March 2019). Eline left more than 500 000 people homeless in Mozambique, caused about 1000 deaths, and severely impacted bridges, roads and drainage systems. Furthermore, over north-eastern South Africa, the storm brought extensive flooding in addition to the damage caused in southern and central Mozambique (Dyson & Van Heerden, 2001). However, tropical cyclones are not the only systems responsible for heavy rainfall over south eastern Africa, TTTs (Hart et al., 2010; Manhique et al., 2011, 2015; Hart et al., 2013) are known to contribute substantially to summer rainfall over South Africa as do mesoscale convective complexes (Blamey & Reason, 2012; 2013).

Southern Africa has a highly variable climate on intraseasonal, interannual, decadal and longer time scales (Tyson et al., 1975; Usman & Reason, 2004; Reason et al., 2006; Washington & Preston, 2006) and is vulnerable to both heavy rainfall and extreme droughts. Both ENSO events (Lindesay, 1988; Reason et al., 2000) and regional SST modes in the South East Atlantic (Hirst and Hasternrath, 1983; Rouault et al, 2003; Hansingo & Reason, 2009) and South Indian Oceans (Reason & Mulenga, 1999; Behera & Yamagata, 2001; Reason, 2001, 2002; Allan et al., 2002; Malherbe et al., 2014) have been implicated as leading to interannual to interdecadal rainfall variability over the region. Although a significant amount of work has

been focused on rainfall variability over subtropical southern Africa, less attention has been devoted to studying tropical cyclones and associated rainfall influences over southern Africa. About 5% of South West Indian Ocean tropical cyclones make landfall on the southern African mainland (Reason & Keibel, 2004), however, when they do cause floods, human loss of life and devastating damage often result. Thus, analysis of Tropical Cyclone Dineo which impacted large areas of Mozambique and northeast and central South Africa is important. Although Tropical Cyclone Dineo contributed substantially to the 2017 late summer rainfall over parts of south-eastern Africa, it only reached category 2 according to the Saffir-Simpson Scale.

To date, not many studies exist that have attempted numerical modelling of tropical cyclones over southern African region that make landfall. Hence, the aim of this study is to investigate the evolution of Tropical Cyclone Dineo and its associated heavy rainfall which was experienced over north-eastern South Africa during February 2017. Output from the WRF model, CFSv2 Reanalyses, TRMM satellite derived rainfall, ASCAT satellite winds and rainfall station data are used for this purpose. Provided that the simulation is validated correctly, it may help provide some useful information that could help in better understanding of the evolution and development of tropical storms. Chapter 2 presents the literature review while Data and Methodology are presented in Chapter 3. Chapter 4 includes the interpretation of the model results and data while the discussion and the conclusions are given in Chapter 5.

Chapter 2

2. Literature Review

2.1 Introduction

Tropical Cyclones are found in all tropical ocean basins except the tropical eastern South Pacific and eastern South Atlantic (to date one case has occurred in the tropical south west Atlantic in March 2004) (Pezza & Simmonds, 2005). They are known as the most destructive weather events that bring about heavy rainfall and high winds leading to loss of life and infrastructure damage to the areas prone to their impact. This Chapter explores the climate of Southern Africa, tropical cyclones globally, particularly the prominent factors involved in their development, as well as rainfall bearing systems of this region. Consequently, this literature review provides a background context within which to study Tropical Cyclone Dineo which was generated over the Mozambique Channel in the South West Indian Ocean (SWIO) during the 2016/17 tropical cyclone season. Based on the studied mechanisms of how other storms have formed over this region, the information may be used to evaluate how the evolution of Dineo is similar or different to them. Finally, the study considers the factors that led to Dineo producing significant amount of rainfall over north-eastern South Africa, helping to improve conditions after the severe 2015-2016 drought in areas such as Mpumalanga and Limpopo.

2.2 Climate of Southern Africa

Southern Africa has a highly variable climate on intraseasonal, interannual, decadal and longer time scales and is vulnerable to both heavy rainfall and extreme droughts (Tyson et al.,1975; Rouault et al., 2003; Usman & Reason, 2004; Washington & Preston, 2006;). El Nino Southern Oscillation (ENSO) events (Kruger, 1999; Reason et al., 2000), regional SST modes in the South East Atlantic (Rouault et al 2003; Fauchereau et al., 2003; Hansingo & Reason, 2009)

and South Indian Oceans (Landman & Mason, 1999; Reason, 1999, 2001, 2002; Behera & Yamagata, 2001; Allan et al., 2002; Malherbe et al., 2014) have been implicated as leading to rainfall variability over the region. The climate of this region is influenced by several factors including its topography, the air-sea interaction of the surrounding oceans with contrasting warm Agulhas Current in the east and upwelling cool Benguela Current in the west, and its geographical location in the subtropics and tropics (Blamey & Reason, 2013; Gimeno et al., 2016).

2.3 Tropical Cyclones

Tropical Cyclones, also known as hurricanes (North Atlantic) or typhoons (North West Pacific) are intense, rapidly rotating, low pressure atmospheric weather systems that form over tropical and subtropical waters with sea surface temperatures of at least 26°C. Additionally, they contain organized deep convection and strongly cyclonic surface wind circulation as well as thunderstorm activity (Fink & Speth, 1998; Pezza & Simmonds, 2005). They fall under the category of deep convective storms due to local processes that result in strong instability with enough low-level convergence of moist air masses as well as regional surface heating to produce strong uplift and relative vorticity (Ferreira & Schubert, 1999). Ferreira and Schubert (1999) studied tropical cyclones as warm core systems whose cyclonic winds decrease with height; and are between 100 and 2000 km in diameter. Furthermore, under extreme cases, the TCs' typical minimum central pressure of 950 hPa can drop below 880 hPa (Pezza & Simmonds, 2005).

A TC can be recognized as a coherent severe weather system that typically persists over the warm tropical oceans for several days (Sippel & Zhang, 2008). Additionally, TCs are primarily maintained by the latent heat release of water vapour extracted from the warm sea surface

waters. Furthermore, when they move over land they typically weaken and lose intensity as their primary energy source is cut off and they evolve into a dissipation phase (Wong et al., 2008).

Despite many observational and numerical modelling studies of tropical cyclones conducted in recent decades, the detailed physical processes associated with the early stages of TC development are still inadequate (Montgomery & Farrell, 1993; Gray, 1998). However, TCs have a lifecycle that is typically divided into three distinct phases, i.e., the first phase is defined as a Tropical Disturbance (TD), followed by Tropical Storm (TS) and lastly a mature storm which is characterised as a Tropical Cyclone (Avila & Pasch, 1992) provided that its sustained winds are sufficiently strong.

In the tropical North Atlantic, the westward moving African Easterly Waves (AEWs), which are alternating wind systems of approximately 2500km wavelength with enhanced convection in their troughs and suppressed convection in their ridges, are associated with convection near the equator (Burpee, 2003; Berry & Thorncroft, 2005). The enhanced convection portion of the trough within the AEW is where a TD is frequently located. Additionally, as the AEWs travel westward during summer months, they gradually organize forming a TD whereby a low-pressure system forms and is accompanied by thunderstorms that enhance production of circular wind flow with maximum sustained winds below 39 mph (Hopsch et al., 2010). These storms may then strengthen into hurricanes if the underlying SST is warm enough and the atmospheric conditions are favourable. Meanwhile, in the tropical South Indian Ocean TDs may evolve from some initial disturbance in the tropical easterly winds typically in the 10-20^{o}S zone (Duvel, 2015).

Most TCs form over warm tropical oceans, near or just pole wards of the Inter-Tropical Convergence Zone (ITCZ). In this region, there is intense surface convergence and low surface pressure in an unstable warm marine air-mass that is favourable for concentrated deep convection which is a basic requirement for the TC formation (Emanuel, 1986; Malherbe et al., 2014).

In the process of TD formation, the winds over the ocean rotate due to the Coriolis Effect. During this process, more energy builds up and, if conditions remain favourable, the TD may strengthen into TS that is driven by latent heat released by condensation of water vapour found within convective rain bands (Fink & Speth, 1998).

A fully developed TC is a nearly circular, warm-cored vortex that occupies the entire height of the troposphere. Additionally, it radially extends hundreds of kilometres and is driven by the energy obtained through oceanic evaporation and subsequent latent heat release. TCs can move at a speed of 10-50 kilometres per hour within the zone of trade winds (Malilay, 1997). Moreover, as discussed in Pielke (1990), Landsea (2000) and Pezza & Simmonds (2005), six environmental conditions tend to favour tropical cyclone development. These are firstly Sea Surface Temperature (SST) warmer than 26.5°C, secondly, weak Environmental Vertical Wind Shear (EVWS) which is the magnitude of the difference between 200 and 850 hPa vector winds of lower than 8 m s^{-1}, thirdly, sufficient upper ocean thermal energy through the upper layer depth of 60m with a temperature warmer than 26°C, fourthly, enhanced mid-troposphere relative humidity, fifthly, lower troposphere relative vorticity to provide favourable environment for aggregation of vorticity seedlings for TC genesis, and finally the warm core of the disturbance which is maintained by the moist interior updrafts. However, the conditions

favourable for the cyclogenesis are not stable due to atmospheric conditions and SST subject to change over time (Emanuel et al., 2004; Pezza & Simmonds, 2005).

2.3.1 Location, Intensity and Seasonality of Tropical Cyclones

a) Location

Globally, Tropical Cyclones occur predominantly in the tropical North Atlantic, northeast Pacific, northwest Pacific, North Indian, South Indian and southwest Pacific Oceans, between latitudes 10°S and 30°S (Gray & Brody, 1967; Goni et al., 2007) but are called hurricanes in the North Atlantic and typhoons in the northwest Pacific. These tropical ocean regions have warmer surface waters (SST above 26^{o}C) during certain times of the year which essentially defines the cyclone season for that region (Graham & Barnett, 1987).

b) Intensification

The Tropical Cyclone Heat Potential (TCHP) which is calculated by summing the heat content in the water column above the 26^{o}C isotherm may play a significant role in influencing the intensity and intensification of TCs (Graham & Barnett, 1987; Wada & Usui, 2007; Goni et al., 2007). Although SST > 26°C is necessary for TCs to develop, warm SST by itself is insufficient for their intensification (Shay et al., 2000). Chun-Chieh Wu (2007) argued that not merely the surface temperature of the ocean, but also the depth of the warm water pool beneath the surface serves as a reservoir of energy for the intensification of TCs. Moreover, research shows that the rapid deepening of a TC central pressure is closely linked to the TCHP that is accumulated from the initial stages of a TC formation to the mature stages than it is with the accumulated SST and its duration (Graham & Barnett, 1987; Wada & Usui, 2007; Goni et al., 2007; Hendricks et al., 2010). Over the South West Indian Ocean, Malan et al (2013) presented

evidence of an increasing tendency in TCHP and in strong TC occurrence in recent decades (category 3 and above).

The rate of intensification of TCs is weakly dependent on environmental conditions.(Hendricks et al., 2010), these conditions include warmer SST, deep layer vertical wind shear, interactions with upper level troughs, and the level of conditional instability in the lower-troposphere. These conditions act together with the internal processes occurring within the storm, which include those responsible for eyewall replacement, potential vorticity mixing between eyewall and eye, as well as convectively coupled vortex Rossby waves (Hendricks et al., 2010). Moreover, the Tropical Upper-Troposphere Trough (TUTT) which is an elongated region of relatively low atmospheric pressure can influence both the development and intensification of the TC by increasing or decreasing the vertical wind shear where the TC is embedded (Ferreira & Schubert, 1999).

The intensity of a TC is measured according to the Saffir-Simpson Scale (**Table. 1**) in which they are classified into categories from one to five as distinguished by the intensities of their sustained winds (Webster et al., 2005). However, the forecasting of Tropical Cyclone intensity remains difficult due to the complex physical properties that play a major role in controlling the TC intensity (Vitart et al., 2003).

Rapid intensification of TCs is more likely to occur when the upper oceanic heat content is greater than 50 kilojoules cm^{-2} (Pasquero & Emanuel, 2008). There have been several examples of intensification of TCs in the South West Indian Ocean in the last decade or so into category

4 or 5 (e.g., Bansi in January 2015). Such cases have been related to large TCHP (Malan et al 2013) or to other important upper ocean characteristics such as barrier layer thickness and variable mixing length temperature (Mawren & Reason, 2017).

c. Seasonality

The TC season in the tropical South West Indian Ocean (defined as 10°S-25°S, 40°E-100°E) occurs during austral summer (November to April) with 1 January to 31 March being the peak TC season (Klinman & Reason, 2008; Vitart et al., 2003). An average of eleven to twelve TCs occurs per season in this region with relatively few making landfall on the southern African mainland, typically central Mozambique. TC Dineo made landfall near Inhambane (~23.5°S) on the south-central coast of Mozambique which is further south than typical. A much larger fraction make landfall on eastern Madagascar, but many dissipate in South West Indian Ocean without ever making landfall. About 5% of tropical storms that develop in SWIO have made landfall over the last 5 decades (Reason & Keibel, 2004; Klinman & Reason, 2008; Fitchett & Grab, 2014).

The seasonal frequency of TC development in the tropical oceans is closely linked to the following six parameters; namely, a non-zero but low value of the Coriolis parameter, low-level relative vorticity, vertical wind shear, ocean thermal energy, potential temperature and relative humidity in the mid-troposphere (Gray & Brody, 1967). These parameters can be thought of in terms of dynamic and thermal potentials in the way that they collectively contribute to the possibility of cyclogenesis. They can be assessed through a TC "seasonal genesis parameter" that may provide a good estimate of the long-term frequency of TC occurrence each season (Gray & Brody, 1967).

2.3.2 El-Nino Southern Oscillation (ENSO) and Tropical Cyclones

Globally, the location, track and frequency of TCs are influenced by ENSO while the South Indian Ocean Dipole (SIOD) contributes to the frequency of TCs over the South Indian Ocean (Fitchett & Grab, 2014).

ENSO is a phenomenon involving the large-scale oscillation of ocean-atmosphere circulation and properties in the tropical Indo-Pacific Oceans on interannual time scales. This phenomenon consists of three phases which are El Niño (warm phase), La Niña (cold phase) as well as the neutral phase (or "normal" conditions). Since ENSO strongly influences the temperatures and circulation throughout the tropics, it is able to have a significant effect on TCs. The phase and intensity of ENSO is defined by observing the indices linked with atmospheric pressure gradient and the SST anomalies over near-equatorial regions (Kuleshov et al., 2008).

In the Southern Hemisphere, ENSO has been observed to contribute to the variability of TC activity during the TC season with about 25 TCs occurring during El Niño and 29 during La Niña, annually (Kuleshov et al., 2008). ENSO alters the regional and global scale atmospheric circulation and upper ocean characteristics; hence it can influence the TC direction of movement or the spatial pattern of the TC genesis (Ash & Matyas, 2012).

There is a potential connection between the state of ENSO and TC landfall over Mozambique with a noticeable tendency for strong TCs forming in SWIO to make landfall during La Niña years (Vitart et al., 2003; Klinman & Reason, 2008). During La Niña summers, there tends to be an easterly (positive) Zonal Steering Flow (ZSF) over the South West Indian Ocean favouring the development of TCs that penetrate westwards (Vitart et al., 2003; Klinman &

Reason, 2008). The ZSF is defined as the vertical average of the zonal wind from 200 to 850hPa over the main SWIO TC cyclogenesis region during the peak TC season (1 January to 31 March) (Vitart et al., 2003).

TCs in the SWIO have a typical trajectory towards the south west, leading to the eastern coast of Madagascar (and sometimes Mozambique) to be prone to their impact (Ash & Matyas, 2012). However, as they move towards the south west and into higher latitudes, they tend to re-curve south eastward and back into the open ocean. Relatively few TCs can cross the mountains of Madagascar into the Mozambique Channel; one notable exception was TC Eline in February 2000 (Klinman & Reason, 2008). When the ZSF is strongly negative (westward), the number of TC crossing Madagascar tends to increase, and TC activity is enhanced in the Mozambique Channel.

Although a few TCs form in the Mozambique Channel, they tend to move southwards into the open ocean rather than making landfall (Reason, 2001). Moreover, TCs that are generated in Mozambique Channel have been observed to be generally weak and short lived (Reason & Keibel, 2004; Klinman & Reason, 2008). A notable exception is TC Idai in March 2019 which reached Category 3 status and lasted for over two weeks.

2.3.3 South Indian Ocean Dipole (SIOD) and Tropical Cyclones

The South Indian Ocean Dipole (SIOD) is considered to be an important mode of climate variability in the Southwest Indian Ocean whereby, during its positive phase, the south-western part of the South Indian Ocean exhibits warm SST anomalies while the south-eastern portion

consists of cool SST anomalies simultaneously during austral summer (Behera and Yamagata, 2001; Reason, 2001, 2002; Ash & Matyas, 2012; Kripalani & Kumar, 2004). During a positive SIOD, large areas of southern Africa tend to receive above average summer rainfall (Reason, 2001, 2002; Behera & Yamagata, 2001). Since the SIOD is associated with large scale pressure anomalies over the South Indian Ocean (Behera & Yamagata, 2001; Hermes & Reason, 2005) it may also influence TC trajectories over the region. To assess this possibility, an interactive consideration of both ENSO events and SIOD is necessary (Ash & Matyas, 2012). During La Nina and positive SIOD summers, TCs over the South West Indian Ocean most commonly exhibit westward trajectories (Klinman & Reason, 2008; Ash & Matyas, 2012). However, SIOD events can occur independently of ENSO, even though these climate modes coincide sometimes and show a strong correlation (Matyas, 2015).

2.4 Main rainfall producing systems over Southern Africa

Southern African climate is mainly affected by three major circulation systems; namely, the semi-permanent high-pressure systems over the subtropical South Indian and South Atlantic Oceans, the Inter-Tropical Convergence Zone (ITCZ) and the Circumpolar Trough located over the Southern Ocean (Reason & Rouault, 2005; Reason et al., 2006). The relationships between these features and the climate variability of this region are still not completely understood (Blamey & Reason, 2013; Driver & Reason, 2017). Two important regional circulation systems in summer, the Angola Low and the Botswana High, influence the development of TTTs and other convective rainfall systems (Cook et al., 2004; Driver and Reason, 2017; Munday and Washington, 2017) and, are in turn, impacted by ENSO which can lead to modulations of the El Nino expected drought such as happened during 1997/98 (Reason and Jagadheesha, 2005) and 2009/10 (Driver at al., 2019). In other cases, such as 2015/16, the

Angola Low is weakened and the Botswana High is strengthened leading to a severe El Nino-induced drought (Blamey et al 2018).

Four main rainfall regions occur in southern Africa; these are the austral winter rainfall region in western South Africa, the all-season rainfall region of the south coast, the bimodal rainfall regions in northern Tanzania and Kenya, and lastly the austral summer region which occurs over the vast majority of southern Africa (Blamey & Reason, 2013; Weldon & Reason, 2014; Engelbrecht et al., 2015) and which is strongly impacted by ENSO events

There are several factors that encourage rainfall production, including low level moisture flux convergence, the extent of atmospheric instability together with upper level divergence (Mason & Jury, 1997; Reason, 1998; Reason & Mulenga, 1999; Reason, 1999; Reason et al., 2000; Malherbe et al., 2014). The most important summer rainfall producing system over subtropical southern Africa is the TTT or tropical-extratropical (TE) cloud band, with organised convection and rainfall occurring over a large NW-SE oriented area that extends out over the South West Indian Ocean (Harrison, 1984; Hart et al., 2010). TTTs are common features in many regions and are identified as elongated cloud bands rooted in the tropics, stretching poleward, exporting moisture and heat to the mid-latitudes (Hart et al. 2010). Up to about 40-50% of summer rainfall over eastern South Africa can be contributed by these systems (Harrison, 1984; Hart et al., 2010).

Based on the analysis of the inter-annual frequency of TTTs over Mozambique and Southwest Indian Ocean, there is a relationship between SSTs and circulation patterns (Manhique et al.,

2011). TTTs occurrence may be related to La Nina and Southern Hemisphere planetary waves that further regulate the subtropical high-pressure cells in the ocean basins surrounding southern Africa (Fauchereau et al., 2009). La Nina events also tend to favour enhanced easterlies over South Indian Ocean and onshore moisture transport flowing towards south-eastern Africa (Manhique et al., 2011).

The Mesoscale Convective Complex (MCC) is another severe weather producing system which is of great interest as it is both damaging and often associated with heavy rainfall. MCCs are by definition a large circular cluster over organised deep convection that lasts for at least 6 hours. In southern Africa, they tend to occur in the eastern regions downstream of topography and near the Agulhas Current and Mozambique Channel, with about nine occurring per year (Blamey & Reason, 2012; 2013) on average. MCC can contribute up to about 20% of the summer rainfall over southern Mozambique and north-eastern South Africa reducing to 6% over the western interior. MCCs can produce more than 100mm of rainfall within 6 hours, which contributes greatly to the seasonal rainfall and leads to the potential for damaging floods (Blamey & Reason, 2012). However, there are still gaps in the available information mainly about the formative mechanisms of MCCs.

Particularly during the transition seasons (spring and autumn), cut-off lows can also make substantial contributions to rainfall over subtropical southern Africa with the potential for flash floods since more than 100 mm of rain may occur in a 24-hour period (Singleton & Reason, 2007a). Cut-off lows form in the middle/upper troposphere and are described as cold cored systems developing from a pre-existing cold trough that shifts equatorward and eventually

becomes cut-off from the westerly flow and remain as a cyclonic closed vortex (Taljaard, 1985; Singleton & Reason, 2007b).

The occurrence of a strong ridge of high pressure over the South Atlantic Ocean is favourable for the development of cut-off lows along with a pronounced upper level westerly trough. A ten-year study (1973-1982) of cut-off lows conducted by Taljaard, (1985) over South Africa indicated that on average, 11 cut-off lows occur per year. An extended study of 30 years (1973-2002) conducted to create climatology of cut-off lows over subtropical southern Africa, revealed that the least number of such events prevailed during December and January and for March, April, May and June, high frequencies were observed with April being the peak month for cut-off lows occurring (Singleton & Reason, 2007a).

Although tropical cyclones tend to only contribute directly to rainfall over Madagascar, Mozambique and eastern Zimbabwe, subsidence around the periphery of these weather systems can make conditions unfavourable for rainfall further inland. Over the past few decades, a great amount of work has been dedicated to the studying of tropical cyclone formation and tracks over the South West Indian Ocean (Ferreira & Schubert, 1999; Emanuel, 2001; Vitart et al., 2003; Reason & Keibel, 2004; Reason, 2007; Klinman & Reason, 2008; Mavume et al., 2009; Ash & Matyas, 2012b; Malan et al., 2013; Fitchett & Grab, 2014; Matyas, 2015; Mawren and Reason, 2017; Rapolaki & Reason, 2018). However, a better understanding of mechanisms responsible for the formation of heavy rainfall and floods during the TC is still needed. In addition, the strong winds and storm surges associated with tropical cyclones often also causes loss of life and damage near where the system makes landfall.

In this thesis, TC Dineo and its associated rainfall over the north-eastern South Africa is considered using South African Weather Service data, atmospheric re-analyses and output from a numerical model simulation (WRF). The WRF simulation is validated using available observations. The objective of the thesis is to better understand the evolution of Tropical Cyclone Dineo and the conditions that led to the rainfall observed over north-eastern South Africa during this month. Dineo is of interest for several reasons. Firstly, it occurred during the 2016/17 SWIO tropical cyclone season which was below average in terms of TC frequency in that it produced only five storms of which three intensified into tropical cyclones. Secondly, it formed in the central Mozambique Channel and then tracked south-westwards to make landfall on the south-central Mozambique coast. Most TCs that make landfall in Mozambique tend to do so somewhat further north. Furthermore, relatively few of the total South West Indian Ocean tropical cyclones actually form in the Mozambique Channel and those that do often track south and out of the Channel (e.g., TC Dera, described in Reason, 2007) or make landfall on western Madagascar. Finally, Dineo contributed greatly to the total February summer rainfall in north-eastern South Africa. Based on the percentage anomalies in the SAWS rainfall maps (**Fig. 2-1**), during 2016/17 early summer, most regions were experiencing dry conditions due to the 2015/2016 strong El Nino which had a wide-ranging effect globally. In October, November and December 2016, the western parts of South Africa were extremely dry with rainfall occurring mostly on the eastern parts. However, January and February 2017 received above average rainfall in most parts of the country with Western Cape and western Northern Cape remaining the driest regions. The late summer rainy season was below average over the rest of South Africa.

Chapter 3:

3 Data and Methods

3.1 Data

3.1.1 Station and Satellite Data

To assess the contribution of Dineo to the total February rainfall, daily rainfall data from 10 and 14 stations in Mpumalanga and Limpopo respectively were provided by South African Weather Service (SAWS). It should be noted that only 10 and 14 stations for Mpumalanga and Limpopo respectively were available. The daily time series were produced for the period 1 to 28 February 2015. The aim was to show the quantity of rainfall received by Mpumalanga and Limpopo from 12 to 17 February 2015 when Dineo was active. Additionally, the contribution of the storm to the total rainfall for each station was calculated and listed (**Table 2).**

Satellite-derived Tropical Rainfall Measuring Mission (TRMM) 3B42 version 6 (Huffman et al., 2010), 3-hourly data were used to show the spatial extent of rainfall over southern Africa using TRMM that is available at the 0.25° x 0.25° spatial resolution, for the period 1997 to near present (Liu et al., 2012). TRMM satellite uses a Microwave Imager (TMI) instrument with a passive remote sensing which occurs at low altitudes of about 402 km and assesses rainfall equatorward of around 40° (Huffman et al., 2010). TRMM data were downloaded from the Goddard Earth Science Data and Information Services Centre (GESDISC) website: http://disc.sci.gsfc.nasa.gov.

Analysing extreme rainfall linked to extreme rainfall events over southern Africa remains challenging due to the limited rain gauge monitoring network. However, relatively high temporal resolution (3-hourly) data sets such as TRMM have enabled extreme rainfall studies.

TRMM data have been used recently (Rapolaki and Reason, 2018) to assess extreme rainfall over south-eastern Africa associated with Tropical Storm Chedza which occurred in January 2015. Furthermore, Tian et al., (2007) showed that TRMM estimates have relatively small biases in estimating storm rainfall volume and the rate of average rainfall, which makes it suitable for this study. However, TRMM overestimate rainfall over the tropics, mostly during the warm season.

In this study, Advanced Scatterometer (ASCAT) was used to evaluate how well the model represents surface wind patterns over the neighbouring oceans. ASCAT is an active sensor on board Meteorological Operation-A (MetOp-A) satellite that was launched by European Organisation for the Exploitation of Meteorological Satellites (EUMETSAT) MetOp-A satellite in October 2006 and started to operate in 2007, additionally, it was upgraded to METOP-B satellite (ASCAT-B) that became operational in 2013 (Figa-Saldaña et al., 2002). These data are available at 0.25^0 x 0.25^0 spatial resolution and with 6-hourly temporal resolution. The daily ASCAT data were downloaded from the Physical Oceanography Distributed Active Archive Centre (PODAAC) website: https://podaac.jpl.nasa.gov/dataset/ASCATB-L2-25km. Please note that the ASCAT satellite derived data only measure the surface winds over the ocean and are only available for 2007-present.

3.1.2 CFS Reanalyses Data

The second version of National Centres for Environmental Prediction (NCEP) Climate Forecast System (CFSv2) 6-hourly dataset was used to provide initial boundary conditions and to validate the WRF model output. CFSv2 is a coupled weather prediction model developed by NCEP and became operational in March 30, 2011 and is available for the 2010-present period

(Saha et al., 2014). Nearly all the aspects of the data assimilation and forecast model elements of the system (CFSR) have been upgraded in this version.

The CFSv2 model is made up of four separate models (atmosphere model, ocean, land/soil, and sea ice), which are integrated to give an accurate representation of atmospheric conditions. The horizontal resolution of CFSv2 is 0.5° x 0.5° and it assimilates data from aircraft, upper air soundings, and satellite observations. The boundary conditions for CFSv2 are provided by the Global Data Assimilation System (GDAS) generated from multiple satellite and surface observations. The CFSv2 model is initialized four times per day (0000, 0600, 1200, 1800 UTC) and its six-hourly land surface, oceanic, and atmospheric forecasts are available at 0.2, 0.5, 1.0, and 2.5- degree horizontal resolutions archived on Research Data Archive (RDA) website (http://rda.ucar.edu/datasets/ds094.0/).

3.2 WRF Model Description

Significant progress has been made in numerical simulations of TCs due to improvements in computing power and advancements in observational data used to force the models. In recent years, several studies have used one of the state-of-the-art mesoscale models, known as WRF to simulate TCs (Rapolaki & Reason, 2018; Pattanayak & Mohanty, 2008). The WRF model has been used widely for simulation of formation, intensification and the direction of the TCs (Raju et al., 2011; Fierro et al., 2009; Pattanayak & Mohanty, 2008), which makes it suitable for simulation of TC Dineo. However, high resolution models are deemed expensive for most research groups with limited computational resources (Kim et al., 2015).

Using models with coarse spatial resolution tends to underestimate the key TC activities such as cyclogenesis location, track, intensity and the central pressure (Kim et al., 2015; Shen et al., 2006). Other than computational issues that result in errors in the simulation of the storms, the validity of physics parameterizations presents another challenge in conducting simulations of ultra-high resolution (Shen et al., 2006). Shen et al., (2006) suggest another way to improve tropical cyclone simulations is by improving initial conditions, resolution, model physics as well as taking into consideration the convection parameterization as it can be another limiting factor affecting the storm representation in the model. In this study, the WRF model was used to simulate Tropical Cyclone Dineo. The model physics, resolution, and boundary conditions were selected carefully based on previous studies (Islam et al., 2015; Nguyen et al. 2014; Shen et al., 2006) to mitigate errors in the simulation as discussed below.

WRF is a fully compressible, terrain-following (sigma) coordinate, non-hydrostatic model on an Arakawa-C grid that is better used for research and weather forecast applications, developed by the National Centre for Atmospheric Research (NCAR) (Skamarock & Klemp, 2008). WRF model is a flexible state-of-the–art atmospheric simulation system suitable for a broad range of applications such as idealised simulations, data assimilation research, parameterization research, and real-time numerical weather prediction (NWP) (Skamarock & Klemp, 2008). The WRF model was chosen for this study because it is freely available and has been used mainly for the simulation and analyses of tropical cyclones (Kim et al., 2015; Cha & Wang, 2013). Furthermore, the model has both one and two-way nesting ability to allow for the interaction between the coarser and finer resolution domains.

In this study, the simulation used two-way nested domains for the processes and circulation simulated in the child domain to be fed back into the lower resolution, outer domain (model domains are displayed in **Fig. 3-1**). The parent domain had 18 km horizontal resolution and the child domain had 6 km resolution. The parent domain had 435 x 281 grid points with 18-km grid spacing, and a time step of 180 seconds. The child domain has 889 x 544 points with 6 km grid spacing, and a time step of 60 seconds. Both domains were initialized at 0000 UTC 10 February 2017 and ran until 1800 UTC 17 February 2017. The selection of the parent domain was so that it lies over southern Africa, including Madagascar, and the neighbouring South West Indian Ocean and a small part of the South East Atlantic Ocean (0N° to 47°S, 5°E to 85°E). The child domain covers southern Africa, the Mozambique Channel and Madagascar to better track the formation location and path of TC Dineo. CFSv2 reanalyses data were used for initialization and boundary conditions. Both domains had 30 vertical levels between the surface and the model top at 10 hPa. To use the same time scale as the CFSv2 reanalyses data, the model was set up to produce six-hourly averages. A 24-hour spin-up period was allowed for the model and the output was analysed from 0000 UTC 12 February 2017 to 1800 UTC 17 February 2017 which is the duration of the storm. Daily high-resolution (0.5° x 0.5°) (Reynolds et al., 2007) optimally interpolated SST was used to provide the lower boundary conditions for the simulation (Kim et al., 2015).

The physics options used for model simulations constituted the WRF Single-Moment3-class (WSM3) simple ice microphysics scheme by (Hong et al., 2004) on the parent domain (18 km) and WSM6-class graupel scheme in child domain (6 km) for cloud microphysics (Hong at al., 2004). This scheme is suitable for simulations of high-resolution as it consists of ice, snow, and graupel processes (Kumar et al., 2008). For convective processes Kain-Fritsch (new-Eta) cumulus parameterization scheme (Kain, 2004) was used as it better simulates precipitation in

mesoscale models (Hong et al., 2004). Shortwave radiation options were chosen based on the Dudhia shortwave radiation scheme (Dudhia, 1989). For surface-layer parameterization, the Yonsei University (YSU) planetary boundary layer scheme was used. Additionally, to represent land surface processes, the Noah land surface model scheme was chosen as it better represents low level temperature and humidity (Ek et al., 2003). The performance of WRF model and its ability to simulate circulation patterns associated with Tropical Cyclone Dineo was evaluated through a comparison of winds and geopotential height simulated by the WRF model and CFSv2 reanalysis.

3.3 Methods

3.3.1 WRF model Comparison

The ability of WRF model to represent the important properties of Tropical Cyclone Dineo and regional atmospheric patterns is investigated through comparing the model output with CFSv2 reanalyses and TRMM TMI and ASCAT satellite datasets. To validate circulation patterns over southern Africa during the storm, the WRF model geopotential height and horizontal winds were interpolated onto 200hPa and 850hPa pressure levels.

Daily WRF model winds and geopotential height patterns produced were validated against CFSv2 reanalyses patterns at 200hPa and 850hPa pressure levels for 12-17 February 2017. The 200 hPa pressure level was chosen to assess the ability of model to produce divergence or anticyclonic flow observed at the top of the storm, while the 850hPa pressure level is just above the height of the interior plateau that covers much of the southern Africa.

To investigate how well the model can simulate near-surface winds (above the ocean) during the period of the storm, u and v wind components of the model at 10 m level were compared with ASCAT satellite derived winds from 12-17 February 2017. In addition, to validate the ability of the model to produce rainfall patterns associate with the storm, TRMM TMI satellite derived rainfall dataset was used. The model output list does not include total rainfall; hence, it was calculated using the following formula:

$$T\_RAIN = PRECIP\_G + PRECIP\_C \ldots\ldots (1)$$

where precip_g (mm) is the accumulated total grid scale precipitation and precip_c (mm) is the accumulative total cumulus precipitation.

3.3.2 Moisture flux and its convergence, uplift and instability

To assess potential regional mechanisms that contributed to the heavy rainfall experienced over the north eastern part of South Africa during the storm, moisture flux convergence (expressed in kg kg^{-1} s^{-1}) was computed using the following variables obtained from the WRF model: specific humidity q (kg kg^{-1}), and horizontal wind components u and v (ms^{-1}). The individual qu and qv components were combined to give a moisture flux vector, which has both direction and magnitude. The magnitude (Q) of the vector was calculated from:

$$\text{Moisture flux magnitude: } Q=\sqrt{(qu)^2+(qv)^2} \ldots\ldots\ldots\ldots\ldots\ldots (2)$$

Moisture flux divergence is given by:

$$\text{Moisture flux divergence } = \left(\frac{\partial qu}{\partial x}\right)+\left(\frac{\partial qv}{\partial y}\right) \ldots\ldots\ldots\ldots\ldots\ldots (3)$$

where $\frac{\partial qu}{\partial x}$, is the change in the zonal moisture flux over longitude and $\frac{\partial qv}{\partial y}$ is the change in the meridional moisture flux over latitude. The moisture flux divergence was plotted over the region 10°S to 40°S and 5°E to 55°E to determine the locations of strong convergence

(negative values in the divergence field). In order to identify areas of strong moisture convergence which may be associated with areas that received high rainfall, moisture flux divergence fields at 700 hPa were plotted. Moisture flux vectors were used to indicate the source of moisture during the event.

To show areas of strong uplift associated with rainfall and cloudiness during the event, daily plots of vertical velocity over the inner domain were computed at 500 hPa for 12 to 17 February 2017. A mid-troposphere level was chosen to indicate whether or not uplift favourable for convective development was present. Positive values of vertical velocity indicate substantial uplift.

Convective instability (°C) was used to show areas of strong instability associated with the storm event (Singleton and Reason, 2007b). Instability was calculated as the magnitude of the temperature difference between potential temperature (θ 850 − θ 500) at 500 hPa and 850 hPa and plotted from 12-17 February 2017

Low level wind shear was calculated from 850 to 500hPa using the following equations:

$$\text{Zonal Wind Shear} = (u_{850} - u_{500}) \ldots\ldots\ldots (4.1)$$

$$\text{Meridional Wind Shear} = (v_{850} - v_{500}) \ldots\ldots\ldots (4.2)$$

Daily plots were computed from 12-17 February 2017.

WRF potential vorticity at 700 hPa was computed from 12-17 February 2017 using the Potential Vorticity (PV) variable from WRF outputs.

To assess the large-scale background environment within which Dineo evolved, NCEP reanalysis data (2.5º horizontal resolution) and NOAA Extended Re-constructed SST were plotted using the following website:

https://www.esrl.noaa.gov/psd/cgi-bin/data/composites/printpage.pl

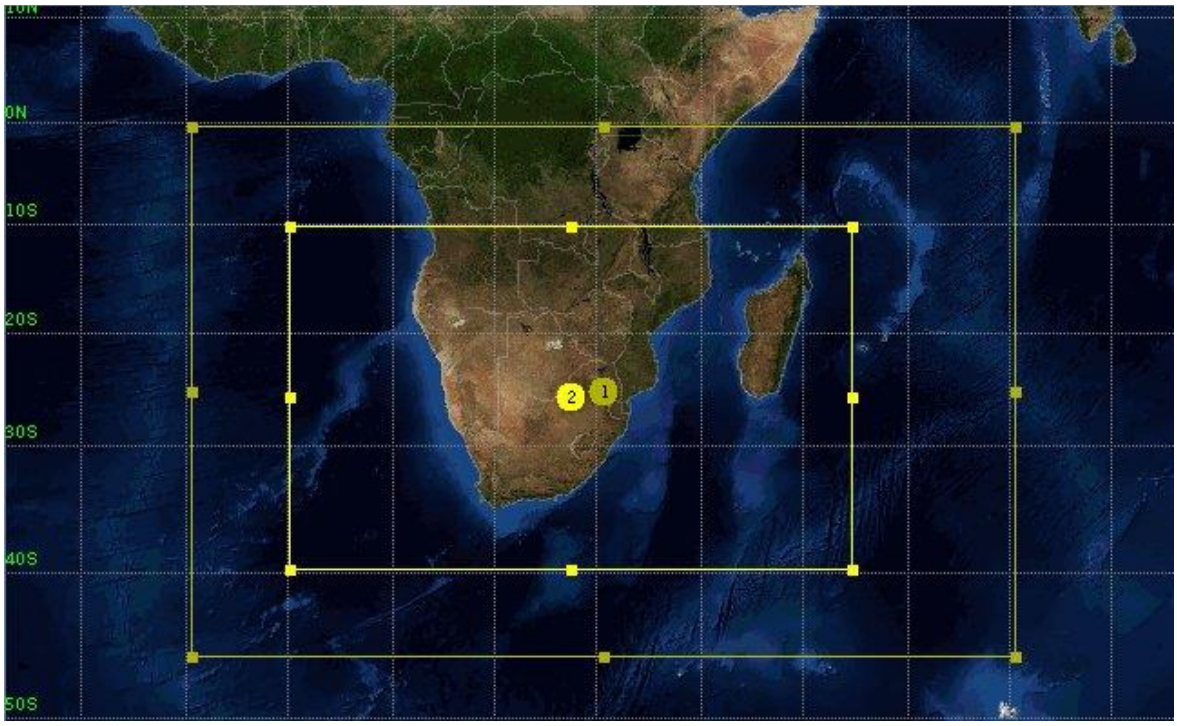

Figure 3-1: Map showing the WRF model domain setup. The symbol 1 refers to the outer domain and 2 refer to the inner domain of the WRF model simulation. The model resolution in the outer domain is 18 km and 6 km in the inner domain.

Chapter 4

4. Results and Discussion

4.1 Synoptic evolution and rainfall

This section describes the evolution of Dineo from the early formation stages to its dissipation stage. The storm developed as a tropical disturbance in the central Mozambique Channel on the 12th of February 2017, strengthened to tropical storm status and named Dineo on the 14th of February before reaching tropical cyclone status on the 15th and making landfall later that day near Inhambane, Mozambique.

Before discussing the synoptic evolution of Dineo, the characteristics of the late summer season during which Dineo occurred are briefly considered. **Fig. 4-1** shows the environmental setting in which TC Dineo developed. **Fig.4-1a** shows the seasonal (JFM) geopotential height anomaly at 850hPa with a high pressure anomaly located over the Mozambique Channel and a stronger high pressure anomaly east of Madagascar. These anticyclonic anomalies were consistent with the reduced TC activity in the South West Indian Ocean during this season. A weaker Angola Low is also evident over south-eastern Angola together with a weaker convergence zone across Zambia, northern Mozambique and the tropical western Indian Ocean implying unfavourable conditions for convection. During this 2016/17 TC season, only five tropical storms occurred, of which three intensified into tropical cyclones. In February, the anticyclonic anomaly in the Mozambique Channel was weaker than that for the season as a whole (**Fig. 4-1b)** but that east of Madagascar was stronger**.** As a result, conditions for cyclogenesis in the Channel may have been more favourable than that east of Madagascar in February 2017. The strong anomaly east of Madagascar suggests enhanced advection of tropical moist marine air towards northern

Madagascar and the Channel. **Fig. 4-1c-d** shows warm SST anomalies in the Mozambique Channel which would also have been favourable for TC activity over the region. The seasonal SST anomalies were positive in the southwest Indian Ocean and negative to the northwest of Australia in a pattern reminiscent of a positive phase of the South Indian Ocean subtropical dipole (Behera and Yamagata, 2001; Reason, 2001, 2002).

Fig. 4-1e-f exhibits zonal wind anomalies at 500 hPa with negative values north of 30°S, which indicates stronger easterlies in the South Indian Ocean towards Madagascar. The easterly anomalies for JFM in the central Mozambique Channel and east of Madagascar are slightly weaker compared to those during February.

Moreover, the strong easterly anomalies present over the central and northern Mozambique Channel and Madagascar during February were favourable for a westward track of Dineo in the middle of that month.

The synoptic evolution of Dineo is first examined using South African Weather Service (SAWS) surface synoptic charts from 12 to 17 February 2017 (**Fig. 4-2**). Other data and figures are going to be included in the description below. The chart for 12 February **(Fig. 4-2a)** shows Dineo developing as a tropical depression with a central isobaric pressure of 1004 hPa, located in the central Mozambique Channel. A coastal low was located over northern KwaZulu Natal and a strong trough was present over Botswana. South of South Africa, there was an eastward moving cold front with a ridging anticyclone approaching from the South East Atlantic and the trailing edge of the previous migratory anticyclone located south and southeast of Madagascar. A TTT linked the front with the trough over Botswana (**Fig. 4-3a**). Ahead of the TTT, there was weak offshore flow over southern Mozambique and northern Kwa-Zulu Natal as well as

weak onshore flow over the central Mozambican coast associated with the developing tropical depression in the Channel.

The presence of the tropical depression in the central Mozambique Channel and its associated onshore flow led to a band of relatively strong rainfall extending northwest to southeast over southern Madagascar on this day, as indicated by TRMM (**Fig. 4-5a)**. TRMM also showed a maximum rainfall of over 100 mm for this day over north-western Namibia and up to about 50 mm in parts of the North West Province and Botswana, consistent with areas of convective cloud evident in the EUMETSAT IR image **(Fig. 4-3a)** and the inland trough over Botswana **(Fig. 4-2a).** However, the rain gauge stations (**Fig. 4-4a and 4-4b)** in Mpumalanga and Limpopo recorded no rainfall.

On the 13th of February, the tropical depression had moved slightly southeast in the Channel to be located just west of the west coast of Madagascar with the central minimum pressure reduced to 996 hPa (**Fig. 4-2b**). As a result, a few regions in southern Madagascar received some rainfall on this day but most occurred over the Channel or over southern Mozambique according to TRMM (**Fig. 4-4b**). Furthermore, the trough located over central Botswana, slightly shifted south causing rainfall in parts of South Africa such as Free State and North West Province, consistent with convective cloud evident there in the EUMETSAT IR image (**Fig. 4-3b**). However, the rain gauge stations (**Fig. 4-4a and 4-4b)** in Mpumalanga and Limpopo recorded no rainfall for this day.

The tropical depression deepened into a severe tropical storm (now named Dineo) with a minimum central pressure of 980 hPa in the Mozambique Channel and tracked south-westwards towards the central coast of Mozambique on the 14th of February (**Fig. 4-2c).** Furthermore, over northern Botswana, the trough developed into a closed tropical low, with a heat low now present over the Northern Cape. Convergence between these systems led to substantial rainfall (40-120 mm) over a band stretching northwest from the Northern Cape to the central Namibian coast according to TRMM (**Fig. 4-5c)**. This rainfall was consistent with the areas of convective clouds, as evident in the EUMETSAT IR image (**Fig. 4-3c)**. The inflow of moist air from the South West Indian Ocean into the Northern Cape low led to some SAWS stations in Mpumalanga (**Fig. 4-4a**) and Limpopo (**Fig. 4-4b**) recording rainfall.

On the 15th of February, Dineo deepened to reach TC status and tracked further westward in the Channel towards the central Mozambique coast (**Fig. 4-2d**). The satellite image (**Fig. 4-3d**) shows the western edge of Dineo impacting coastal Mozambique around 6 UTC. Later on this day, it made landfall near Inhambane on the south-central coast. The synoptic chart for this day shows Dineo with a central minimum pressure of 974 hPa and average wind speed of 65 knots. A strong anticyclone was present in the mid-latitude South West Indian Ocean and acted to block the tropical cyclone from tracking further south in the Mozambique Channel into the open ocean.

The rainfall observed over Namibia southeast to Lesotho was associated with the heat low present over the Northern Cape and moist air advected over eastern South Africa by the anticyclone to the southeast of South Africa (**Fig. 4-2d**). This heat low and associated pressure gradients over the Northern Cape were weaker than the previous day, consistent with the

reduced rainfall maximum in the TRMM rainfall band (**Fig. 4-5d**) as well as reduced convective activity according to the IR image (**Fig. 4-3d)**. Furthermore, relatively low amounts of rainfall were recorded at stations in Mpumalanga and Limpopo (**Fig. 4-4a and 4-4b**) on this day. However, TRMM showed substantial rainfall over central Mozambique / eastern Zimbabwe associated with Dineo as well as a westerly shift of the band of rainfall (up to about 40 mm) extending from Namibia southeast to Lesotho (**Fig. 4-5d**).

On the 16th of February, the former Dineo was downgraded to a tropical depression and had moved further inland to be located over eastern Zimbabwe with a minimum central pressure of 996 hPa (**Fig. 4-2e**). Bands of convective cloud circling around a relatively clear centre over southern Mozambique are apparent in the satellite image (**Fig. 4-3e).** The high-pressure system in the mid-latitude South West Indian Ocean had strengthened and tracked south-eastwards reinforcing the moist south-east onshore flow towards eastern South Africa. As a result, some Mpumalanga and Limpopo stations near the escarpment recorded substantial rainfall on this day (**Fig. 4-4a and 4-4b**) (e.g., Graskop and Tshivasie Tea Venda which received 98 and 45 mm respectively). TRMM (**Fig. 4-5e**) showed some rainfall over Zimbabwe and central Mozambique associated with ex-Dineo. The heavier rainfall received over northern Mozambique, Malawi and Zambia was associated with a new tropical low that had developed over northern Mozambique (**Fig. 4-2e**). Another region of rainfall was present in TRMM over the North West Province and Gauteng which appears to be located between the inland heat low over the Northern / East Cape Provinces and ex-Dineo to its northeast.

Ex-Dineo was still present as a tropical depression with a central pressure of about 1004 hPa on 17 February (**Fig. 4-2f**) and located slightly further west over Zimbabwe. Its associated

convective cloud had become more diffuse and less organised into circular bands according to the satellite image (**Fig. 4-3f).** The anticyclone in the mid-latitude South West Indian Ocean further tracked south-eastwards causing moist south-east onshore flow towards eastern South Africa. A narrow band of relatively high rainfall with 60 mm maximum was evident in TRMM over eastern South Africa for this day (**Fig. 4-5f**). These large amounts were particularly evident over Mpumalanga Province, where Graskop received over 125 mm daily rainfall (**Fig. 4-4a**). Additionally, **Fig.4-4a** and **Fig. 4-4b** indicated that the 17th as well as the previous day were the wettest days in February 2017 in several stations in Mpumalanga and Limpopo. TRMM also shows large falls over Zambia and Malawi with daily totals of more than 120 mm near the northern margins of ex-Dineo and nearby convective cloud (**Fig. 4-3f).**

This section has described the evolution of tropical cyclone Dineo as resolved in the SAWS synoptic charts and satellite images together with the rainfall patterns associated with Dineo and the TTT as indicated by TRMM. The next section presents the WRF simulation of Dineo and a validation thereof.

4.2 Modelling Tropical Cyclone Dineo using WRF model

Validation of WRF model output

This section assesses the ability of WRF model to reproduce the features of Tropical Cyclone Dineo and regional atmospheric patterns through comparing the model atmospheric circulations with CFSv2 and satellite datasets from TRMM and ASCAT. To validate pressure and wind patterns, geopotential height and wind components (u and v) were interpolated onto 200 and 850 hPa pressure levels.

The WRF Model was initialized at 00 UTC 12 February and ran until 23 UTC 17 February with two-way nested grids of 18km and 6 km horizontal resolution respectively. Both domains were centred at 25°S, 30°E in the Mozambique Channel.

Figure 4-6 and **Fig. 4-7** show the daily sequence of 850hPa and 200hPa geopotential height respectively over the outer domain at 0000 UTC for 12-17 February 2017 from the WRF simulation (left) and CFSv2 reanalyses (right). The evolution of Tropical Cyclone Dineo after generation in the central Mozambique Channel and subsequent track to make landfall near Inhambane on the south-central Mozambique coast are apparent. In general however, the intensity of Dineo is shown to be stronger in WRF than in the CFSv2 reanalyses. Both also indicate a strong anticyclone over and south of Madagascar that strengthened with time and expanded westward. This location of the anticyclone was favourable for Dineo to track westward towards Mozambique rather than southwards in the Channel into the open South West Indian Ocean as quite often happens with TCs generated in the Channel such as TC Dera in 2001 (Reason 2007).

On the 13th of February, the storm was observed to intensify, with a central minimum geopotential height of less than 1400m in WRF, whereas in CFSv2 reanalyses the minimum height was more like 1430m. Both WRF and CFSv2 reanalyses clearly showed the anticyclone in the South West Indian Ocean to extend further west towards south-eastern Africa compared to the previous day. This westward extension of the anticyclone continued on the 14th of February (**Fig. 4-6c**) along with a strengthening while Dineo moved closer to the Mozambican coast and intensified further.

On the 15th of February, the anticyclone further strengthened and extended over eastern South Africa making conditions unfavourable for Dineo to move further south in the Channel. On this day, both WRF and CFSv2 reanalyses showed the storm slightly shifting westwards and made landfall over southern-central Mozambique. However, WRF showed the eye of Tropical Cyclone Dineo to lie over southern-central Mozambique, meanwhile in the CFSv2 reanalyses, the eye was still slightly offshore of the south-central coast of Mozambique (**Fig. 4-6d**).

After Dineo made landfall and tracked further west towards the border between Mozambique and Limpopo, its intensity weakened on 16 February, where the central minimum geopotential height was about 1480m. Meanwhile, the strengthening of the anticyclone persisted over the South West Indian Ocean (**Fig. 4-6e)** and **(Fig. 4-6f)**. On February 17, the remnants of the Dineo (now a tropical depression) were located over Botswana, as seen in WRF model (**Fig. 4-6f)** whereas the CFSv2 reanalyses indicated that ex-Dineo had merged in with the Angola Low to form a broader cyclonic system extending over Botswana, Namibia and Angola. In WRF, a coherent Angola Low is evident over southern Angola / northern Namibia separate from ex-Dineo.

At 200hPa on the 12th of February **(Fig. 4-7a),** WRF showed a strong anticyclone located in the central Mozambique Channel and another notable anticyclonic feature lying over Botswana, Namibia and north-western South Africa. However, in CFSv2 reanalyses, there was a single anticyclonic feature located over subtropical southern Africa. During 13 and 14 February, these two upper level anticyclones in WRF seemed to merge over southern Africa resulting in a stronger and elongated high pressure system very similar to that in the CFSv2 data **(Figs. 4-7b, c).** A closed upper level anticyclone is evident on 15 February in WRF over the south-central coast of Mozambique, indicating the position of Dineo, but this is less clearly apparent in CFSv2 **(Fig. 4-7d).** During 16 to 17 February when Dineo tracked overland and dissipated, the core of the upper level anticyclones moved further west over subtropical southern Africa and were larger in spatial extent in CFSv2 than in WRF **(Fig. 4-7e** and **Fig. 4-7f).**

Figure 4-8 shows the daily sequence of winds at 850 hPa for the duration of the storm from the WRF simulation (left) and CFSv2 reanalyses (right) over the outer domain at 0000 UTC. Both sequences mainly showed similar wind patterns overall, however, some notable differences in the wind magnitude were observed. On the 12th of February, CFSv2 reanalysis winds in the central Mozambique Channel where the storm developed are stronger than in WRF (**Fig. 4-8a).** From 13-14 February, both WRF and CFSv2 reanalyses showed similar wind patterns, however, the wind magnitude in WRF was enhanced and the storm more tightly defined compared to that of CFSv2 reanalyses (**Fig. 4-8b** and **Fig. 4-8c**). On the 15th of February, WRF again showed stronger winds and a more tightly defined Tropical Cyclone Dineo than does the CFSv2 reanalyses. Also, the eye is nearer the southern central Mozambique coast in WRF than it is in the CFSv2 reanalyses (**Fig. 4-8d).** Although both WRF and CFSv2 reanalyses showed decreased wind magnitudes during 16-17 February over the

southern Mozambique region where the weakening ex-Dineo tracked further inland, WRF showed the core and the stronger winds to be further west than do the CFSv2 reanalyses (**Fig. 4-8e-f)**.

Comparison of near-surface winds over the oceanic parts of the domain between WRF and the ASCAT satellite scatterometer derived winds is a tougher test of the model since the ASCAT data are completely independent unlike the re-analyses. However, it must be noted that the WRF winds in **Fig. 4-9** are at 10m above sea-surface whereas the ASCAT data are derived from scatter from the waves on the sea surface. Both WRF and ASCAT show similar wind patterns in general. However, in WRF the strengthening tropical depression on 12 February has wind magnitudes of about 15 ms^{-1} in the central Mozambique Chanel whereas the ASCAT winds here are much weaker (**Fig. 4-9a**). Also, the area of strong winds (9-12ms^{-1}) south of Madagascar in the South West Indian Ocean was also larger in WRF than in ASCAT on this day. The maximum wind surface showed by ASCAT was over 12 ms^{-1}.

On the 13th of February, both WRF and ASCAT showed similar strong surface winds in the central Mozambique Channel associated with Dineo with the core in the same location (**Fig. 4.9b)**. However, just south of Madagascar, the winds were stronger in WRF than in ASCAT.

The westward extension of the strong winds above 12 ms^{-1} in the western Mozambique Channel towards the Mozambican coast on 14 February is evident in WRF but less so in ASCAT (**Fig. 4.9c)** whereas on February 15 (**Fig. 4.9d**), this extension can be seen in both data sets. Additionally, when WRF surface winds were plotted at 1000 hPa pressure level (not shown), the winds on the 14th of February reached 29 ms^{-1}(104 $kmhr^{-1}$) and were associated

with tropical storm (Dineo) near the coast. On 15 February, the surface maximum winds reached 36 ms^{-1} causing Dineo to reach Tropical Cyclone status (category 1)

On 16 and 17 February, the winds in the southern Mozambique Channel weaken as ex-Dineo moves inland while those south of Madagascar strengthen (**Figs. 4.9e-f).** The latter are associated with the anticyclone seen in **Fig. 4-6.** In general however, the regions of stronger winds in these two locations are more spatially extensive in WRF than in ASCAT. Although there are some differences in wind magnitude, the WRF and ASCAT near-surface winds are in reasonable agreement with each other. It should be noted that ASCAT dataset were daily averages whereas WRF was 6 hourly averages, hence the relatively weak winds were observed throughout the duration of the storm in ASCAT.

Even though regional climate models are powerful tools for simulations of weather events, they may still feature systematic errors particularly with respect to rainfall (Jakob et al., 2011). Hence, it is of interest to see how the rainfall patterns produced by WRF model during Dineo compare to the rainfall estimated by TRMM. **Fig. 4-5** and **Fig. 4-10** suggest that there are some differences in the rainfall spatial distribution both near Dineo and over the larger southern African region.

In general, because of the models finer resolution (6km), WRF tended to show higher rainfall >120mm over the regions where the storm was located, meanwhile TRMM (~50 km) depicted far less rainfall in the region of Dineo. From 12 to 14 February, WRF captured significant rainfall in parts of tropical southern Africa, whereas TRMM showed no rainfall (**Figs. 4-5 and**

4-10). However, TRMM indicated more rainfall over eastern South Africa on 12 February than did WRF (**Figs. 4-5a and 4-10a**).

On 14 February, TRMM showed a narrow band of relatively heavy rainfall stretching northwest from the Northern Cape to the central Namibian coast; meanwhile WRF indicated a less well-defined band of weak patchy rainfall over this region (**Fig. 4-5c and 4-10c**). By contrast on this day, the heavy rainfall associated with Dineo in the southern Mozambique Channel was clearly evident in WRF while that in TRMM in the southern Channel and neighbouring Mozambique was weak and disorganised. During 15-16 February, as Dineo tracked inland over southern Mozambique, this heavy rainfall persisted in the WRF simulation but not in TRMM which only showed significant rainfall to the north of Dineo.

On the 17th of February when the remnants of Dineo were observed over southern Zimbabwe, Botswana and north-east South Africa, WRF showed rainfall again above 120 mm over these regions, meanwhile TRMM indicated a narrow band of rainfall of up to 60 mm stretching south-eastwards from the North West Province of South Africa across Lesotho to the Eastern Cape coast. On the other hand, TRMM estimated heavy rainfall over northern Mozambique (over 120 mm) whereas WRF only showed relatively low rainfall of 20 mm here (**Fig. 4-5f and 4-10f**).

Daily WRF rainfall time series were compared with SAWS station data rainfall for the duration of the Dineo (**Figure 4-11**). Considering the wettest stations in Limpopo and Mpumalanga, Both WRF and station data showed rainfall on 16-17 February which were the wettest days

during the storm. However, for most stations, WRF underestimated the rainfall received. Considering Tzaneen and Bourkes Luck on 16 February, WRF was able to capture rainfall like that of station data.

In summary, there were some discrepancies between the WRF model and CFSv2 reanalyses in terms of the position and strength of Dineo. However, the evolution of the storm from development to its dissipation stage was represented correctly by WRF. The WRF surface winds compared with ASCAT winds showed not much difference in terms of the storm position and wind direction in the storm region. However, WRF tended to show stronger winds of up to 22 ms^{-1} maximum compared to ASCAT maximum winds of 20 ms^{-1}. Additionally, ASCAT misrepresented the position of Dineo on 14 and 15 February.

There were however more obvious differences between WRF and TRMM estimates of rainfall. Surprisingly, TRMM did not clearly show the organised heavy rainfall associated with Dineo unlike WRF. Although the resolution of TRMM is 25 km, it should still be able to capture heavy rainfall associated with a tropical cyclone. Instead, TRMM appeared to over-emphasize the rainfall associated with the TTT over southern Africa to the west of Dineo and then, after Dineo had made landfall, it appeared to overestimate the rainfall over northern Zambia and northern Mozambique. The rainfall at some SAWS stations (e.g. Tzaneen, Tshivhasie Tea Estate, Graskop and Bourke's Luck) in north-eastern South Africa on 16 and 17 February as ex-Dineo tracked further inland are consistent with the WRF estimates for these days. However, WRF had difficulties in capturing the extreme rainfall for individual station regardless of whether the WRF time series was plotted using the nearest grid-point to the station

or the average of the surrounding grid points. This difficulty is not surprising given the very steep topography of the region where these stations are located.

4.3 Contribution of TC Dineo to rainfall over north-east South Africa.

Having shown that there is reasonable confidence in the WRF simulation of Dineo and its associated rainfall, this section uses WRF output to understand the circulation patterns and potential mechanisms that might have contributed to the substantial rainfall received during February 2017 over Mpumalanga and Limpopo Province.

As mentioned above, north-east South Africa received large amounts of rainfall in February 2017 which was associated with Tropical Cyclone Dineo. Following the drought over southern Africa which resulted from the strong 2015/16 El Nino (Blamey et al., 2018) ,it is of interest to see how much impact Tropical Cyclone Dineo had on the region in terms of rainfall.

Tables 2-3 list the contribution of Dineo to the monthly total rainfall for February 2017 recorded at various Mpumalanga and Limpopo stations. The contribution was calculated using the following formula:

$$Storm\ Contribution\ (\%) = \left(\frac{total\ rainfall\ during\ the\ storm}{monthly\ rainfall}\right) x\ 100$$

These range from essentially no contribution at stations on the Highveld such as Ermelo and Witbank to as much as 80% at lowveld stations (Skukuza). Largest contributions (> 40%) occur at or near the windward slope of the escarpment in Mpumalanga. The percentage contributions (but not necessarily the actual amounts) from Dineo are greater in Mpumalanga than in Limpopo. In terms of amount, Dineo contributed most at Graskop (242 mm) in Mpumalanga

with Tzaneen in Limpopo (99 mm) being the third wettest station overall. Thus, Dineo led to significant contributions to the summer rainfall totals at several places in eastern Mpumalanga and eastern Limpopo; these regions are important to the national economy for both agriculture (mainly fruit, vegetables and macadamia nuts) and tourism (e.g., Kruger National Park).

Figs. 4-4a and b show the timing of the daily rainfall at each station during February 2017. At the eastern stations with heavy rainfall like Graskop, Bourkes Luck, Kruger Mpumalanga International Airport, Tzaneen and Tshivasie, the heavy rainfall tends to occur on 16 and 17 February as ex-Dineo tracked from southern Mozambique further inland. Some of these stations received little or no rainfall earlier in the month highlighting the importance of this event. The period from 19-26 February also showed significant falls at many stations across both provinces as ex-Dineo contributed along with an active Angola Low to producing favourable conditions for convective rainfall over subtropical southern Africa.

To better understand the circulation patterns that may be associated with the rainfall that occurred from 12 to 17 February 2017 during the lifespan of Dineo, plots of moisture flux at 850hPa, moisture flux divergence at 700hPa, vertical velocity at 500hPa, convective instability calculated between 850 and 500hPa, zonal wind shear calculated between 850 and 500hPa, meridional wind shear between 850 and 500hPa as well as potential vorticity at 700hPa were produced.

Figures 4-12 - 4-14 show strong cyclonic moisture fluxes impacting on south-western Madagascar from the southern Mozambique Channel with areas of convergence and uplift that

are largely consistent with the WRF rainfall (**Fig. 4-10**), on the 12th of February while TRMM (**Fig. 4-5a**) shows more extensive rainfall including to the south of Madagascar. The cyclonic fluxes in the southern Channel represent the tropical depression that developed into TC Dineo and are associated with favourable conditions such as warm SST (not shown), relatively large convective instability (**Fig. 4-15a)**, relatively weak wind shear (**Figs. 4-16a, 4-17a**) and negative vorticity at 700 hPa (**Fig. 4-18a**). The convective instability plot suggests the presence of a relatively unstable marine air mass in lower and midlevel troposphere over the central Mozambique Channel where Dineo developed. Over the southern African mainland, areas of moisture flux convergence and uplift can be matched up with rainfall in WRF (**Fig. 4-10a**) over northern Namibia and Zambia. **Fig. 4-12a** suggests that the rainfall over these regions was associated with a strong northeast monsoonal flow from the tropical western Indian Ocean that fed into the interior tropical troughs present over Botswana and Zambia seen in the synoptic chart for this day (**Fig. 4-2a**).

On the 13th of February, the tropical depression had moved slightly southeast in the Channel and was adjacent to the southwest coast of Madagascar with the central minimum pressure reduced to 996 hPa (**Fig. 4-2b**). The regions of strong moisture fluxes were located over the southern Mozambique Channel and central subtropical southern Africa ((**Fig. 4-12b**). Furthermore, these regions of enhanced moisture flux are associated with those of moisture flux convergence (**Fig. 4-13b**); enhanced uplift (**Fig. 4-14b**) large convective instability (**Fig. 4-15b**), relatively weak wind shear (**Fig. 4-16b, 4-17b**) and negative vorticity (**Fig. 4-18b**). **Figure 4-12b**, suggests that the rainfall over southern Mozambique was associated with the convergence around the tropical depression, meanwhile, the rainfall over Zambia, Namibia, Angola was associated with the on-going northeast monsoonal flow feeding the interior tropical low (**Fig. 4-10b**). Additionally, WRF shows another region of rainfall over southeast South

Africa, which is associated with the convection in the TTT activity, as evident in EUMETSAT IR image (**Fig. 4-3b**). However, both Mpumalanga and Limpopo stations did not receive rainfall on this day (**Fig. 4-4a and 4-4b**).

The tropical depression deepened into a severe tropical storm in the Mozambique Channel and tracked south-westwards towards the central coast of Mozambique on the 14th of February (**Fig. 4-2c).** The cyclonic moisture fluxes impact the central coast of Mozambique with convergence (**Fig. 4-13c**), relatively strong uplift (**Fig. 4-14c**), enhanced convective instability (**Fig. 4-15c**), weak wind shear (**Fig. 4-16c, 4-17c**) and negative vorticity (**Fig. 4-18c)** near Dineo. The areas of large convective instability over the southern Mozambique Channel, where the storm was located, indicated unstable marine air in the lower and mid-level troposphere. As a result, WRF showed heavy rainfall over the southern Mozambique Channel on this day with weaker rainfall near the Mozambican coast (**Fig. 4-10c).** Moisture flux and convergence plots (**Fig. 4-12, 13c)** indicated that the rainfall produced over northern Zimbabwe, Zambia, Angola and Nambia was due to the trough located over northern Botswana (**Fig. 4-2c).** The convergence between this trough and the heat low present over the Northern Cape, led to substantial rainfall (40-120 mm) over a band stretching northwest from the Northern Cape to the central Namibian coast (**Fig. 4-5c),** consistent with the EUMETSAT IR image (**Fig. 4-3c**). The inflow of moist air from the South West Indian Ocean into the Northern Cape low led to some stations in eastern Mpumalanga (**Fig. 4-4a**) (Belfast 40 mm, Secunda 25 mm and Graskop 20 mm) and Limpopo (**Fig. 4-4b**) (Tzaneen Westfalia Estate 35 mm) recording rainfall.

On the 15th of February, Dineo deepened to reach TC status and tracked further westward in the Channel towards the central Mozambique coast (**Fig. 4-2d**). The cyclonic fluxes located

over southern Mozambique in WRF indicated tropical cyclone Dineo making landfall near Inhambane. Strong moisture flux convergence (**Fig. 4-12d**), relatively strong uplift (**Fig. 4-14d**), enhanced convective instability (**Fig. 4-15d**), weak wind shear (**Fig. 4-16d, 4-17d**) and negative vorticity (**Fig. 4-18d)** were all favourable for the strengthening of Dineo**.** Over southern Mozambique, the convective instability plot confirmed the presence of unstable air mass in the lower and mid-level troposphere over the TC region. Areas of moisture flux convergence and relatively strong uplift were in agreement with the rainfall regions in WRF (**Fig. 4-10d). Fig. 4-12d** suggests that the rainfall observed over northern Mozambique, Zimbabwe and Zambia was associated with the on-going north-easterly monsoonal flow, which fed into the interior tropical lows located over northern Botswana and Northern Cape. Rainfall over Namibia extending southeast towards Lesotho was associated with the heat low present over the Northern Cape and moist air advected over eastern South Africa by the anticyclone to the southeast of South Africa (**Fig. 4-2d**). Additionally, the EUMETSAT IR image (**Fig. 4-3d)**, indicated a reduced convective activity over Namibia and Botswana, but substantial activity over south-eastern South Africa. However, over both Mpumalanga (**Fig. 4-4a**) and Limpopo (**Fig. 4-4b**) SAWS stations, no rainfall was recorded for this day.

On the 16th of February, the former Dineo was downgraded to a tropical depression and had moved further inland to be located over eastern Zimbabwe (**Fig. 4-2e**). Strong moisture fluxes are evident in WRF over southern Mozambique, eastern Zimbabwe and north-eastern South Africa (**Fig. 4-12e**). There were areas of strong moisture flux convergence (**Fig. 4.13e**), relatively strong uplift (**Fig. 4-14e**), enhanced convective instability (**Fig. 4-15e**), weak wind shear (**Fig. 4-16e, 4-17e**) and negative vorticity (**Fig. 4-18e).** The area of enhanced convective instability between southern Mozambique and north-eastern South Africa where ex-Dineo was located was characterised by instability in the lower and mid-level troposphere. The moisture

flux convergence and strong uplift over this region were consistent with the rainfall in WRF (**Fig. 4-10e**). The moisture flux plot (**Fig. 4-12e**) suggests that the rainfall received over this area was associated with convergence between the northeast monsoonal flow from the western Indian Ocean and moist southeast inflow due to the anticyclone located in the mid-latitude south west Indian Ocean as seen in the synoptic chart (**Fig. 4-2e**). Moist south-east onshore flow towards eastern South Africa driven by this anticyclone led to some Mpumalanga and Limpopo stations near the escarpment recording substantial rainfall on this day (**Fig. 4-4a and 4-4b**) (e.g., Graskop and Tshivasie Tea Venda which received 98 and 45 mm respectively).

Ex-Dineo was still present as a tropical depression on 17 February (**Fig. 4-2f**) and located slightly further west over Zimbabwe. The large cyclonic fluxes over Botswana, north-eastern South Africa, and Zimbabwe, due to ex-Dineo, were associated with areas of moisture flux convergence (**Fig. 4-13f**), relatively strong uplift (**Fig. 4-14f**), enhanced convective instability (**Fig. 4-15f**), weak wind shear (**Fig. 4-16f, 4-17f**) and negative vorticity (**Fig. 4-18f).** Northern South Africa and south-eastern Botswana show strong convective instability where ex-Dineo was situated with an unstable air mass present in the lower and mid-level troposphere. The regions of enhanced moisture flux convergence and uplift over eastern Botswana, western Mozambique and north-eastern South Africa can be matched up with the rainfall in WRF (**Fig. 4-10f**). The moisture flux plot (**Fig. 4-12f**) indicated that the rainfall over these regions was associated with a strong moist south-east onshore flow from the anticyclone in the mid-latitude South West Indian towards eastern South Africa. The rainfall seen over Namibia and Angola was associated with the Angola Low which was located over southern Angola / northern Namibia (**Fig. 4-2f**). A few rainfall stations in Mpumalanga received some rainfall with Graskop as the wettest station (over 126 mm) (**Fig. 4-3a**) on this day. Several other stations in Limpopo Province received substantial amount of rainfall with Tzaneen receiving over 60 mm,

Levubu 38mm, Tshivase 45 mm, Mukumbani Tea Estate Venda 48 mm and Punda Maria 35 mm (**Fig. 4-3b**).

In summary, assessing the WRF model fields during the storm event suggests that the rainfall regions shown during the storm event matched up with the regions of large convective instability, low level moisture flux convergence and strong uplift. Warm SST in the Mozambique Channel (not shown), relatively large convective instability, relatively weak wind shear, and negative vorticity were all favourable for the generation and subsequent strengthening of Dineo. The low-level moisture flux plots helped to identify the sources of moisture that fed the precipitation over different locations. The main primary source of moisture for the rainfall received over the Mozambique Channel and north-eastern regions of southern African mainland was the strong northeast monsoonal flow from western Indian Ocean. The moisture source for rainfall over Namibia, Angola and Botswana was associated with the heat low located over Namibia. Finally, for the north-eastern South Africa rainfall, the anticyclone over mid-latitude South West Indian Ocean caused a strong moist southeast inflow towards South Africa where Mpumalanga and Limpopo received several days of heavy rainfall associated with ex-Dineo as it tracked inland.

Table 1: Saffir-Simpson scale (Source: https://www.nhc.noaa.gov/aboutsshws.php)

Type	Category	Pressure (mb)	Wind(mph)	Wind(kmph)	Surge(m)
Tropical Depression	TD	----	<39	<62	----
Tropical Storm	TS	----	39-73	63-118	----
Tropical Cyclone	1	>980	74-95	119-153	1.2-1.5
Tropical Cyclone	2	965-980	96-110	154-177	1.6-2.4
Tropical Cyclone	3	945-965	111-130	178-209	2.5-3.6
Tropical Cyclone	4	920-945	131-155	210-250	3.7-5.4
Tropical Cyclone	5	<920	>155	>250	>5.4

Table 2 showing February 2017 total rainfall for various stations and the storm's contribution over Mpumalanga Province.

Station	**Lat**	**Lon**	**February total (mm)**	**Storm Contribution (mm)**	**Storm Contribution (%)**
Secunda	26.4970	29.1860	145	25.4	18
Ermelo	26.4970	29.9830	3.2	0.0	0.0
Witbank	25.8320	29.1920	127.8	0.8	0.6
Belfast	25.6910	30.0340	180.7	52	29
Machado Dorp	25.7150	30.2300	37.0	0.6	1.6
Komatidraai	25.5140	31.9100	78.6	43.6	55
Kruger Mpumalanga Int. Air	25.3870	31.0990	206.2	82.8	40
Bourkes Luck	24.6720	30.3090	269.8	107	40
Graskop	24.9350	30.8390	597	242	40
Skukuza	24.9920	31.5880	52.4	42	80

Table 3: showing February 2017 total rainfall for various stations and the storm's contribution over Limpopo Province.

Station	Lat	Lon	February total (mm)	Storm Contribution (mm)	Storm Contribution (%)
Oudestad	25.1810	29.3390	95.0	0.8	0.8
Warmbad Toowoomba	24.8990	28.3230	69.4	18.4	27
Mokopane	24.1960	29.0060	34.8	6.4	18
Lephalale	23.6760	27.7050	95.6	0.8	0.8
Market	23.5940	28.3870	169.6	8.4	5
Polokwane	23.8570	29.4510	40.0	14.6	37
Tzaneen Westfalia Estate	23.7360	30.1120	317.8	99	31
Mara	23.1440	29.5570	22.8	6.4	28
Levubu	23.0940	30.2860	211.6	44.8	21
Giyani	23.3140	30.6840	90.2	32.4	36
Tshivhasie Tea Venda	22.9600	30.3540	409.0	59.4	15
Mukumbani Tea Estate Venda	22.9160	30.4050	301.0	61.2	20
Punda Maria	22.6920	31.0150	117.0	44.4	38
Venetia Mine	22.4510	29.3310	42.8	20.4	48

(a) (b)

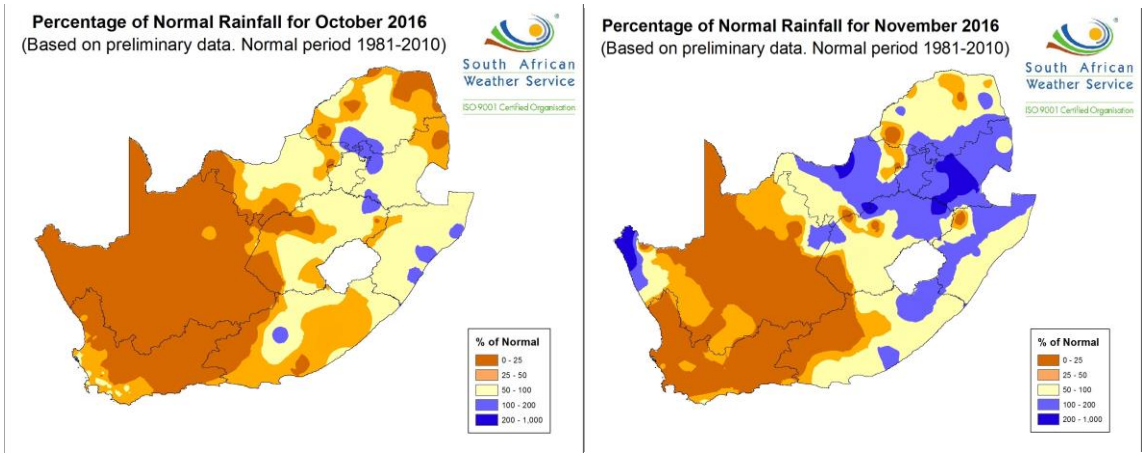

(c) (d)

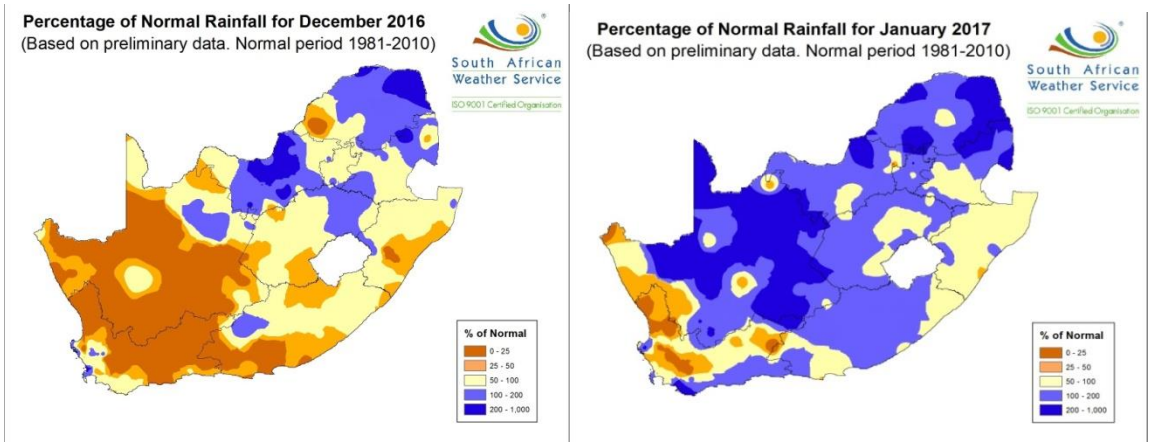

(e) (f)

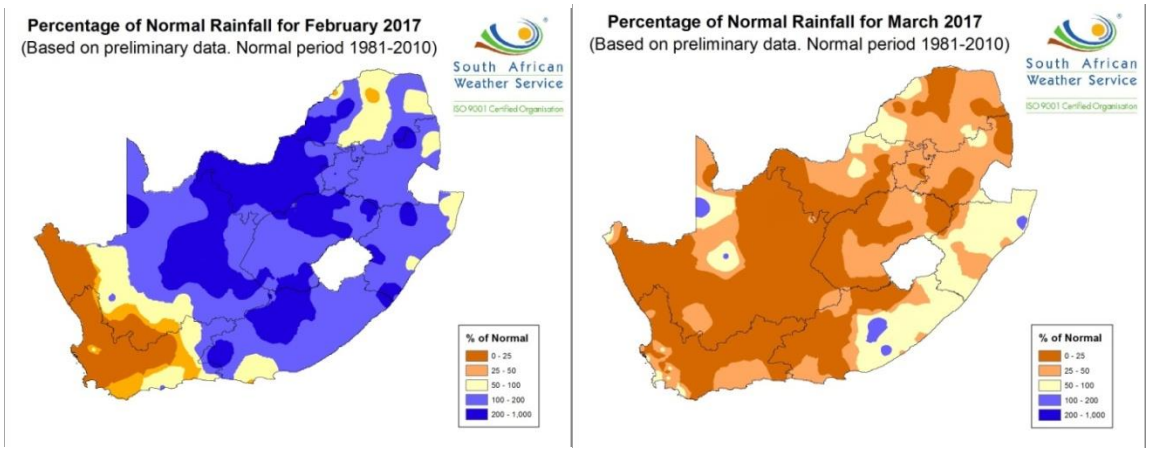

Figure 2-1: Showing percentage of normal rainfall for October 2016 (early summer) to March 2017 (late summer) over South Africa.

(a) (b)

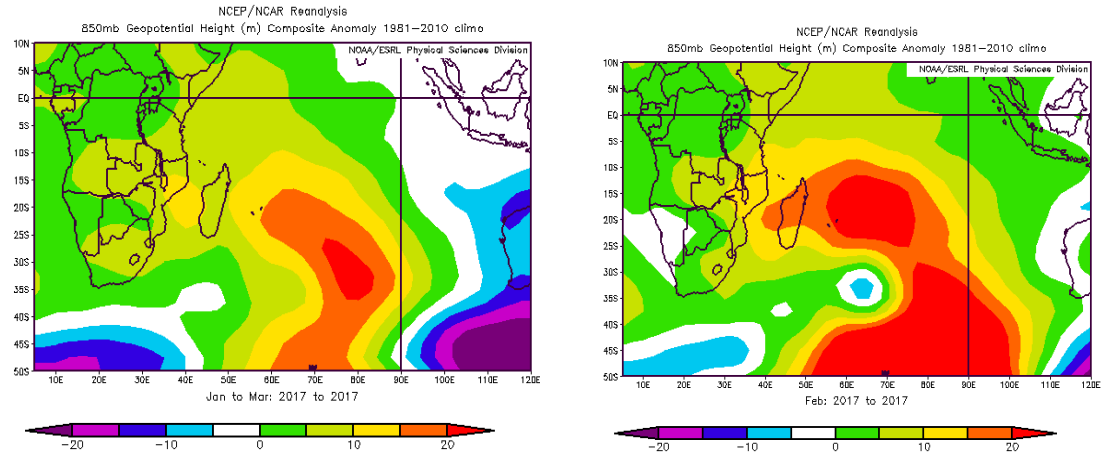

(c) (d)

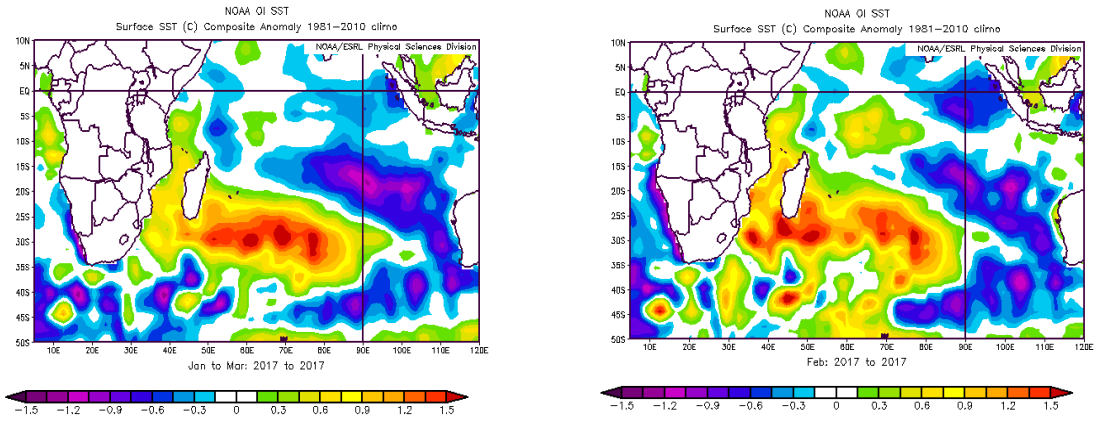

(e) (f)

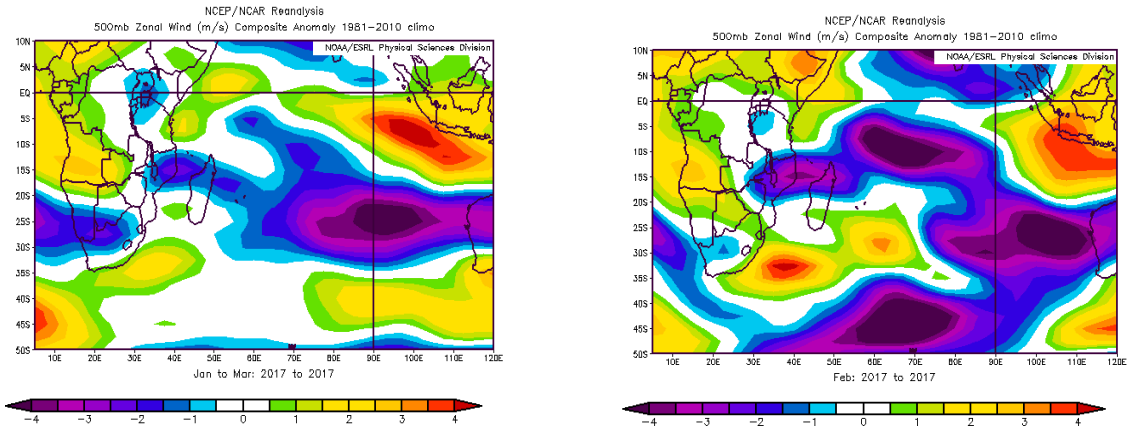

Figure 4-1: Showing (a) seasonal (JFM) geopotential height anomaly at 850hPa, (b) geopotential height anomaly at 850hPa for February 2017, (c) Seasonal (JFM) SST anomaly, (d) SST anomaly for February 2017, (e) Seasonal (JFM) zonal winds at 500hPa and (f) zonal winds for February 2017 at 500hPa.

(a) (b)

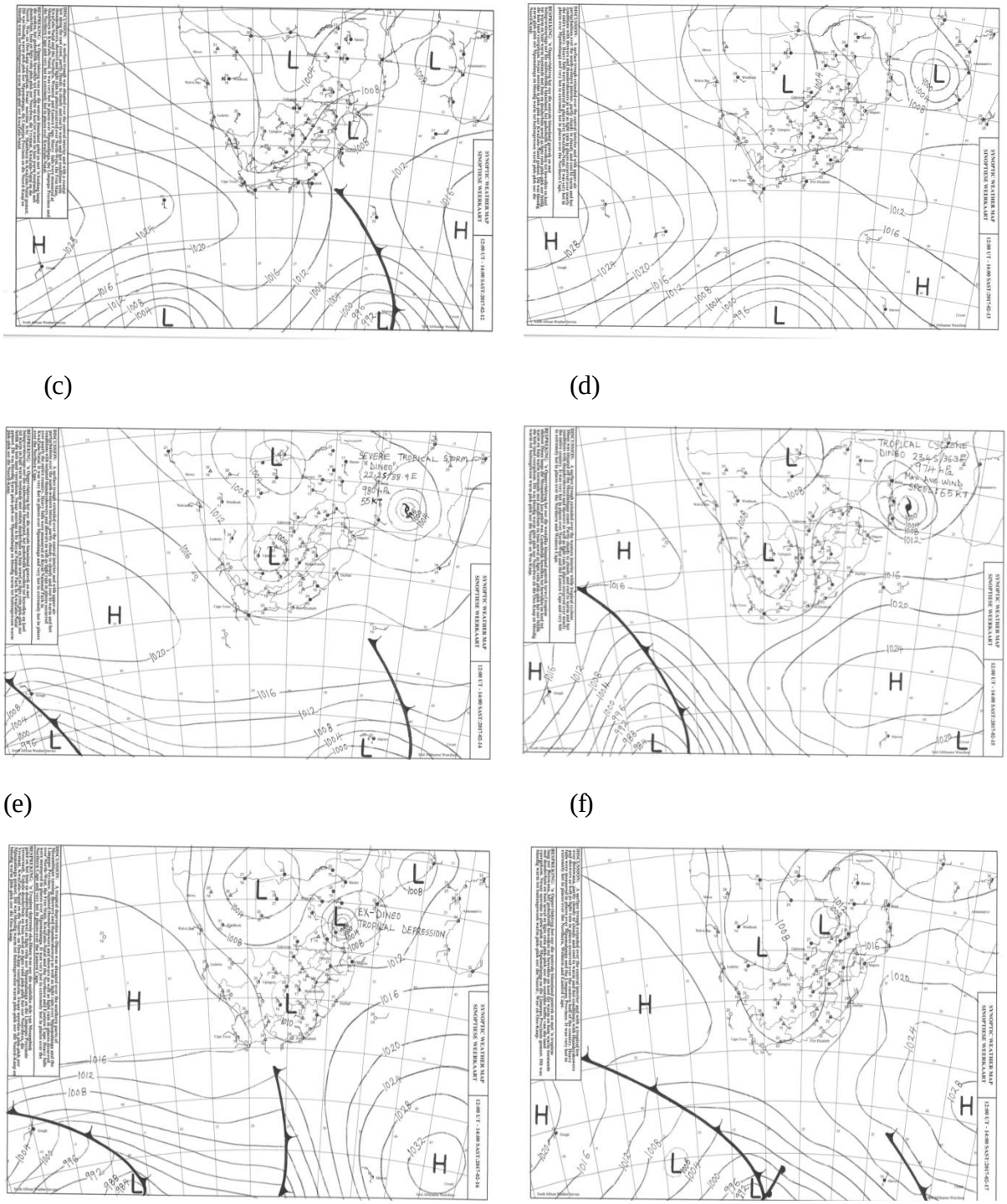

Figure 4-2: Synoptic charts produced by SAWS, showing surface conditions over southern Africa from (a) 12 to (f) 17 February 2017.

(a) (b)

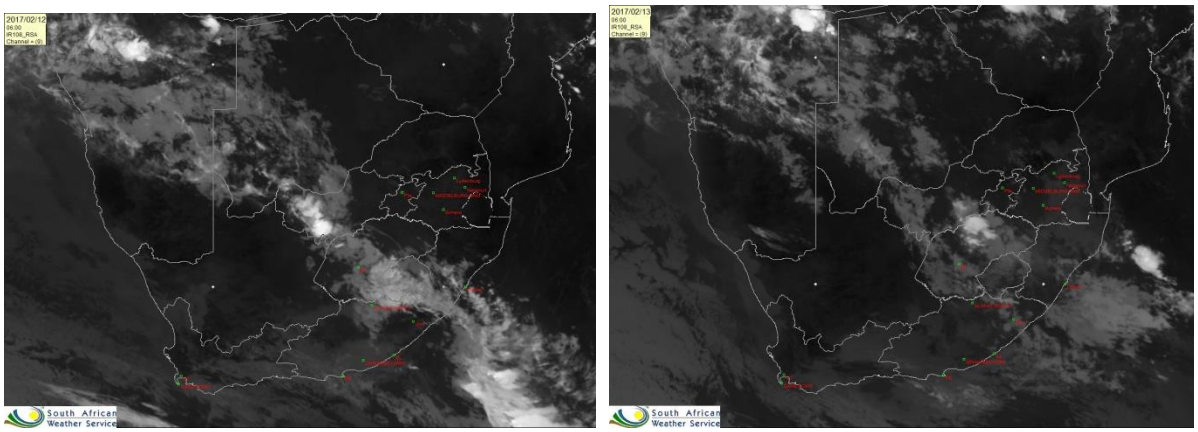

(c) (d)

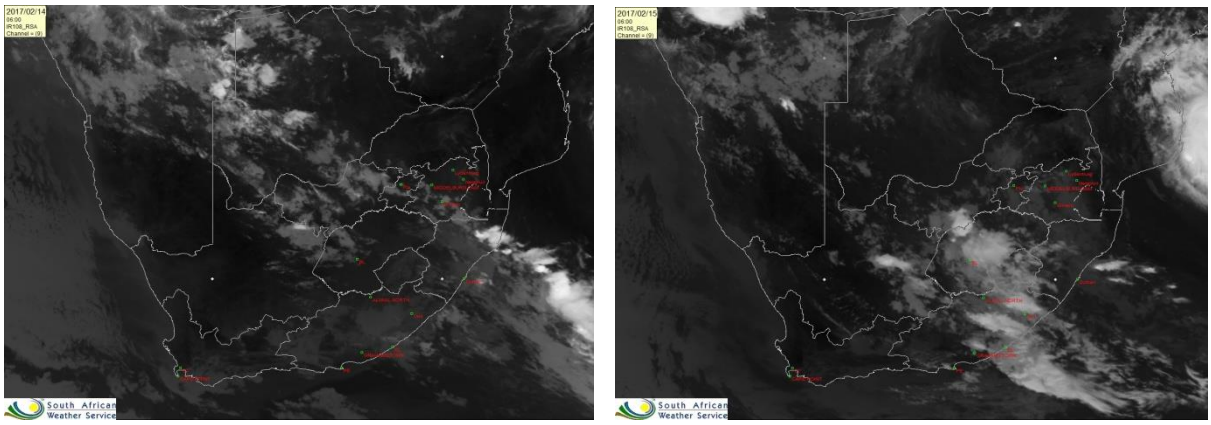

(e) (f)

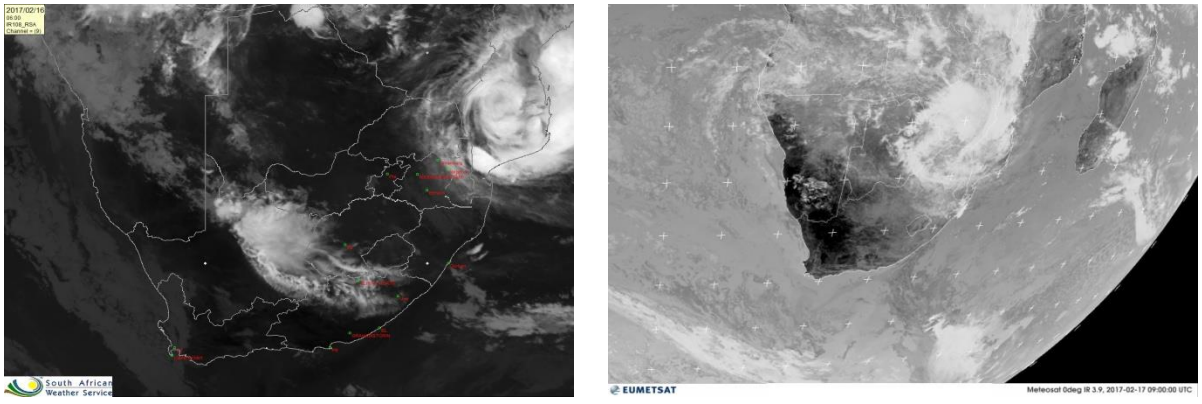

Figure 4-3: EUMETSAT IR images showing atmospheric conditions over southern Africa from (a) 12 to (f) 17 February 2017.

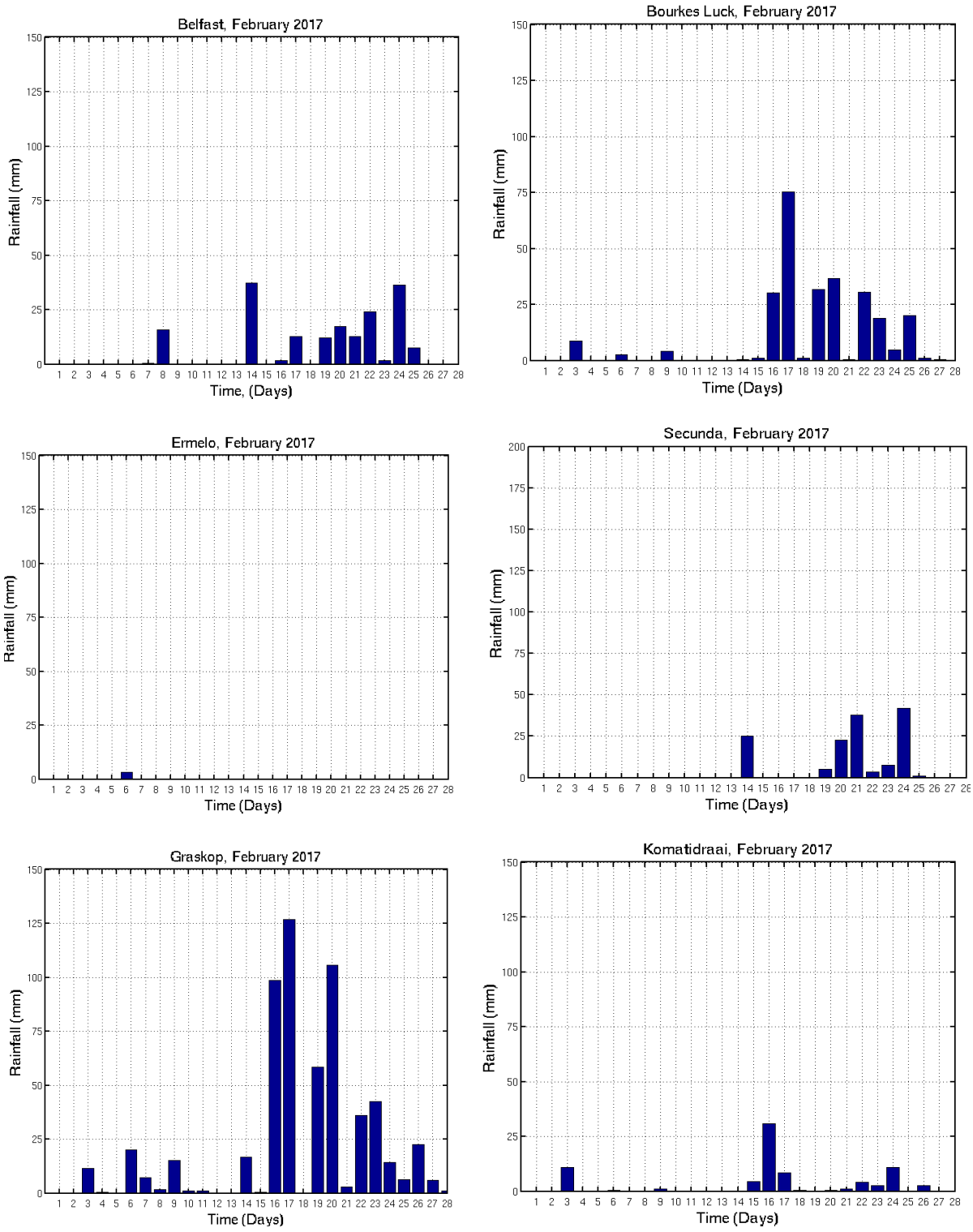

Figure 4-4a: Observed daily rainfall (mm) from 10 stations located in Mpumalanga Province from 1 to 28 February 2017 (Continued on next page).

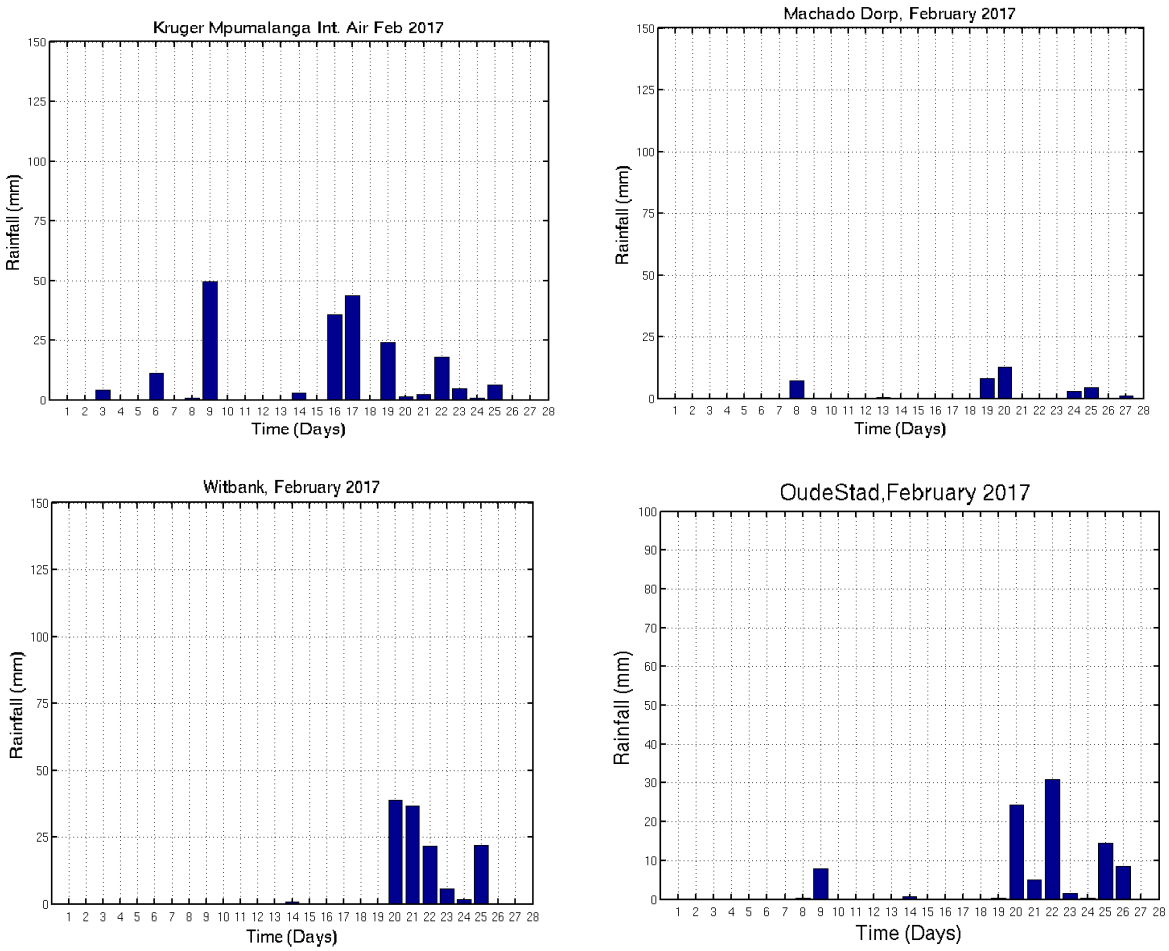

Figure 4-4a: (Continued) Observed daily rainfall (mm) from 10 stations over Mpumalanga Province from 1 to 28 February 2017.

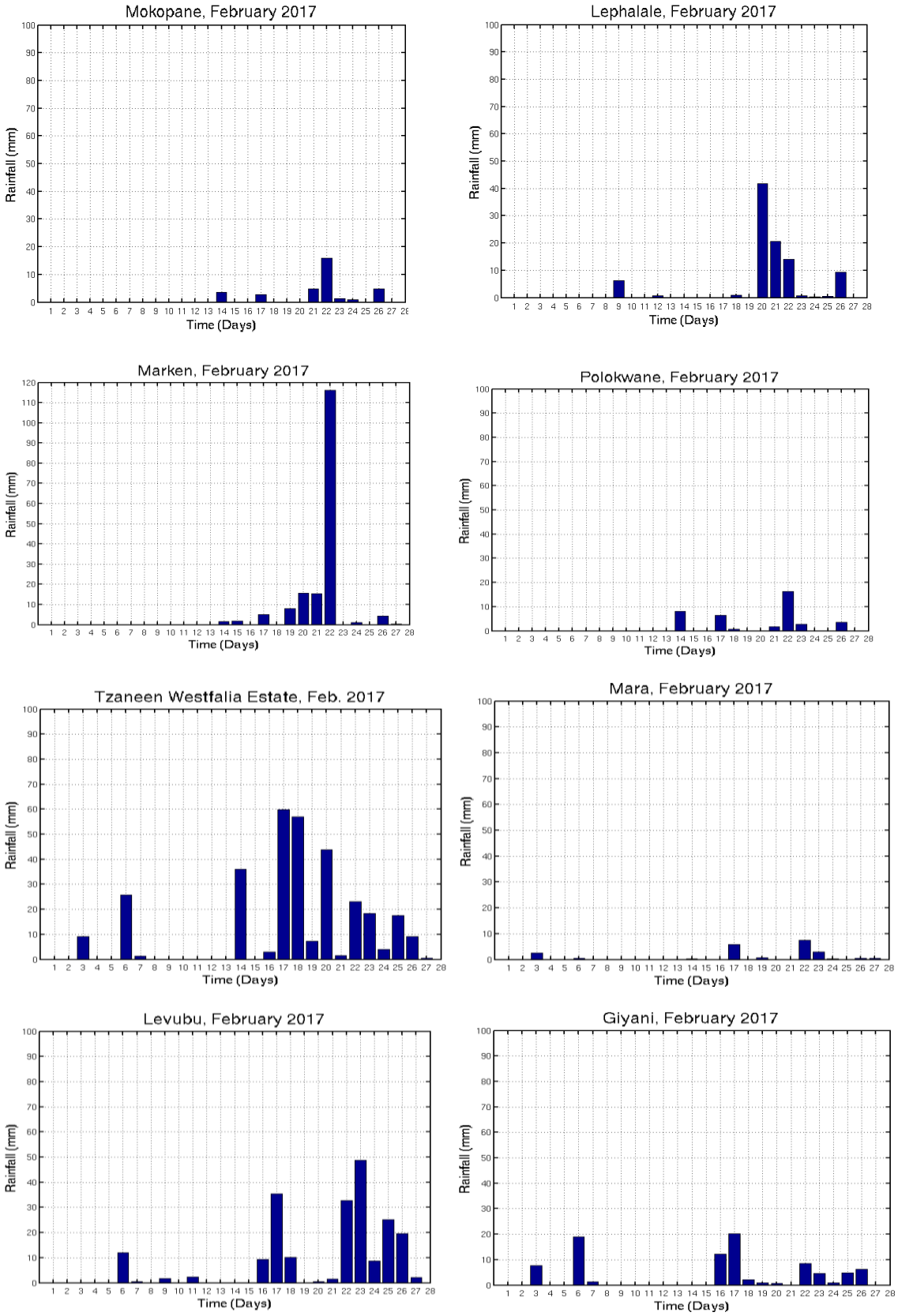

Figure 4-4b: Observed daily rainfall (mm) from 14 stations located in Limpopo Province from 1 to 28 February 2017 (Continued on next page).

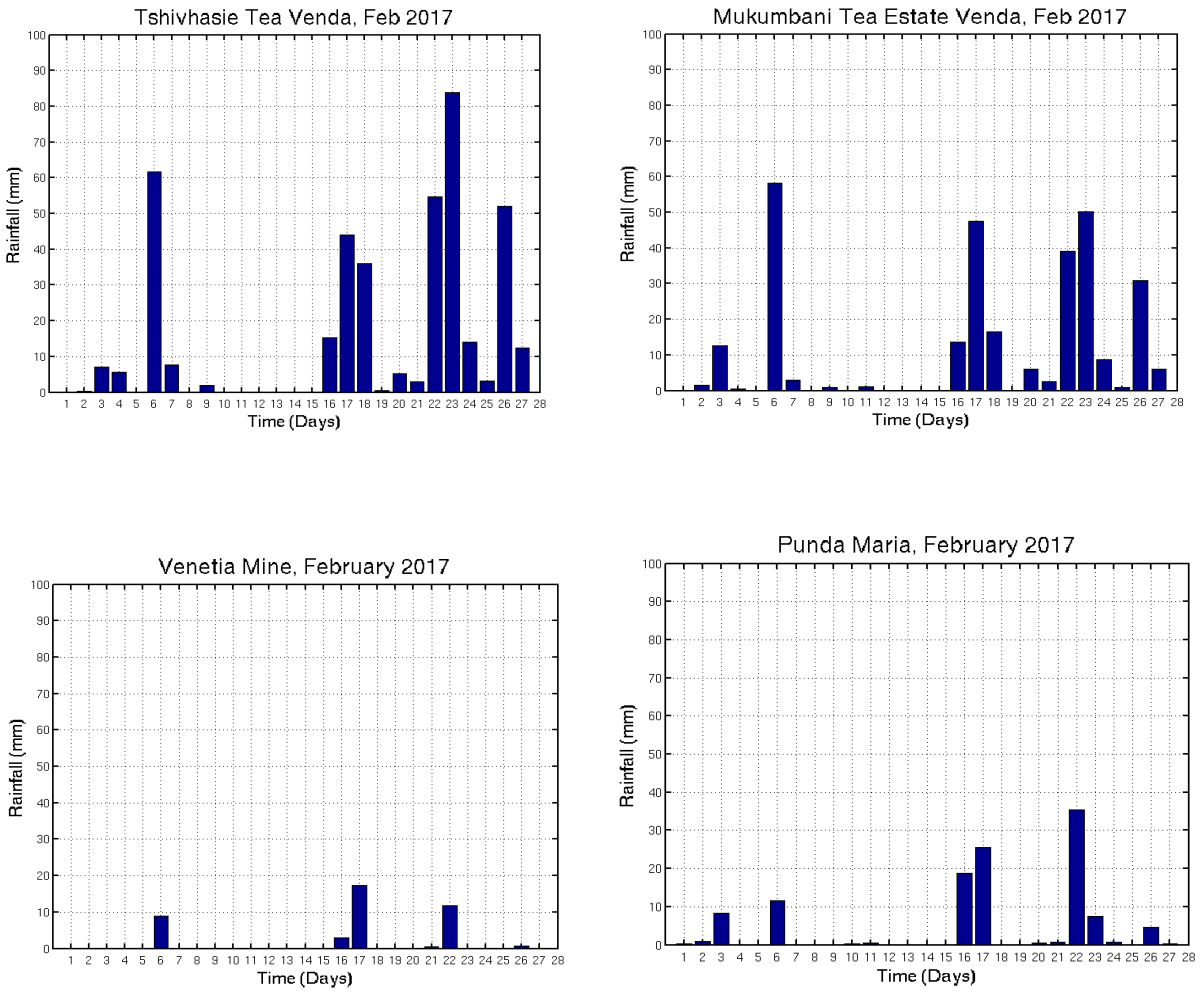

Figure 4-4b: (Continued) Observed daily rainfall (mm) from 14 stations over Limpopo Province from 1 to 28 February 2017.

(a)

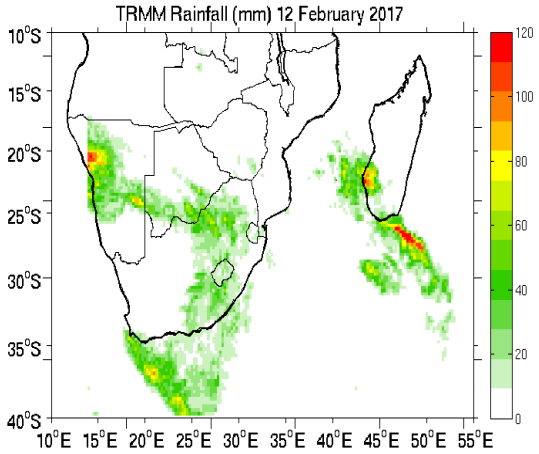

(b)

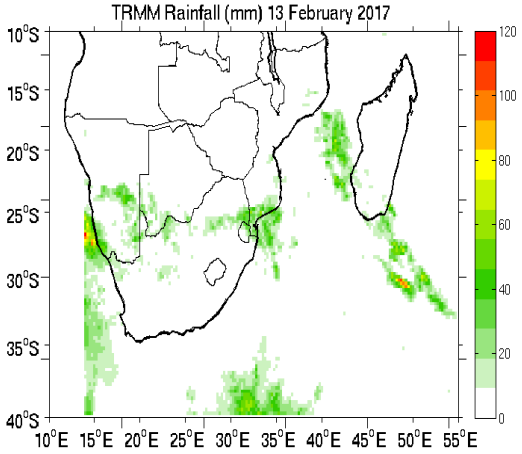

(c)

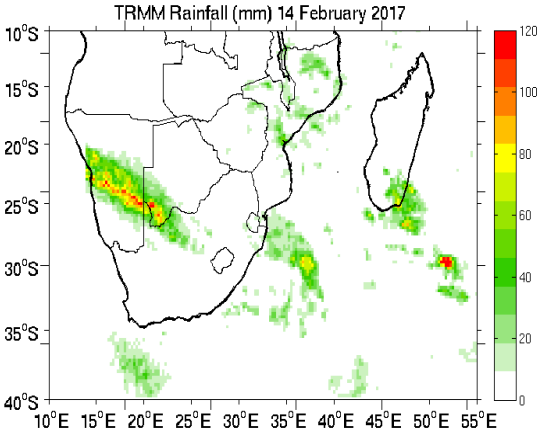

(d)

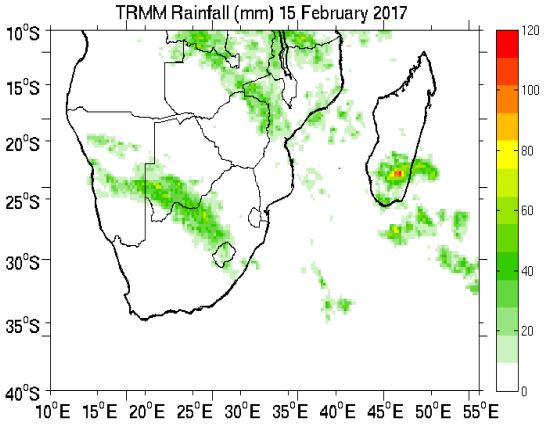

(e)

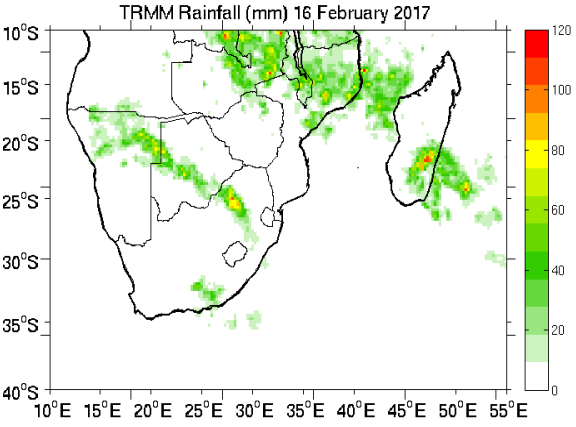

(f)

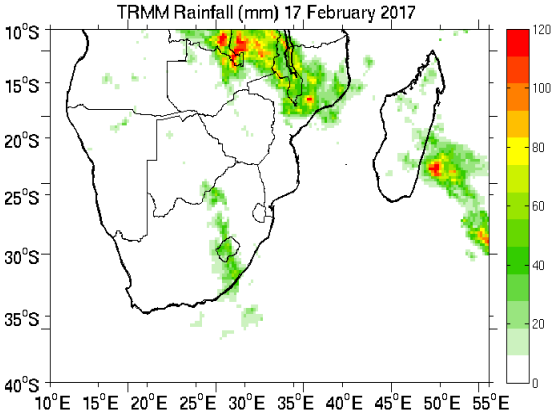

Figure 4-5 Showing TRMM Satellite daily rainfall (mm) over southern Africa from 12 to 17 February 2017.

(a)

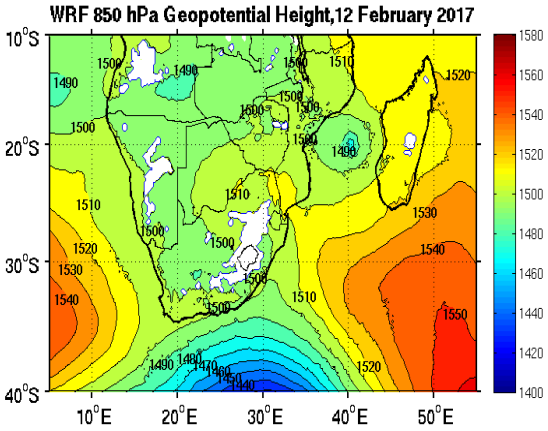

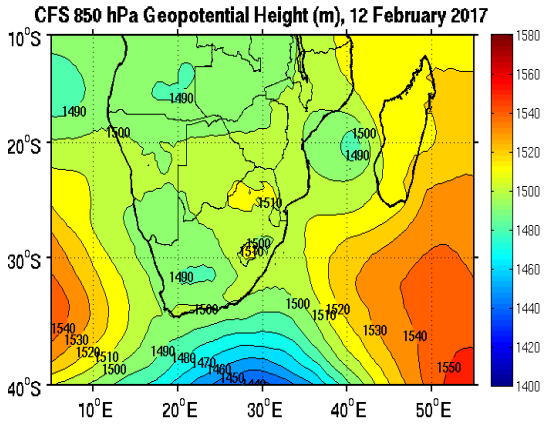

(b)

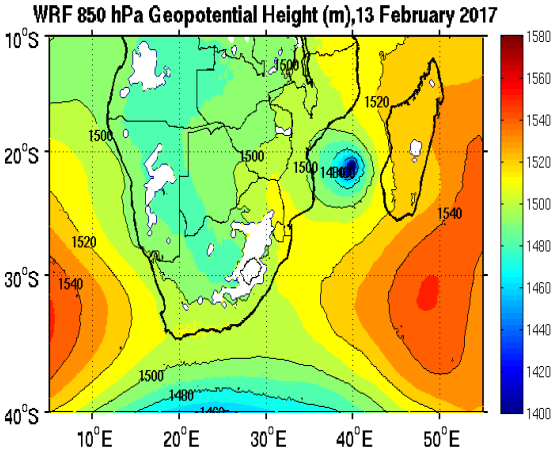

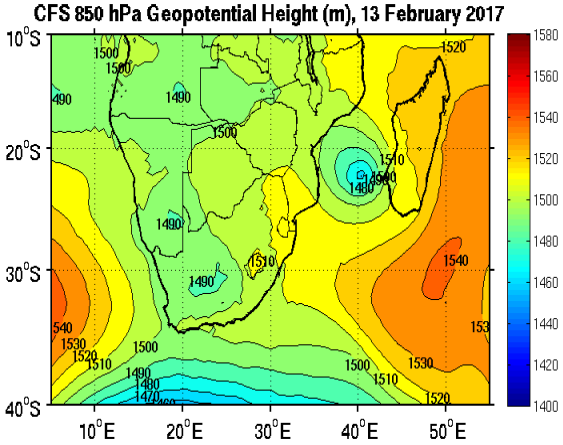

(c)

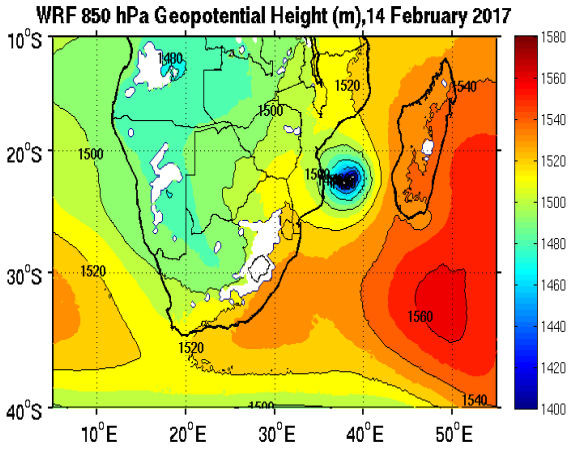

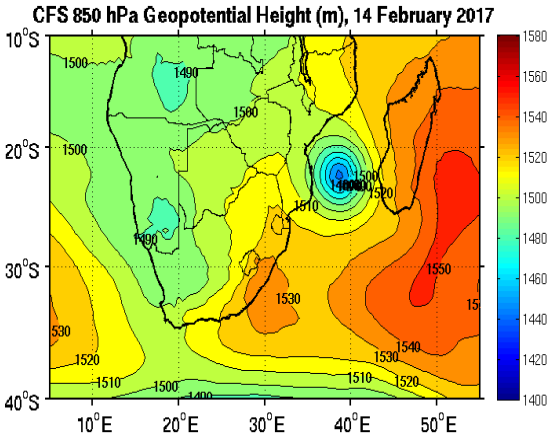

Figure 4-6: 850 hPa geopotential height (m) comparison between WRF simulation (left) and CFS Reanalyses from 12 to 17 February 2017 at 0000 UTC (Continued on next page).

(d)

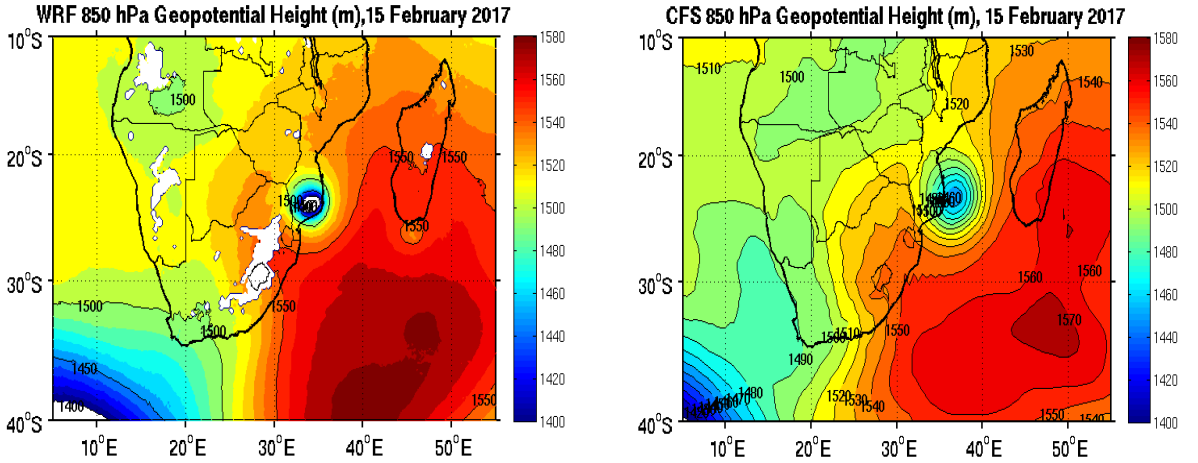

(e)

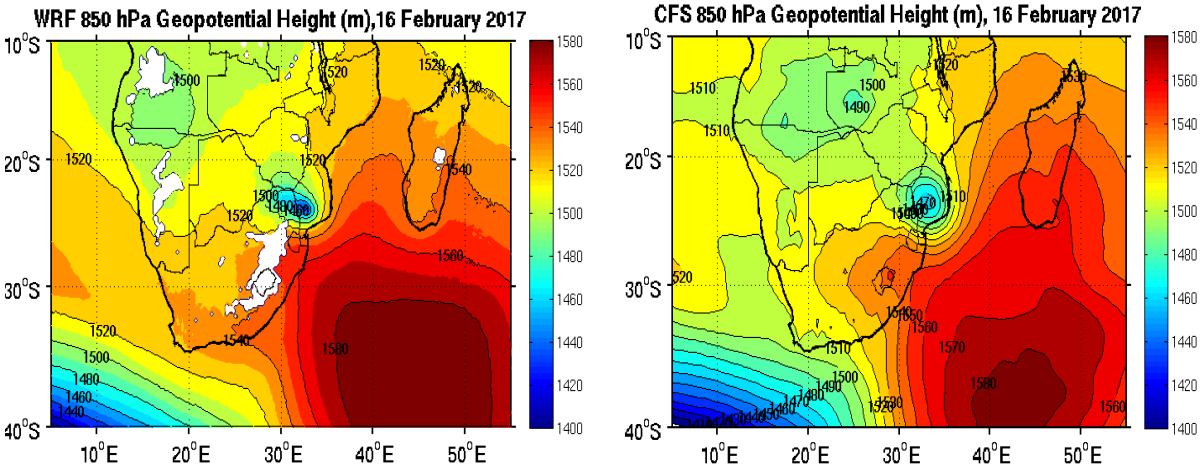

(f)

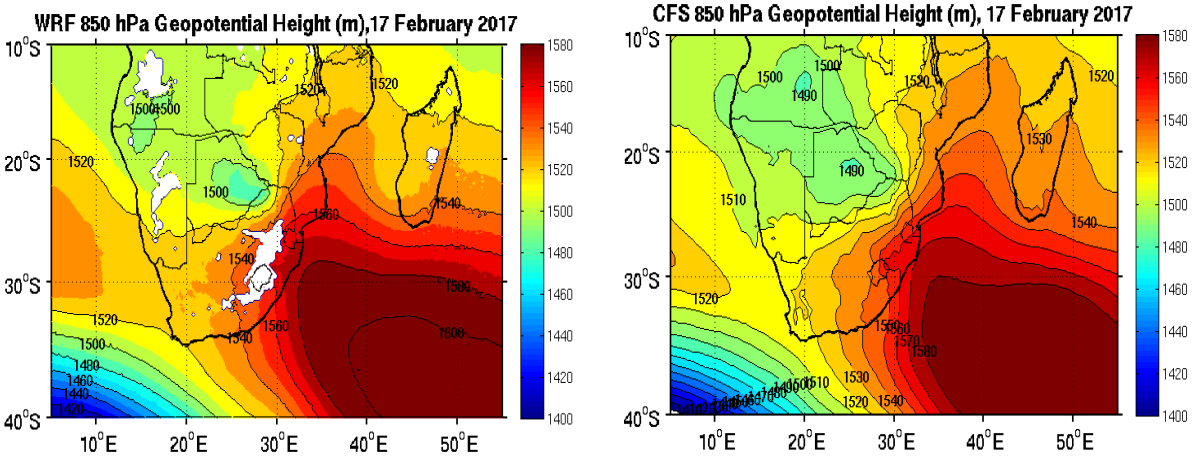

Figure 4-6: (Continued) 850 hPa geopotential height (m) comparison between WRF simulation (left) and CFS Reanalyses from 12 to 17 February 2017 at 0000 UTC.

(a)

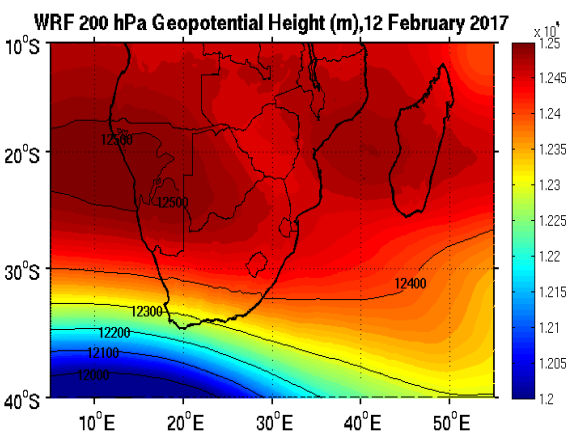

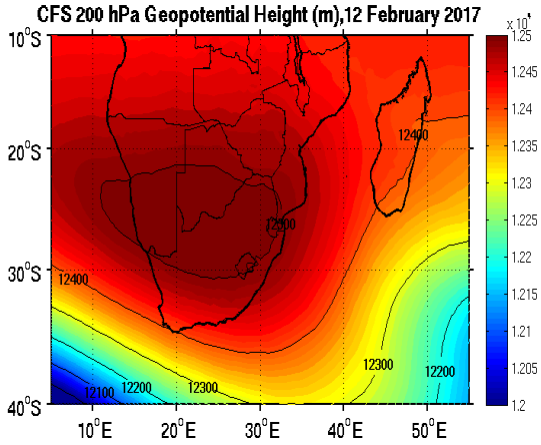

(b)

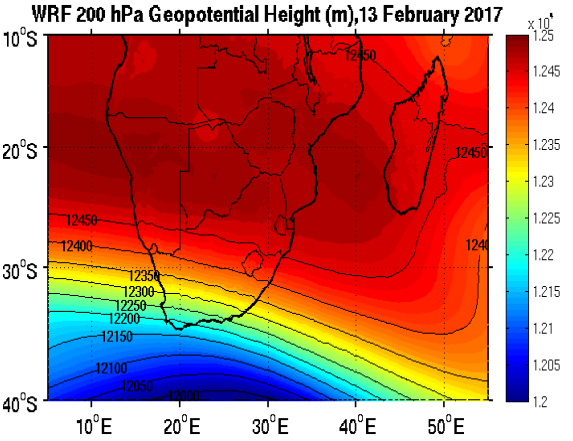

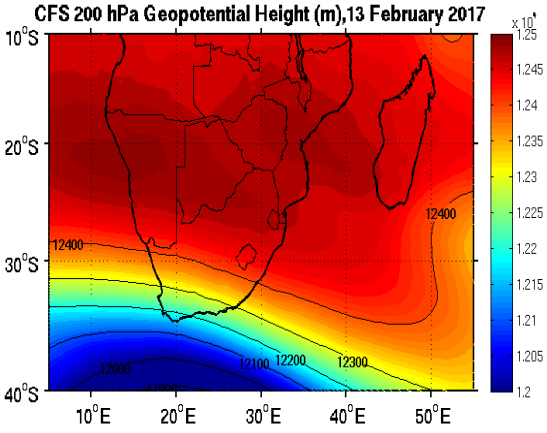

(c)

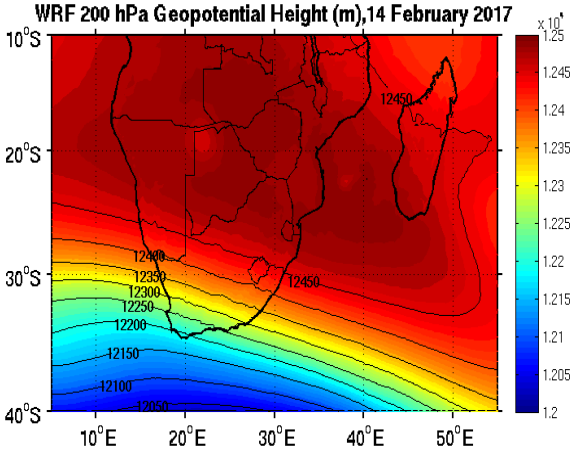

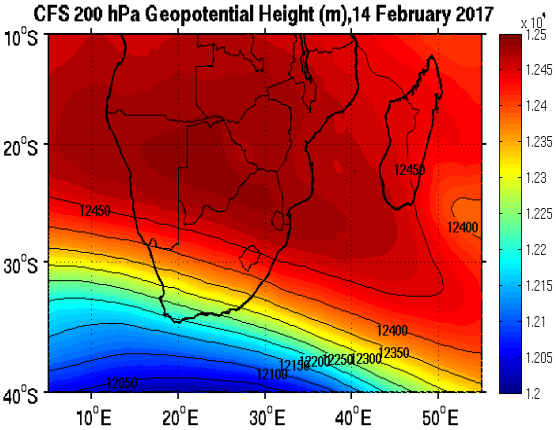

Figure 4-7: 200 hPa geopotential height (m) comparison between WRF simulation (left) and CFS Reanalyses from 12 to 17 February 2017 at 0000 UTC. (Continued on next page)

(d)

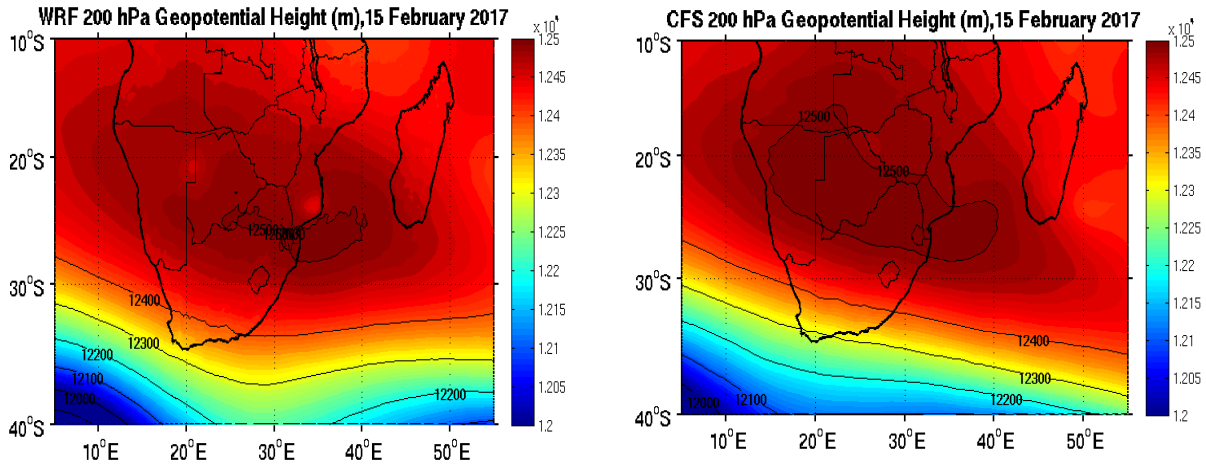

(e)

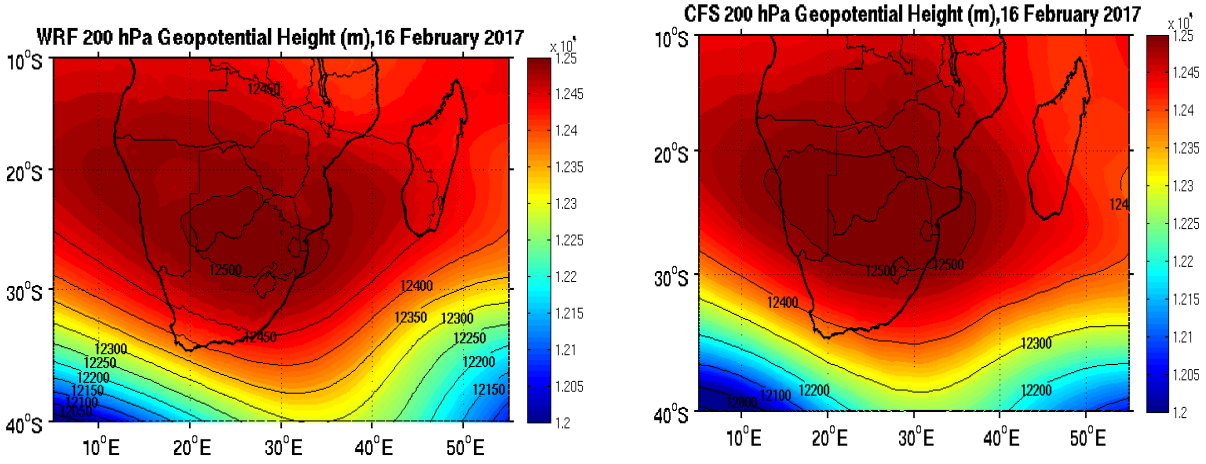

(f)

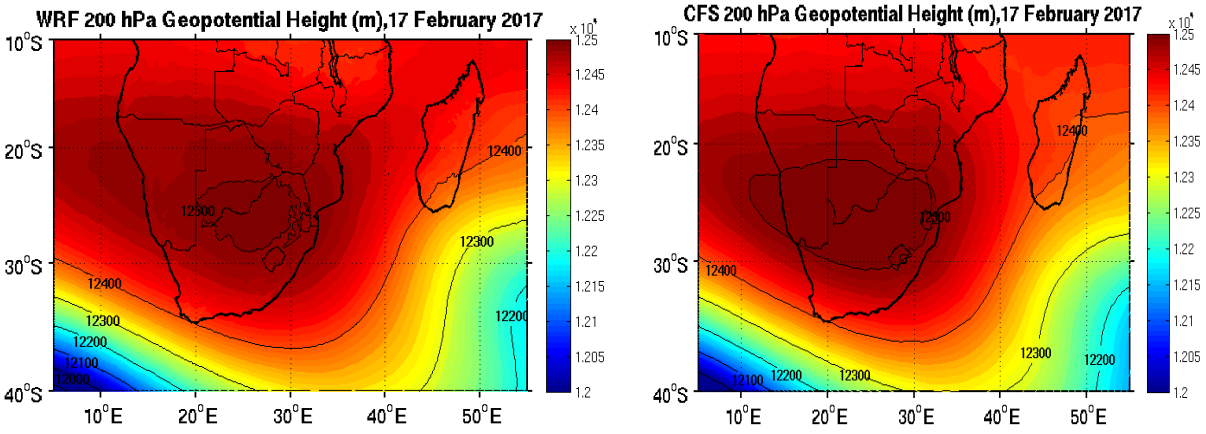

Figure 4-7: (Continued) 200 hPa geopotential height (m) comparison between WRF simulation (left) and CFS Reanalyses from 12 to 17 February at 0000 UTC.

(a)

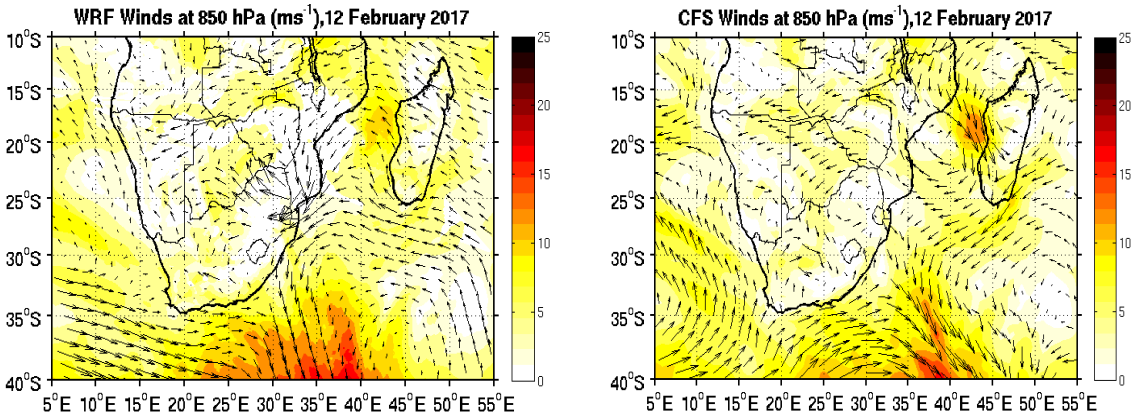

(b)

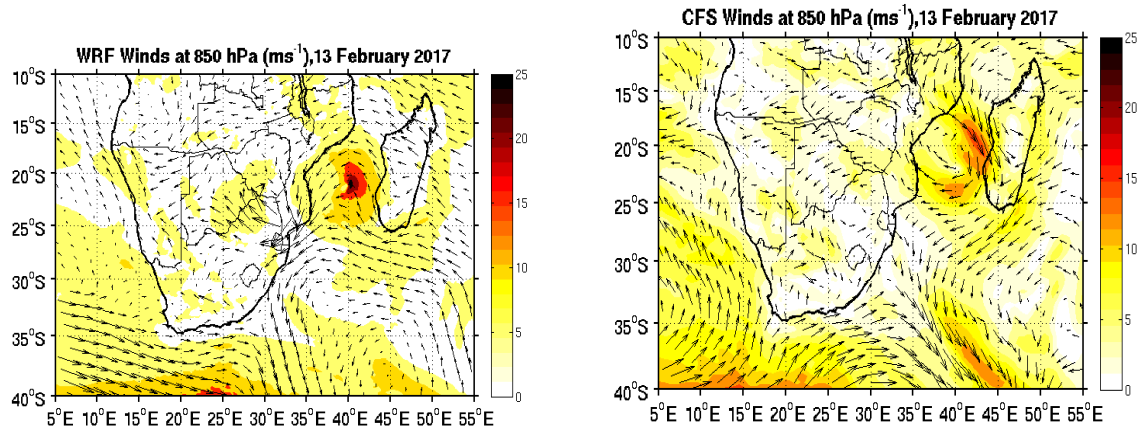

(c)

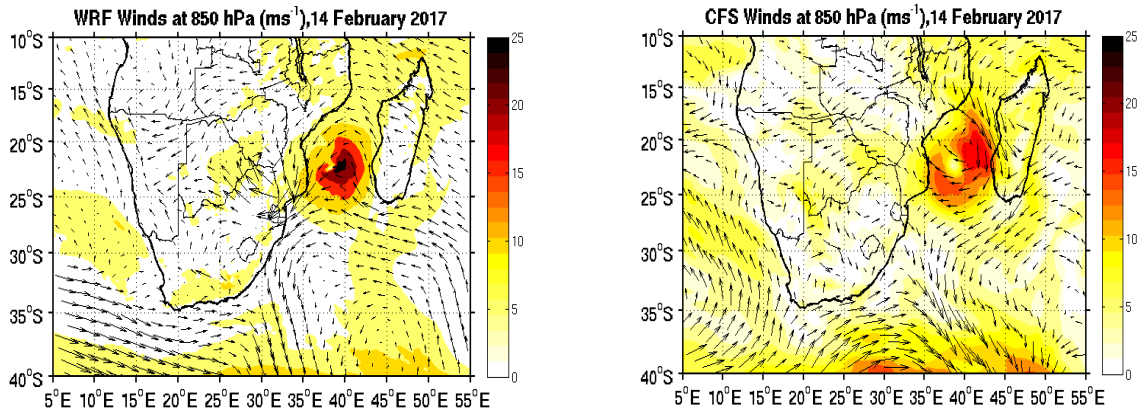

Figure 4-8: 850 hPa wind fields (ms^{-1}) comparison between WRF model simulation (left) and CFS Reanalyses (right) from 12 to 17 February 2017 at 0000 UTC. The arrows denote the wind direction and the shaded areas show wind magnitude. (Continued on next page)

(d)

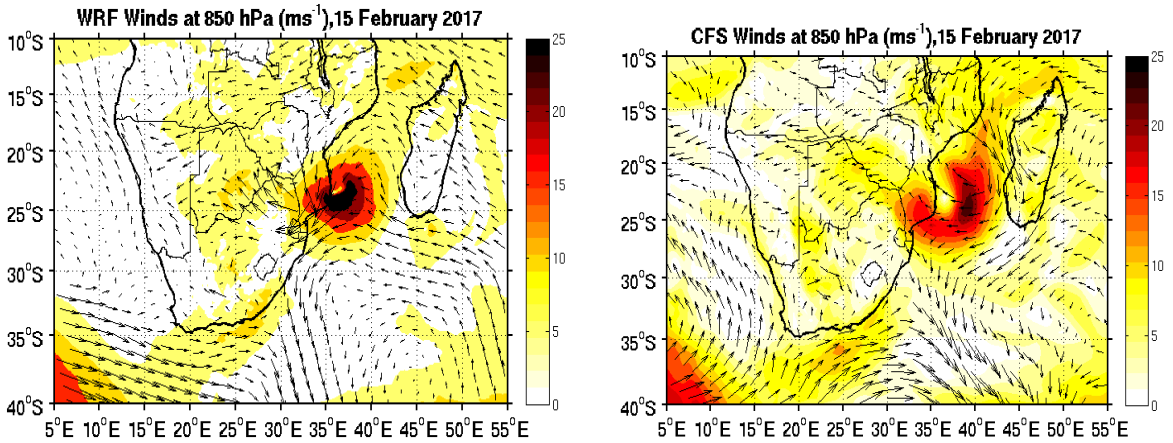

(e)

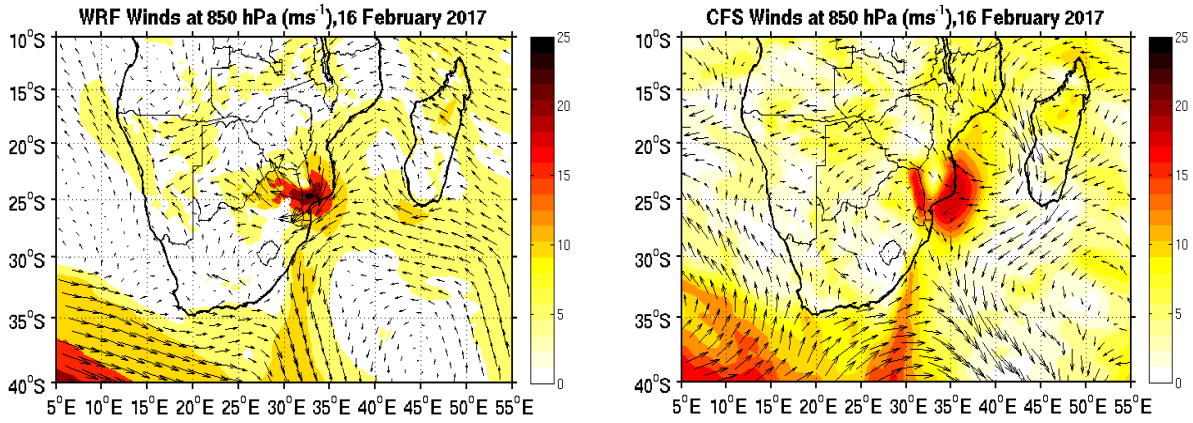

(f)

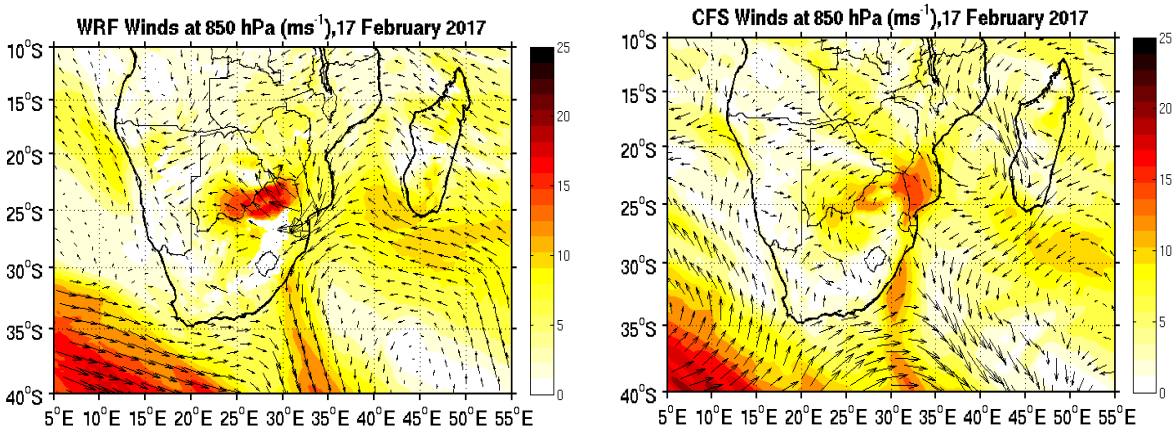

Figure 4-8: (Continued) 850 hPa wind fields (m s^{-1}) comparison between WRF model simulation (left) and CFS Reanalyses (right) from 12 to 17 February 2017 at 0000 UTC. The arrows denote the wind direction and the shaded areas show wind magnitude.

(a)

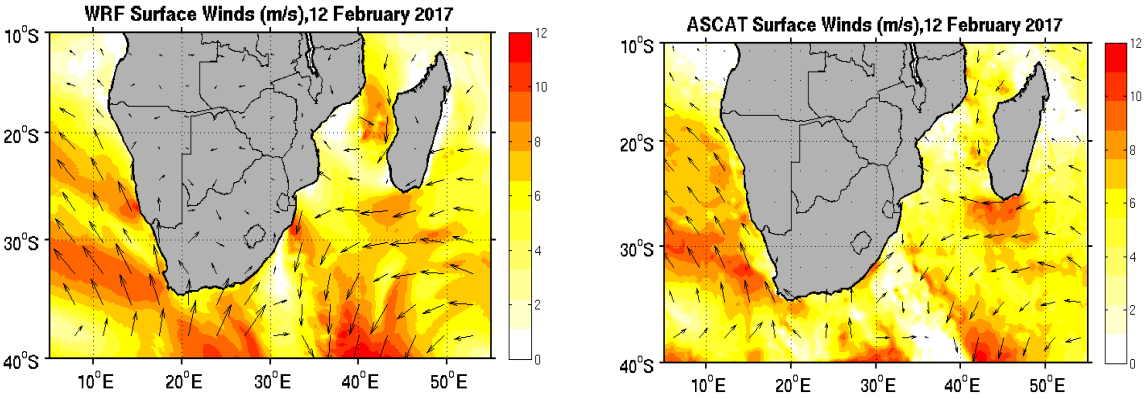

(b)

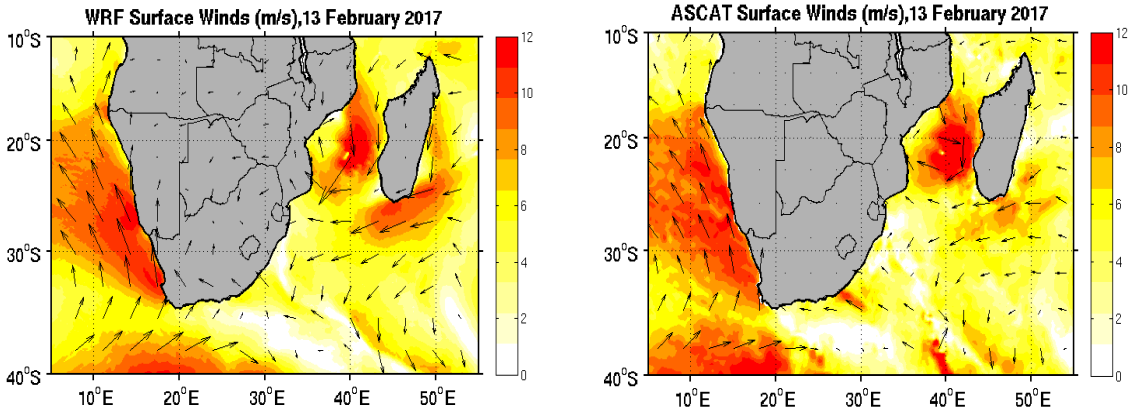

(c)

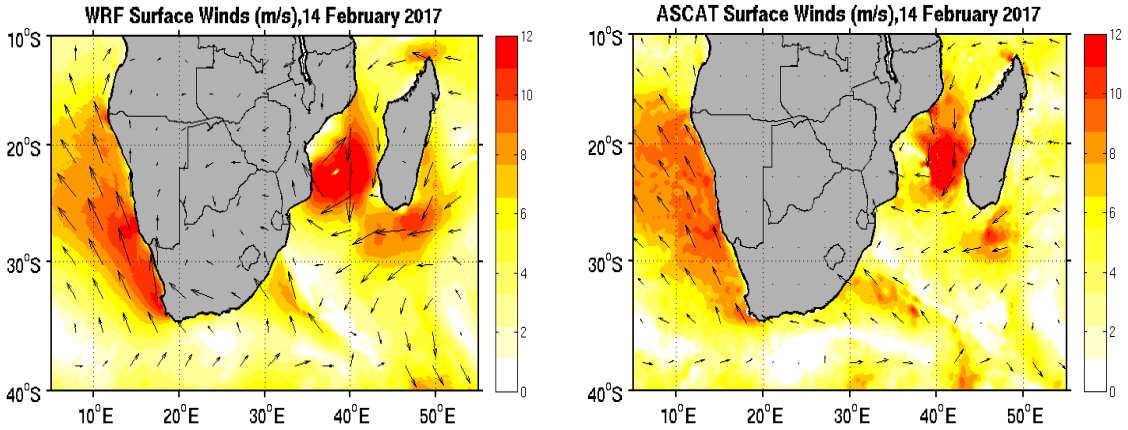

Figure 4-9: Showing daily surface wind fields (m s^{-1}) comparison between 10-m WRF winds (left) and ASCAT winds (right), from 12 to 17 February 2017 (Continued on next page).

(d)

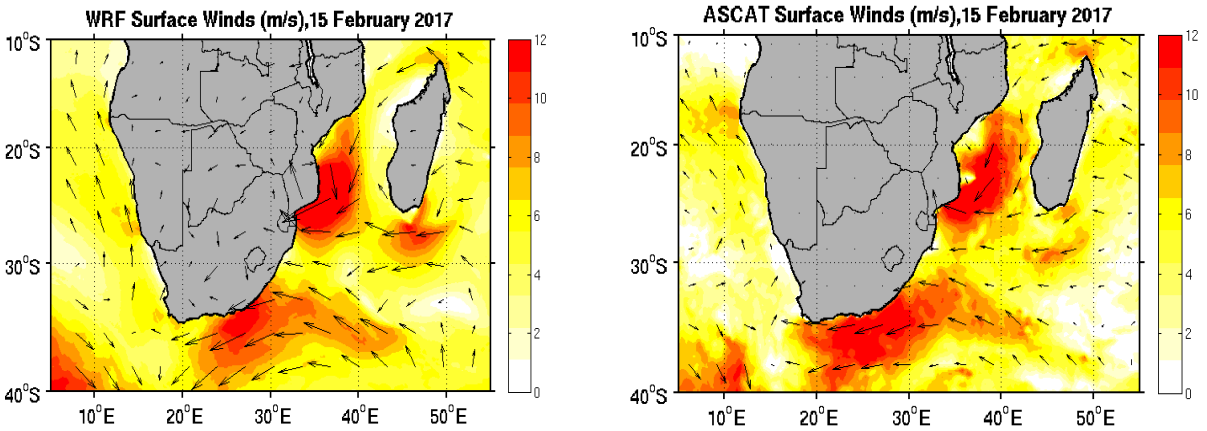

(e)

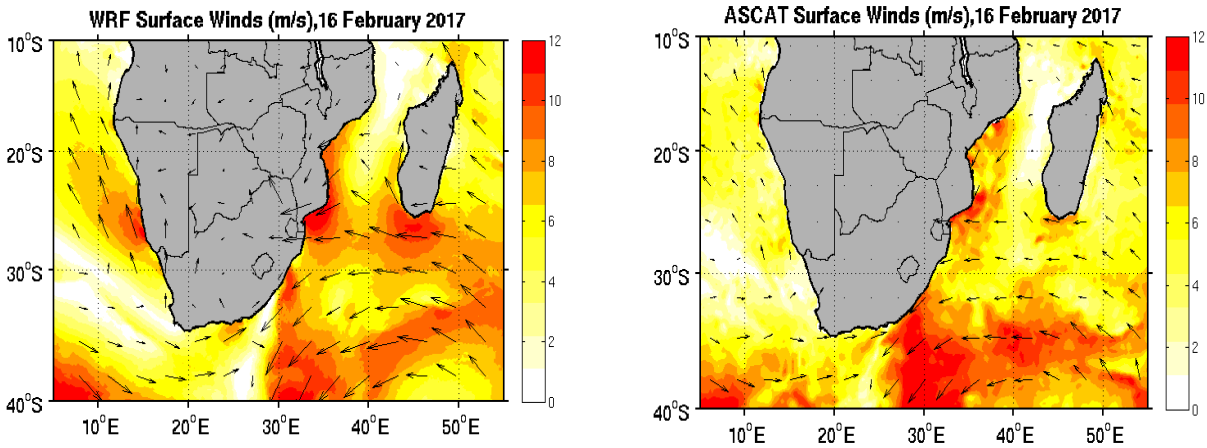

(f)

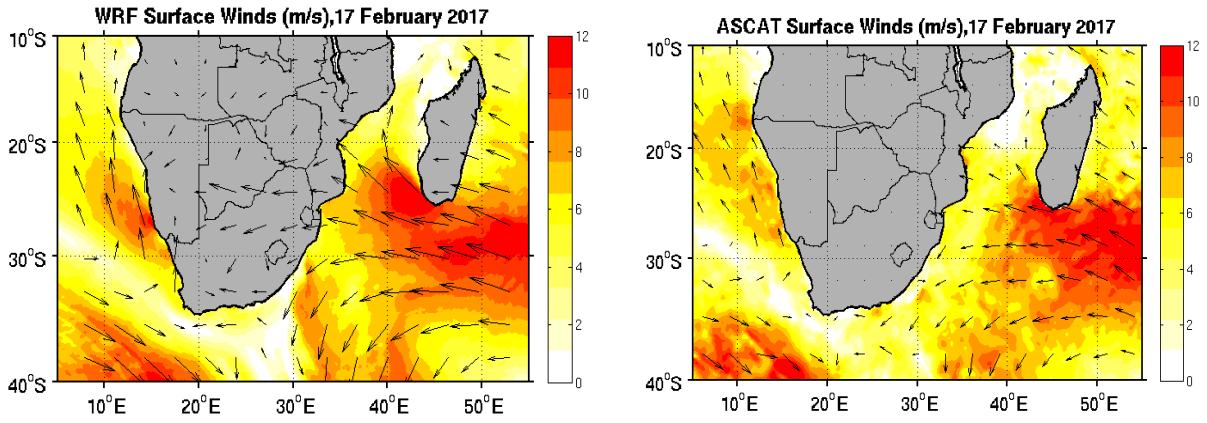

Figure 4-9: (Continued) Daily surface wind fields (m s^{-1}) comparison between 10-m WRF wind (left) and ASCAT wind (right) from 12 to 17 February 2017.

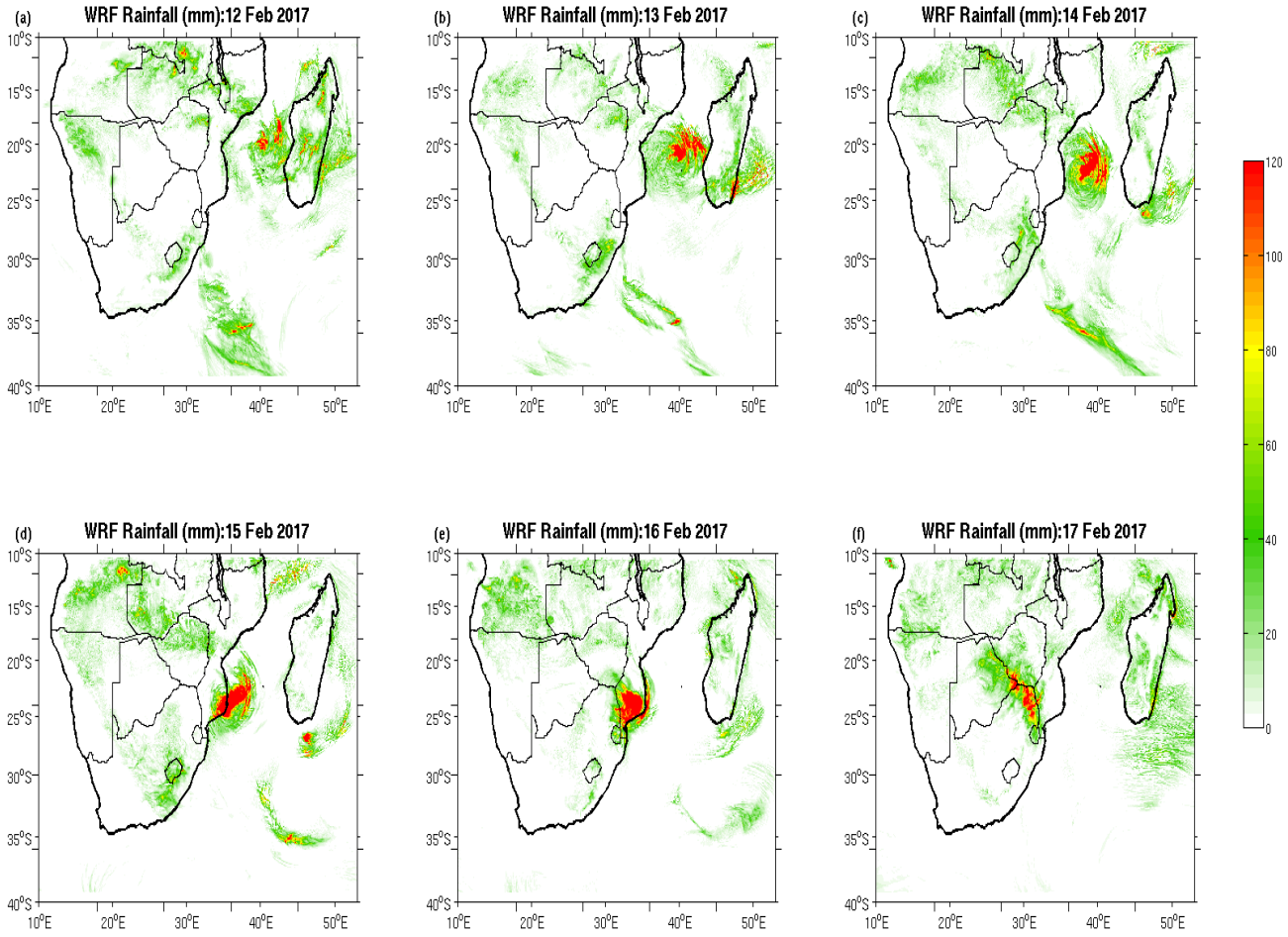

Figure 4-10: Showing WRF daily rainfall (mm) over southern Africa from 12 to 17 February 2017.

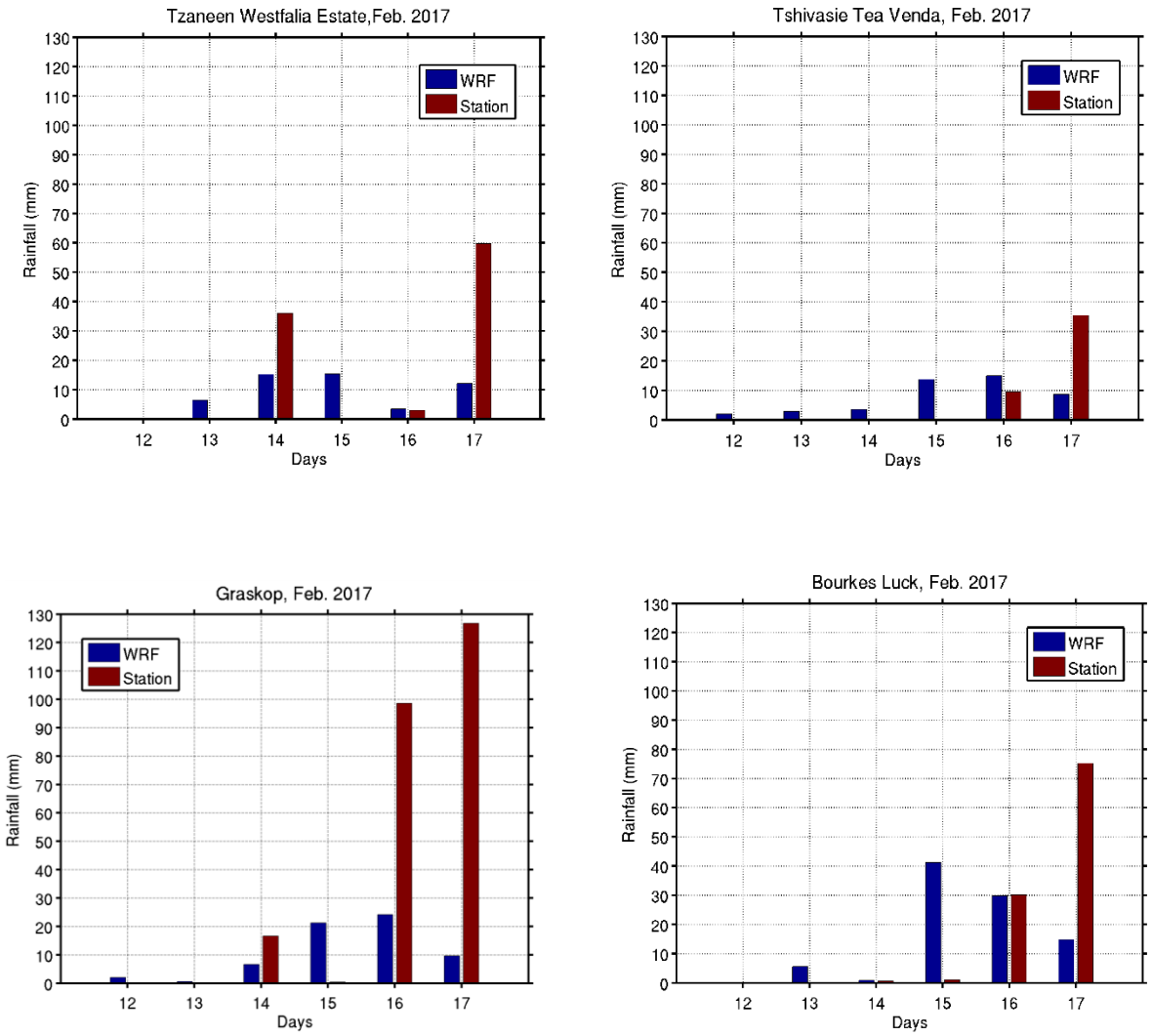

Figure 4-11: Showing daily WRF rainfall time series from 12-17 February 2017 compared with SAWS station rainfall.

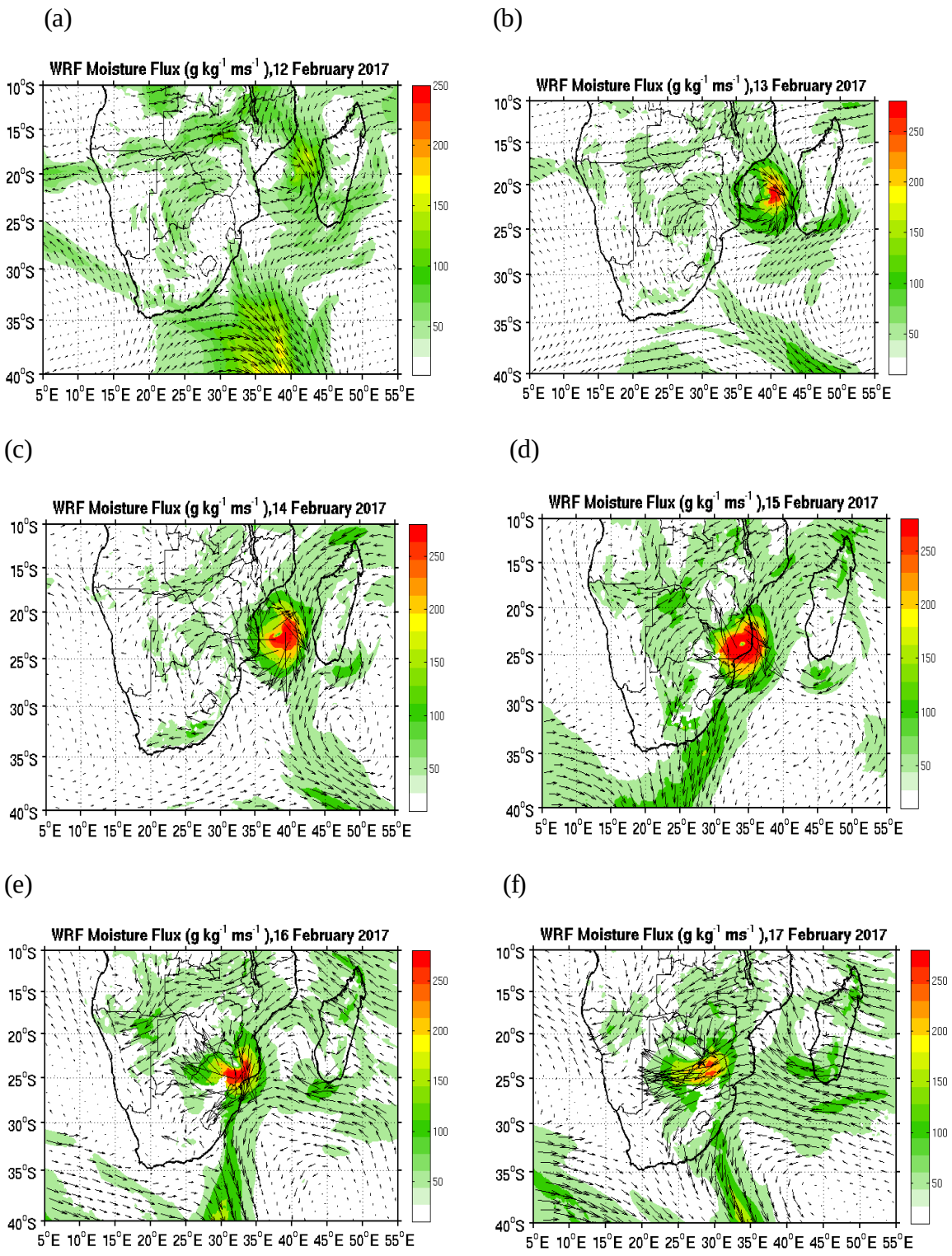

Figure 4-12: WRF model daily moisture flux (shaded, kg kg^{-1} ms^{-1}) at 850 hPa from 12 to 17 February 2017. The actual magnitude of the flux is given in the colour bar.

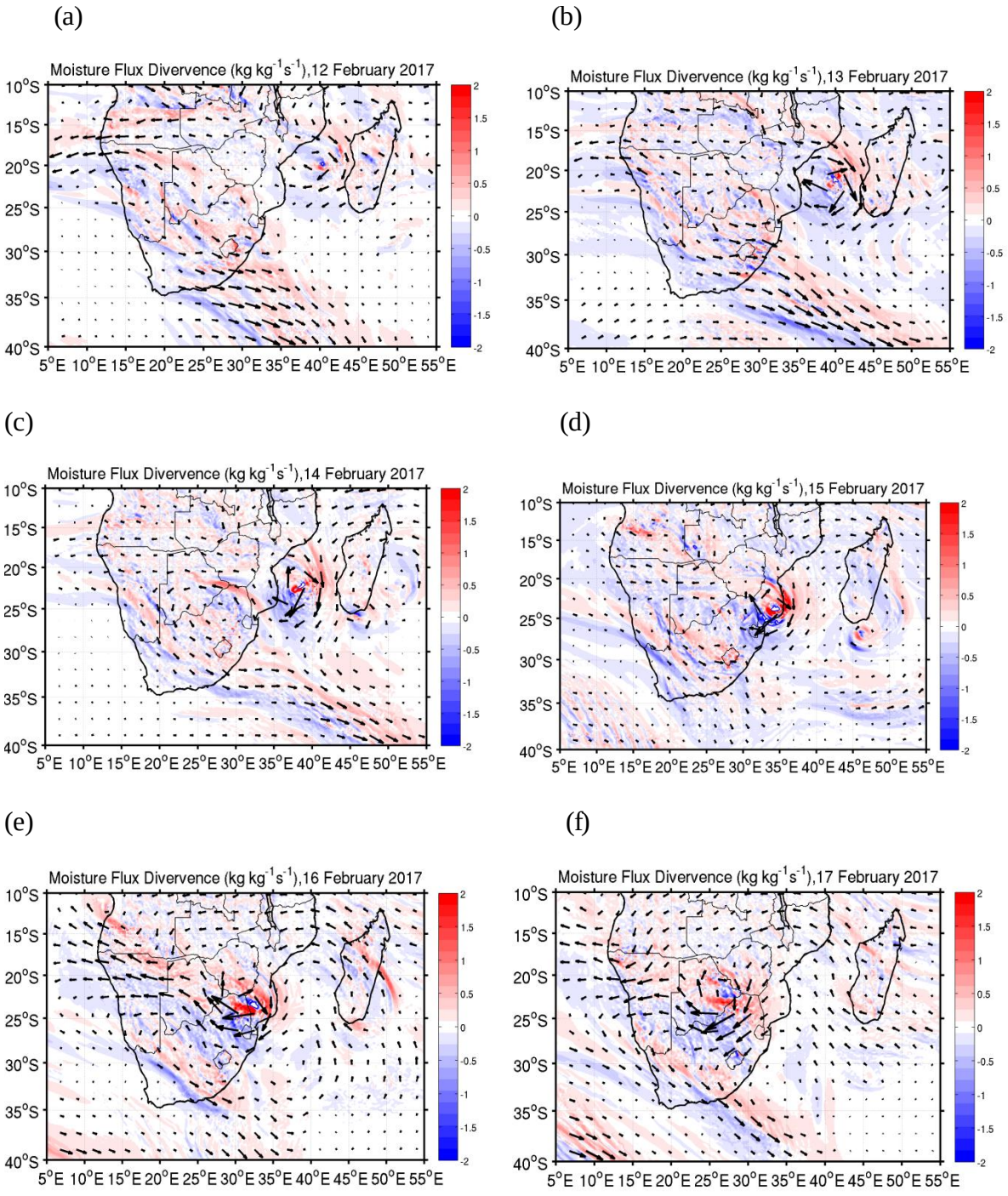

Figure 4-13: WRF model daily moisture flux divergence (shaded, kg kg^{-1} s^{-1}) at 700 hPa from 12 to 17 February 2017. Negative (positive) values imply convergence (divergence). The actual magnitude of the flux is given in the colour bar.

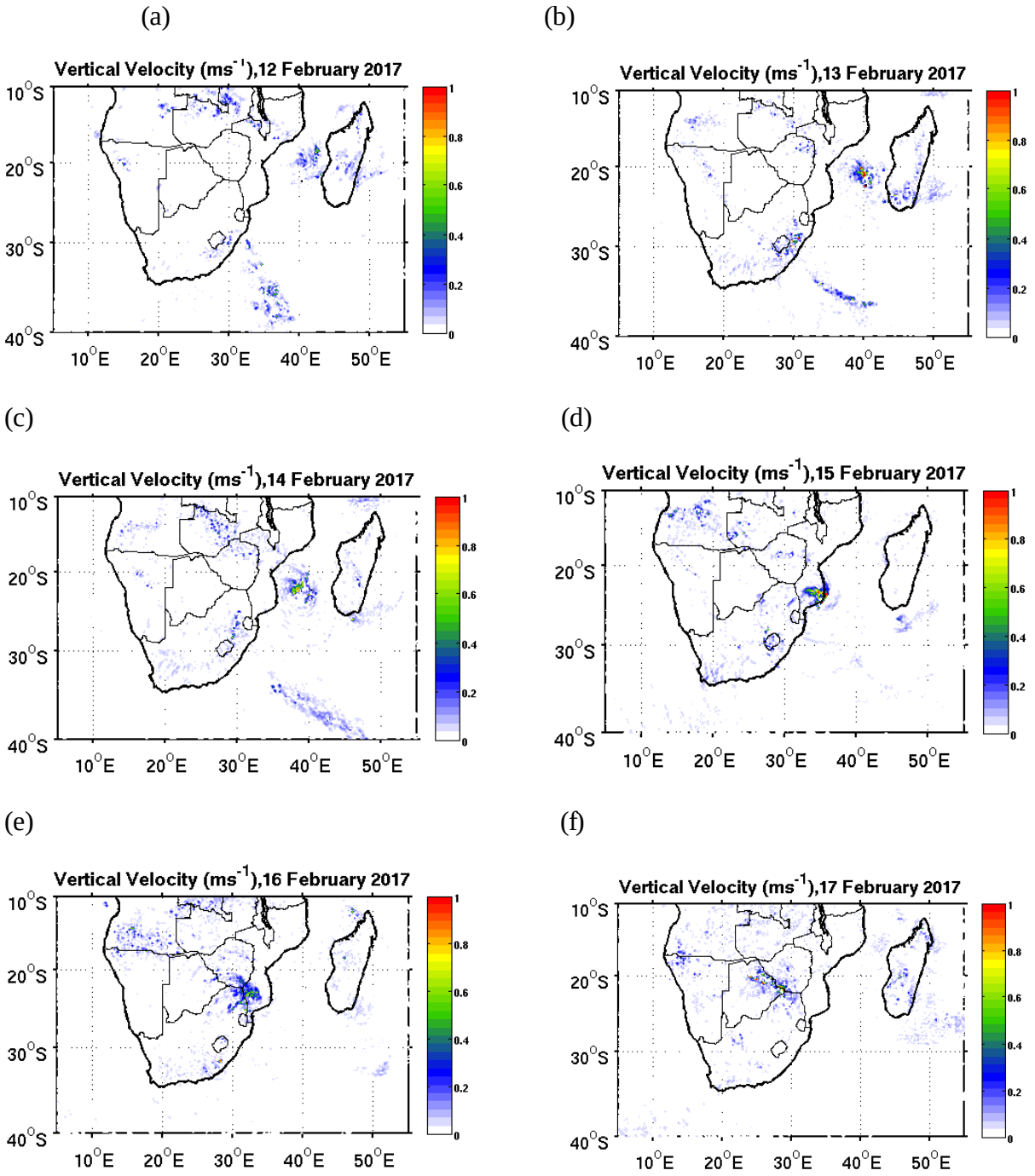

Figure 4-14: WRF model daily 500 hPa vertical wind velocity (ms^{-1}) from 12 to 17 February 2017. Only positive values (uplift) were plotted.

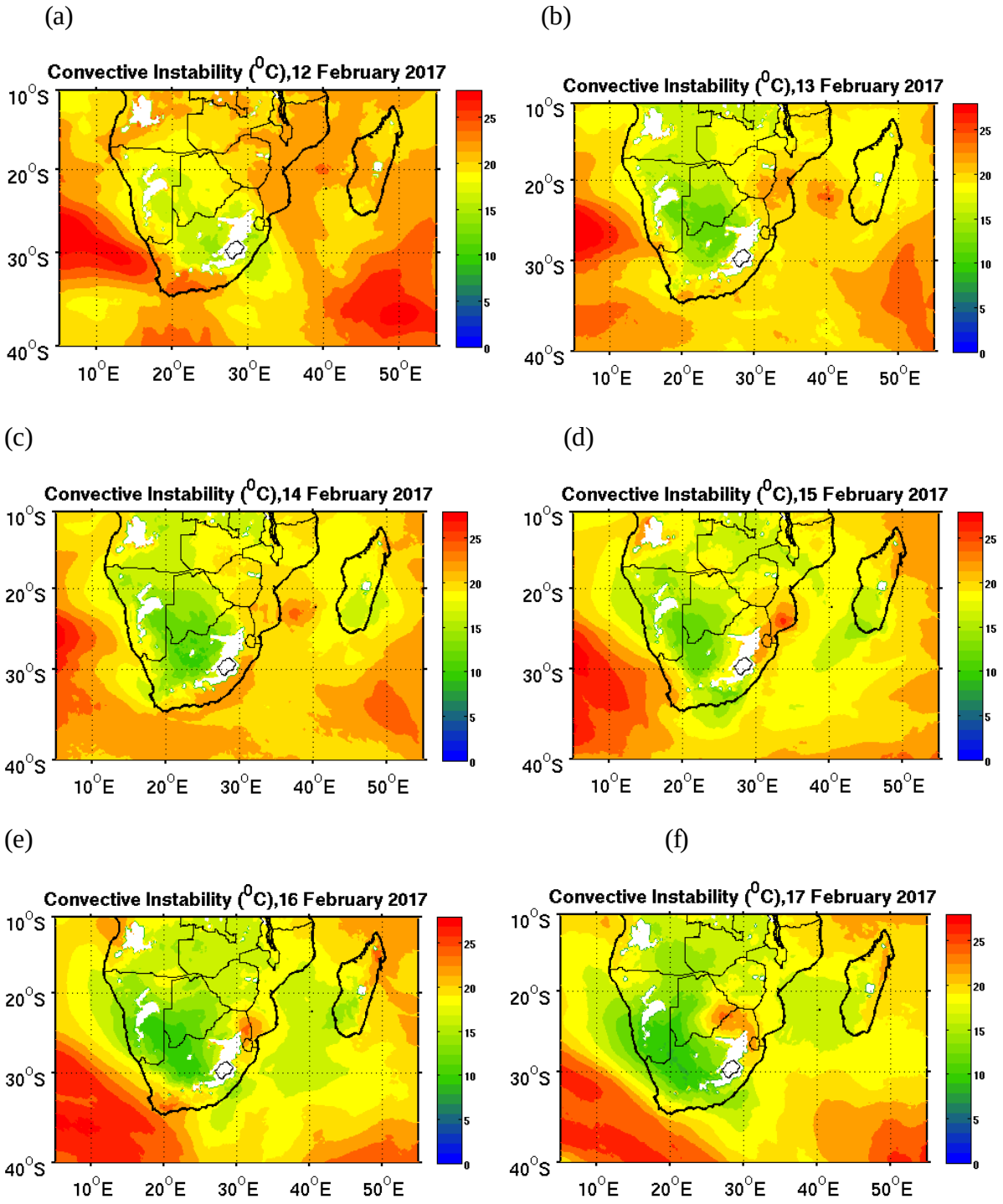

Figure 4-15: WRF model daily convective instability (°C) calculated between 850 hPa and 500 hPa pressure levels $(\theta_{850} - \theta_{500})$ from 12 to 17 February 2017.

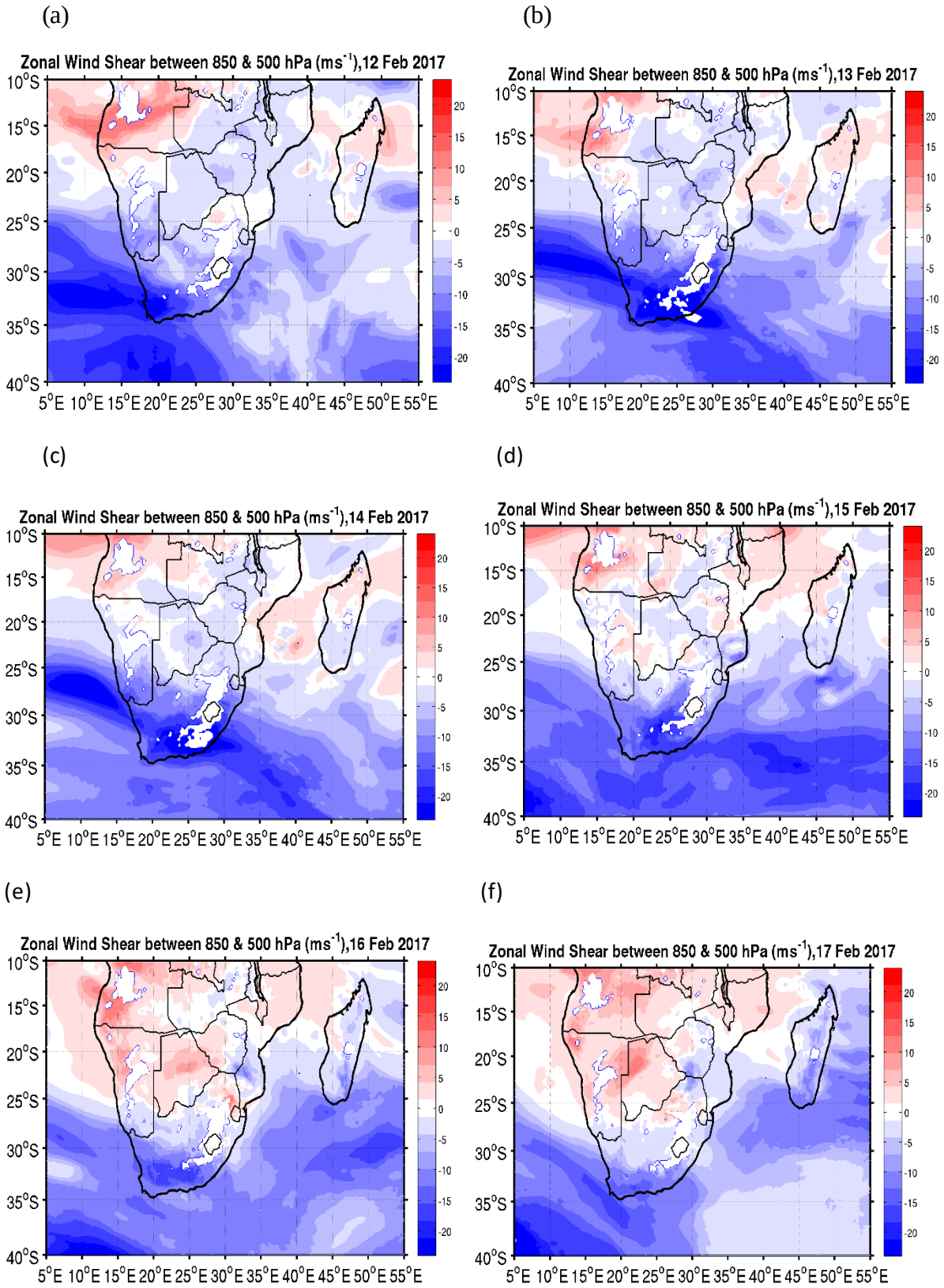

Figure 4-16: WRF daily zonal wind shear (m/s) calculated between 850 and 500 hPa from 12 to 17 February 2017. Positive (negative) values represent eastwards (westerly) flow.

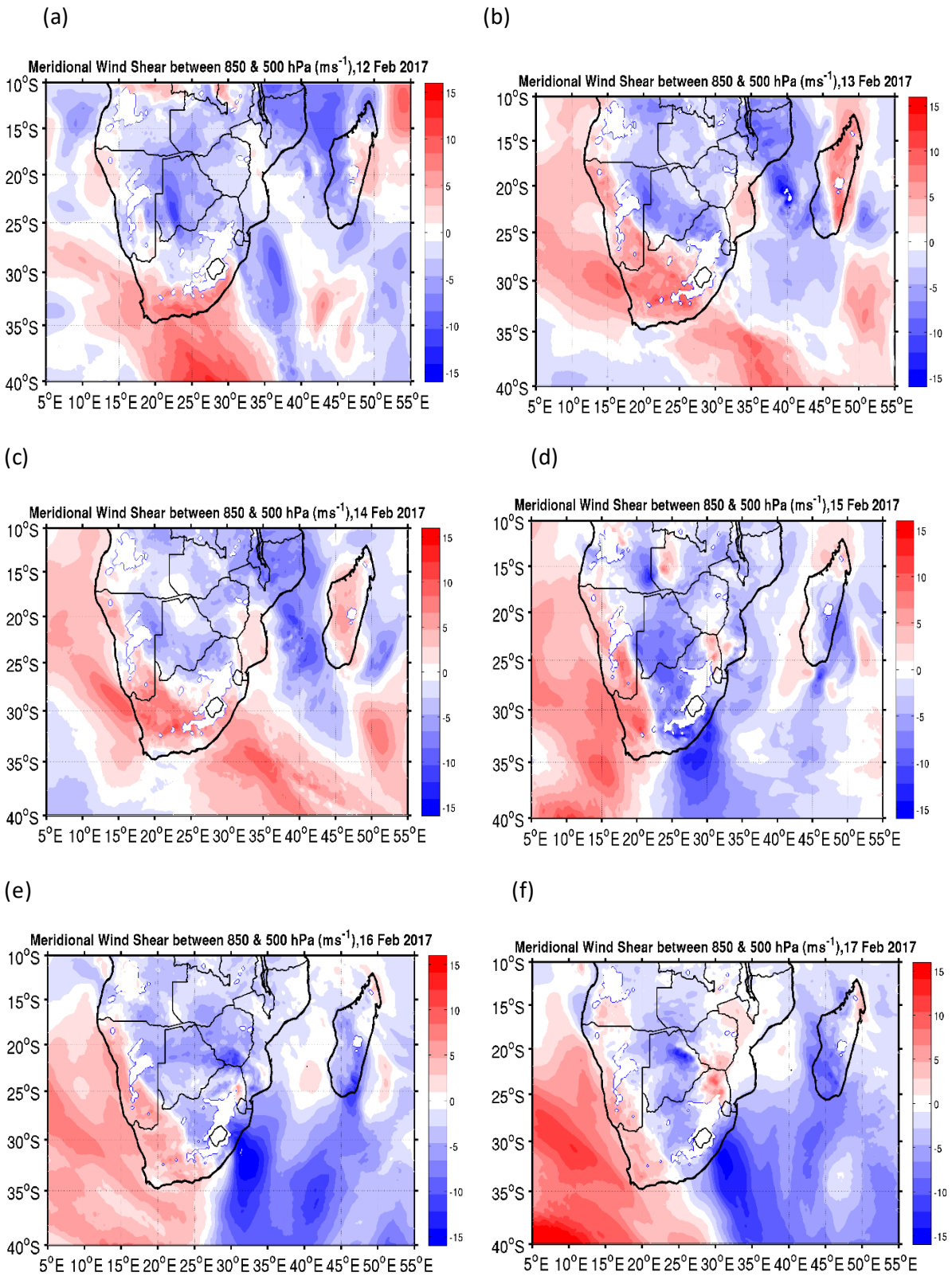

Figure 4-17: WRF daily meridional wind shear (m/s) calculated between 850 and 500 hPa from 12 to 17 February 2017. Positive (negative) values represent northerly (southerly) flow.

(a)

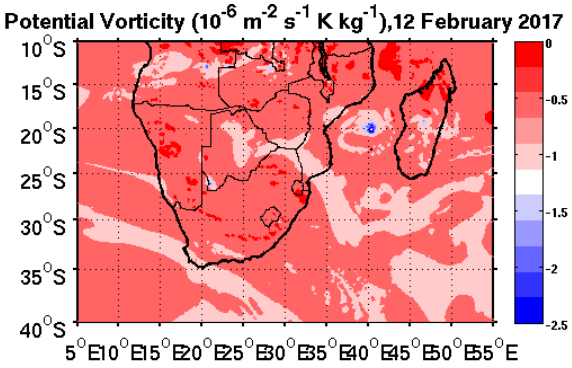

(b)

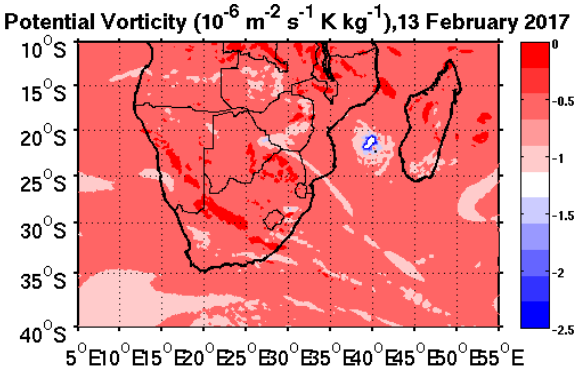

(c)

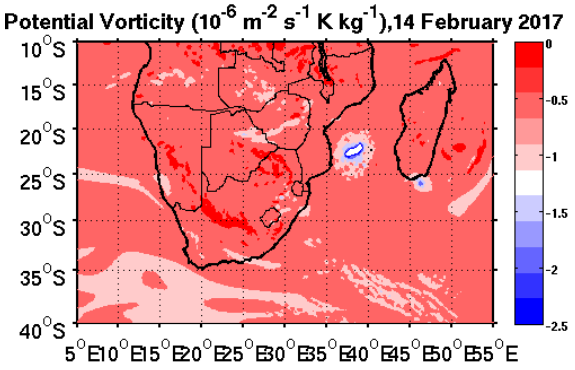

(d)

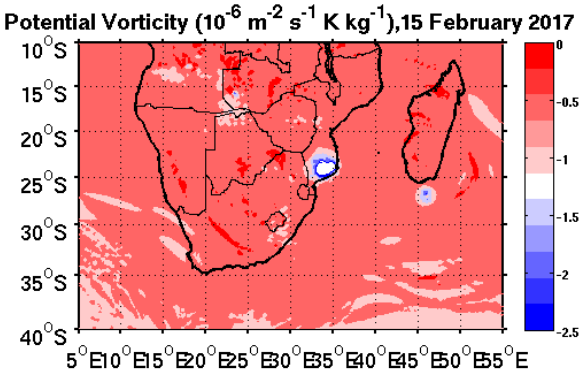

(e)

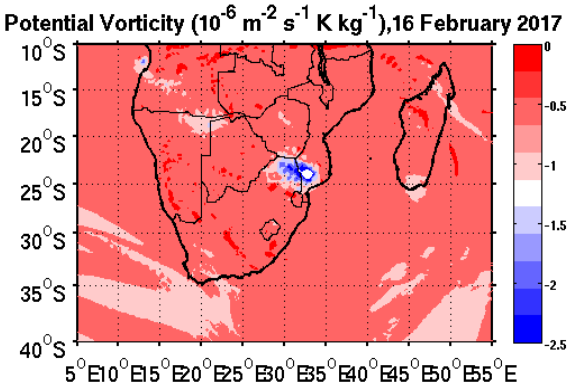

(f)

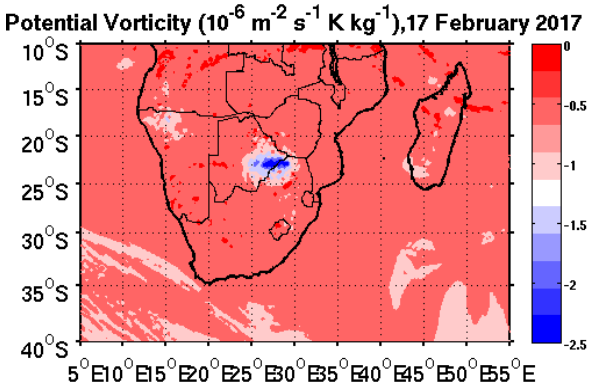

Figure 4-18: WRF model daily Potential Vorticity calculated at 700 hPa from 12 to 17 February 2017.

Chapter 5: Conclusions

The present study assessed Tropical Cyclone Dineo which developed over the Mozambique Channel on 12-17 February 2017. Outputs from the WRF model, CFSv2 Reanalyses, TRMM satellite derived rainfall, ASCAT satellite winds and rainfall station data were used for this purpose. The motivation to study TC Dineo was that it occurred during the 2016/17 SWIO tropical cyclone season which was below average in terms of TC frequency in that it produced only five storms of which three intensified into tropical cyclones. Secondly, it formed in the central Mozambique Channel and then tracked south-westwards to make landfall on the southern Mozambique coast. Most TCs that make landfall in Mozambique tend to do so somewhat further north. Furthermore, relatively few of the total South West Indian Ocean tropical cyclones actually form in the Mozambique Channel and those that do often track south and out of the Channel (e.g., TC Dera, described in Reason, 2007) or make landfall on western Madagascar. Finally, Dineo made important contributions to the total February summer rainfall in north-eastern South Africa (Mpumalanga and Limpopo).

The main objective of this study was to examine the WRF model output for the duration of the storm event, as well as to observe whether the WRF model fields could be used to better understand the mechanisms associated with the above average rainfall produced over north-eastern South Africa from 12-17 February 2017. A comparison of WRF circulation patterns, winds and rainfall with CFS Reanalyses, ASCAT satellite derived winds and TRMM rainfall provided confidence in the ability of WRF outputs to effectively study the storm evolution and the associated rainfall.

Dineo evolved during a below average SWIO tropical cyclone season. The presence of an anomalously strong anticyclonic circulation over the SWIO during this summer was consistent with the reduced TC activity over SWIO. However, this anticyclonic pattern was weaker in February than at other times during the summer making conditions more favourable for Dineo to be generated. The zonal winds at 500hPa were strongly negative between 0º and 30ºS, particularly in the central Mozambique Channel, northern Madagascar, as well as in the open ocean, which indicated westward movement of the storm and promoting subsequent landfall over southern Mozambique. Most TCs that make landfall in Mozambique tend to do so somewhat further north; however, the general meridional wind patterns were mainly southwards over Mozambique Channel during the storm period, which encouraged a more southward location of Dineo than might otherwise have been expected.

Regions of low-level moisture flux convergence, mid-level uplift and convective instability shown by the WRF model were favourable for the production of rainfall and occurrence of convective weather systems. The WRF moisture flux fields were generally consistent with the areas of rainfall, particularly, over Namibia, Botswana, Zimbabwe, Zambia, Mozambique and north-east South Africa. It could be noted that based on the recorded station rainfall for Mpumalanga and Limpopo, several stations recorded significant amounts of rainfall only after 17 February. Regions such as Mozambique and Zimbabwe mainly received substantial rainfall during the developmental stages of Dineo when moist marine air was advected into these regions and enhanced convective activity which led to rainfall. Other regions like Namibia, western Botswana, and northern South Africa received most of their rainfall from the convective activities that resulted from the tropical low over Botswana and the associated cloud band that were present prior to Dineo making landfall. Finally, the heavy rainfall received by north-east South Africa on 16-17 February was associated with ex-Tropical Cyclone Dineo

after it made landfall over southern Mozambique and shifted westward to Zimbabwe, eastern Botswana and north-east South Africa.

Overall, the WRF model simulated the general flow patterns during the storm period reasonably well. However, there were some discrepancies observed such as the minimum central pressure of the storm when WRF was compared with CFSv2 Reanalyses respectively. The WRF geopotential height at 850 hPa was consistent with CFSv2 Reanalyses pressure patterns; however, there were some obvious discrepancies, particularly in the position and intensity of TC Dineo from 15 to 17 February. Moreover, WRF model showed a very small low-pressure system south of Madagascar on 14-15 February, which was well represented in the 850 hPa geopotential height plot (**Fig. 4-6c**), WRF rainfall (**Fig. 4-9c**) as well as WRF moisture flux divergence (**Fig. 4-11c**). It could be suggested that the visibility of this low-pressure system may be due to the finer resolution of WRF model which was able to capture and resolve small scale features than CFSv2 Reanalyses.

Generally, WRF model winds at 10 m above the surface were consistent with the ASCAT satellite derived winds over the outer domain. However, the WRF model tended to show winds stronger than ASCAT in the regions where Dineo was located.

The WRF and TRMM broad-scale rainfall patterns were mostly consistent with each other. However, there were visible differences, whereby WRF showed larger amounts of rainfall than did TRMM in regions where the storm was located. In other regions WRF showed little to no rainfall, meanwhile, TRMM showed some rainfall. Comparisons with station data showed that

WRF generally tended to underestimate the large amounts received at certain stations like Graskop, Bourkes Luck, Tzaneen and Tshivhasie Tea Station. However, these stations are located in regions of very steep topography which will not be completely resolved by the 6km horizontal grid of WRF. Hence, such discrepancies are not unexpected.

As previously mentioned, there is a potential connection between the state of ENSO and tropical cyclone landfall over Mozambique with a noticeable tendency for strong TCs forming in SWIO to make landfall during La Niña years. However, based on the strength of Ocean Nino 3.4 index, JFM 2017 evolved from very weak La Niña conditions to neutral; hence, relatively few tropical cyclones in the SWIO during this period is not unexpected. The development of a relatively strong westward steering flow in the Mozambique Channel region in February then provided favourable conditions for the landfall of Dineo on the south central coast of Mozambique.

Bibliography

Allan RJ, Reason CJ, Carroll P, Jones PD. (2002). 'A reconstruction of Madras (Chennai) mean sea-level pressure using instrumental records from the late 18th and early 19th centuries. *Int J Climatology* **22**: 1119-1142.

Ash KD, Matyas CJ. (2012b). 'The influences of ENSO and the subtropical Indian Ocean Dipole on tropical cyclone trajectories in the southwestern Indian Ocean', *International Journal of Climatology* **32**: 41-56.

Avila LA, Pasch RJ. (1992). 'Atlantic tropical systems of 1991', *Monthly Weather Review* **120**: 2688-2696.

Behera SK, Yamagata T. (2001). 'Subtropical SST dipole events in the southern Indian Ocean'. *Geophysics Res Lett* **28**: 327-330.

Berry GJ, Thorncroft C. (2005). 'Case study of an intense African easterly wave'. *Mon Weather Rev* **133**: 752-766.

Blamey RC, Reason C. (2013). 'The role of mesoscale convective complexes in southern Africa summer rainfall', *J Clim* **26**: 1654-1668.

Blamey RC, Kolusu SR, Mahlalela P, Todd MC, Reason C. (2018). 'The role of regional circulation features in regulating El Niño climate impacts over southern Africa: A comparison of the 2015/2016 drought with previous events', *Int J Climatology* **38**: 4276-4295.

Blamey RC, Reason C. (2012). 'Mesoscale convective complexes over southern Africa', *J Clim* **25**: 753-766.

Burpee RW. (2003). Characteristics of African easterly waves. In Anonymous *A Half Century of Progress in Meteorology: A Tribute to Richard Reed*. Springer, p 91-108.

Cook, C., Reason, C. J.C., Hewitson, B. C. (2004). Wet and dry spell within particularly wet and dry summers in the South African summer rainfall region. Climate Research, 26, 17-31.

Cha D, Wang Y. (2013). 'A dynamical initialization scheme for real-time forecasts of tropical cyclones using the WRF model', *Mon Weather Rev* **141**: 964-986.

Driver P, Reason C. (2017). 'Variability in the Botswana High and its relationships with rainfall and temperature characteristics over southern Africa', *Int J Climatology* **37**: 570-581.

Driver, P., B. Abiodun, and C. Reason, 2019: Modelling the precipitation response over southern Africa to the 2009–2010 El Niño using a stretched grid global atmospheric model. Climate. Dynamics., 52, 3929-3949.

Dudhia J. (1989). 'Numerical study of convection observed during the winter monsoon experiment using a mesoscale two-dimensional model', *J Atmos Sci* **46**: 3077-3107.

Duvel J. (2015). 'Initiation and intensification of tropical depressions over the southern Indian Ocean: Influence of the MJO', *Mon Weather Rev* **143**: 2170-2191.

Dyson LL, Van Heerden J. (2001). 'The heavy rainfall and floods over the north-eastern interior of South Africa during February 2000', *S Afr J Sci* **97**: 80-86.

Ek MB, Mitchell KE, Lin Y, Rogers E, Grunmann P, Koren V, Gayno G, Tarpley JD. (2003). 'Implementation of Noah land surface model advances in the National Centers for Environmental Prediction operational mesoscale Eta model', *Journal of Geophysical Research: Atmospheres* **108**.

Emanuel K. (2001). 'Contribution of tropical cyclones to meridional heat transport by the oceans', *Journal of Geophysical Research: Atmospheres* **106**: 14771-14781.

Emanuel K, DesAutels C, Holloway C, Korty R. (2004). 'Environmental control of tropical cyclone intensity', *J Atmos Sci* **61**: 843-858.

Emanuel KA. (1986). 'An air-sea interaction theory for tropical cyclones. Part I: Steady-state maintenance', J *Atmos Sci* **43**: 585-605.

Engelbrecht F, Adegoke J, Bopape M, Naidoo M, Garland R, Thatcher M, McGregor J, Katzfey J, Werner M, Ichoku C. (2015). 'Projections of rapidly rising surface temperatures over Africa under low mitigation', *Environmental Research Letters* **10**: 085004.

Fauchereau N, Trzaska S, Rouault M, Richard Y. (2003). 'Rainfall variability and changes in southern Africa during the 20th century in the global warming context', *Nat Hazards* **29**: 139-154.

Fauchereau N, Pohl B, Reason C, Rouault M, Richard Y. (2009). 'Recurrent daily OLR patterns in the Southern Africa/Southwest Indian Ocean region, implications for South African rainfall and teleconnections', *Clim Dyn* **32**: 575-591.

Ferreira RN, Schubert WH. (1999). 'The role of tropical cyclones in the formation of tropical upper-tropospheric troughs', *J Atmos Sci* **56**: 2891-2907.

Fierro, A. O., R. F. Rogers, F. D. Marks, and D. S. Nolan, (2009): The impact of horizontal grid spacing on the microphysical and kinematic structures of strong tropical cyclones simulated with the WRF-ARW model. Mon.Weather Rev., 137, 3717-3743.

Figa-Saldaña J, Wilson JJ, Attema E, Gelsthorpe R, Drinkwater MR, Stoffelen A. (2002). 'The advanced scatterometer (ASCAT) on the meteorological operational (MetOp) platform: A follow on for European wind scatterometers', *Canadian Journal of Remote Sensing* **28**: 404-412.

Fink AH, Speth P. (1998). Tropical cyclones. *Naturwissenschaften* **85**: 482-493.

Fitchett JM, Grab SW. (2014). 'A 66-year tropical cyclone record for south-east Africa: temporal trends in a global context', Int *J Climatol* **34**: 3604-3615.

Gimeno L, Dominguez F, Nieto R, Trigo R, Drumond A, Reason CJ, Taschetto AS, Ramos AM, Kumar R, Marengo J. (2016). 'Major mechanisms of atmospheric moisture transport and their role in extreme precipitation events', Annual *Review of Environment and Resources* **41**: 117-141.

Goni GJ, Knaff J, Lin II. (2007). 'Tropical cyclone heat potential', *State of the Climate in:* 43-45. .

Graham NE, Barnett TP. (1987). 'Sea surface temperature, surface wind divergence, and convection over tropical oceans', *Science* **238**: 657-659.

Gray WM. (1998). 'The formation of tropical cyclones. *Meteorology and atmospheric physics* **67**: 37-69.

Gray WM, Brody LR. (1967). *Global view of the origin of tropical disturbances and storms,* Citeseer.

Hansingo K, Reason C. (2009). 'Modelling the atmospheric response over southern Africa to SST forcing in the southeast tropical Atlantic and southwest subtropical Indian Oceans', *International Journal of Climatology: A Journal of the Royal Meteorological Society* **29**: 1001-1012.

Harrison M. (1984). 'The annual rainfall cycle over the central interior of South Africa', *South African Geographical Journal* **66**: 47-64.

Harrison M. (1984). 'A generalized classification of South African summer rain-bearing synoptic systems', *Journal of Climatology* **4**: 547-560.

Hart N, Reason C, Fauchereau N. (2010). 'Tropical–extratropical interactions over southern Africa: Three cases of heavy summer season rainfall', *Mon Weather Rev* **138**: 2608-2623.

Hart NC, Reason CJ, Fauchereau N. (2013). 'Cloud bands over southern Africa: seasonality, contribution to rainfall variability and modulation by the MJO'. *Clim Dyn* **41**: 1199-1212.

Hendricks EA, Peng MS, Fu B, Li T. (2010). 'Quantifying environmental control on tropical cyclone intensity change', *Mon Weather Rev* **138**: 3243-3271.

Hermes JC, Reason C. (2005). 'Ocean model diagnosis of interannual coevolving SST variability in the South Indian and South Atlantic Oceans', *J Clim* **18**: 2864-2882.

Hirst AC, Hastenrath S. (1983). 'Atmosphere-ocean mechanisms of climate anomalies in the Angola-tropical Atlantic sector', *J Phys Oceanogr* **13**: 1146-1157.

Hong S, Dudhia J, Chen S. (2004). 'A revised approach to ice microphysical processes for the bulk parameterization of clouds and precipitation', *Mon Weather Rev* **132**: 103-120. .

Hopsch SB, Thorncroft CD, Tyle KR. (2010). 'Analysis of African easterly wave structures and their role in influencing tropical cyclogenesis', *Mon Weather Rev* **138**: 1399-1419.

Huffman GJ, Adler RF, Bolvin DT, Nelkin EJ. (2010). The TRMM multi-satellite precipitation analysis (TMPA). In Anonymous *Satellite rainfall applications for surface hydrology*. Springer, p 3-22.

Islam T, Srivastava PK, Rico-Ramirez MA, Dai Q, Gupta M, Singh SK. (2015). 'Tracking a tropical cyclone through WRF–ARW simulation and sensitivity of model physics', *Nat Hazards* **76**: 1473-1495.

Jakob Themeßl M, Gobiet A, Leuprecht A. (2011). 'Empirical-statistical downscaling and error correction of daily precipitation from regional climate models', *Int J Climatol* **31**: 1530-1544.

Kain JS. (2004). 'The Kain–Fritsch convective parameterization: an update', *J Appl Meteorol* **43**: 170-181.

Kim D, Jin C, Ho C, Kim J, Kim J. (2015). 'Climatological features of WRF-simulated tropical cyclones over the western North Pacific', *Clim Dyn* **44**: 3223-3235.

Klinman MG, Reason C. (2008). 'On the peculiar storm track of TC Favio during the 2006–2007 Southwest Indian Ocean tropical cyclone season and relationships to ENSO', *Meteorology and Atmospheric Physics* **100**: 233-242.

Kripalani RH, Kumar P. (2004). 'Northeast monsoon rainfall variability over south peninsular India vis-à-vis the Indian Ocean dipole mode', *Int J Climatology* **24**: 1267-1282.

Kruger AC. (1999). 'The influence of the decadal-scale variability of summer rainfall on the impact of El Niño and La Niña events in South Africa', *International Journal of Climatology: A Journal of the Royal Meteorological Society* **19**: 59-68.

Kuleshov Y, Qi L, Fawcett R, Jones D. (2008). 'On tropical cyclone activity in the Southern Hemisphere: Trends and the ENSO connection', *Geophysics Res Lett* **35**.

Kumar A, Dudhia J, Rotunno R, Niyogi D, Mohanty UC. (2008). 'Analysis of the 26 July 2005 heavy rain event over Mumbai, India using the Weather Research and Forecasting (WRF) model', *Q J R Meteorol Soc* **134**: 1897-1910.

Landman WA, Mason SJ. (1999). 'Change in the association between Indian Ocean sea-surface temperatures and summer rainfall over South Africa and Namibia', *International Journal of Climatology: A Journal of the Royal Meteorological Society* **19**: 1477-1492.

Landsea CW. (2000). 'Climate variability of tropical cyclones: past, present and future', *Storms.Routledge, New York*: 220-241.

Lindesay JA. (1988). 'South African rainfall, the Southern Oscillation and a Southern Hemisphere semi-annual cycle', *Journal of Climatology* **8**: 17-30.

Liu Z, Ostrenga D, Teng W, Kempler S. (2012). 'Tropical Rainfall Measuring Mission (TRMM) precipitation data and services for research and applications', *Bull Am Meteorol Soc* **93**: 1317-1325.

Malan N, Reason C, Loveday BR. (2013). 'Variability in tropical cyclone heat potential over the Southwest Indian Ocean', *Journal of Geophysical Research: Oceans* **118**: 6734-6746.

Malherbe J, Landman WA, Engelbrecht FA. (2014). 'The bi-decadal rainfall cycle, Southern Annular Mode and tropical cyclones over the Limpopo River Basin, southern Africa', *Clim Dyn* **42**: 3121-3138.

Malilay J. (1997). 'Tropical Cyclones'. *The public health consequences of disasters* **207**: 227.

Manhique AJ, Reason C, Rydberg L, Fauchereau N. (2011). 'ENSO and Indian Ocean sea surface temperatures and their relationships with tropical temperate troughs over Mozambique and the Southwest Indian Ocean', *Int J Climatol* **31**: 1-13.

Manhique AJ, Reason C, Silinto B, Zucula J, Raiva I, Congolo F, Mavume AF. (2015). 'Extreme rainfall and floods in southern Africa in January 2013 and associated circulation patterns', *Nat Hazards* **77**: 679-691.

Mason SJ, Jury MR. (1997). 'Climatic variability and change over southern Africa: a reflection on underlying processes', *Prog Phys Geogr* **21**: 23-50.

Matyas CJ. (2015). 'Tropical cyclone formation and motion in the Mozambique Channel', *Int J Climatol* **35**: 375-390.

Mavume AF, Rydberg L, Rouault M, Lutjeharms JR. (2009). 'Climatology and landfall of tropical cyclones in the south-west Indian Ocean', *Western Indian Ocean Journal of Marine Science* **8**.

Mawren D, Reason C. (2017). 'Variability of upper-ocean characteristics and tropical cyclones in the South West Indian Ocean', *Journal of Geophysical Research: Oceans* **122**: 2012-2028.

Montgomery MT, Farrell BF. (1993). 'Tropical cyclone formation', *J Atmos Sci* **50**: 285-310.

Moore AM, Loschnigg JP, Webster PJ, Leben RR. (1999). 'Coupled ocean-atmosphere dynamics in the Indian Ocean during 1997-98', *Nature* **401**: 356-360. 10.1038/43848.

Munday C, Washington R. (2017). 'Circulation controls on southern African precipitation in coupled models: The role of the Angola low'. *Journal of Geophysical Research: Atmospheres* **122**: 861-877.

Nguyen LT, Molinari J, Thomas D. (2014). 'Evaluation of tropical cyclone center identification methods in numerical models', *Mon Weather Rev* **142**: 4326-4339.

Pasquero C, Emanuel K. (2008). 'Tropical cyclones and transient upper-ocean warming', *J Clim* **21**: 149-162.

Pattanayak S, Mohanty UC. (2008). 'A comparative study on performance of MM5 and WRF models in simulation of tropical cyclones over Indian seas',*Current Science (00113891)* **95**.

Pielke, R. A., 1990: The Hurricane. Routledge, 225 pp.

Pezza AB, Simmonds I. (2005). 'The first South Atlantic hurricane: Unprecedented blocking, low shear and climate change', *Geophys Res Lett* **32**.

Rapolaki, R. S., R. C. Blamey, J. C. Hermes, and C. J. Reason, (2019): A classification of synoptic weather patterns linked to extreme rainfall over the Limpopo River Basin in southern Africa. Clim.Dyn., 1-15.

Rapolaki RS, Reason CJ. (2018). Tropical storm Chedza and associated floods over south-eastern Africa. *Nat Hazards* **93**: 189-217.

Raju, P., J. Potty, and U. C. Mohanty, (2011): Sensitivity of physical parameterizations on prediction of tropical cyclone Nargis over the Bay of Bengal using WRF model. Meteorology and Atmospheric Physics, 113, 125.

Reason C. (2007). 'Tropical cyclone Dera, the unusual 2000/01 tropical cyclone season in the South West Indian Ocean and associated rainfall anomalies over Southern Africa', *Meteorology and Atmospheric Physics* **97**: 181-188.

Reason C. (2001). 'Subtropical Indian Ocean SST dipole events and southern African rainfall', *Geophys Res Lett* **28**: 2225-2227.

Reason, C.J.C. (2002). Sensitivity of the southern African circulation to dipole SST patterns in the South Indian Ocean. International Journal of Climatology, 22, 377-393

Reason C. (1999). 'Interannual warm and cool events in the subtropical/mid-latitude South Indian Ocean Region', *Geophys Res Lett* **26**: 215-218.

Reason C. (1998). 'Warm and cold events in the southeast Atlantic/southwest Indian Ocean region and potential impacts on circulation and rainfall over southern Africa', *Meteorology and Atmospheric Physics* **69**: 49-65.

Reason C, Jagadheesha D. (2005). 'A model investigation of recent ENSO impacts over southern Africa', *Meteorology and Atmospheric Physics* **89**: 181-205.

Reason C, Rouault M. (2005). 'Links between the Antarctic Oscillation and winter rainfall over western South Africa', *Geophys Res Lett* **32**.

Reason C, Keibel A. (2004). Tropical cyclone Eline and its unusual penetration and impacts over the southern African mainland. *Weather and forecasting* **19**: 789-805. .

Reason C, Mulenga H. (1999). 'Relationships between South African rainfall and SST anomalies in the southwest Indian Ocean', *International Journal of Climatology: A Journal of the Royal Meteorological Society* **19**: 1651-1673.

Reason C, Landman W, Tennant W. (2006). 'Seasonal to decadal prediction of southern African climate and its links with variability of the Atlantic Ocean', *Bull Am Meteorol Soc* **87**: 941-956.

Reason C, Allan RJ, Lindesay JA, Ansell TJ. (2000). 'ENSO and climatic signals across the Indian Ocean basin in the global context: Part I, Interannual composite patterns', *Int J Climatol* **20**: 1285-1327.

Reynolds, R.W., Smith, T. M., Lui, C., Chelton, D. B., Casey, K. S., Schlax, M. G. (2007). Daily high-resolution blended analyses for sea surface temperature. Journal of Climate, 20, 5473-5496.

Rouault M, Florenchie P, Fauchereau N, Reason CJ. (2003). 'South East tropical Atlantic warm events and southern African rainfall', *Geophys Res Lett* **30**.

Saha S, Moorthi S, Wu X, Wang J, Nadiga S, Tripp P, Behringer D, Hou Y, Chuang H, Iredell M. (2014). The NCEP climate forecast system version 2. *J Clim* **27**: 2185-2208.

Shay LK, Goni GJ, Black PG. (2000). 'Effects of a warm oceanic feature on Hurricane Opal', *Mon Weather Rev* **128**: 1366-1383.

Shen B, Atlas R, Reale O, Lin S, Chern J, Chang J, Henze C, Li J. (2006). 'Hurricane forecasts with a global mesoscale-resolving model: Preliminary results with Hurricane Katrina (2005)'. *Geophys Res Lett* **33**.

Singleton AT, Reason C. (2007a). 'A numerical model study of an intense cut off low pressure system over South Africa', *Mon Weather Rev* **135**: 1128-1150. Sippel JA, Zhang F. (2008). 'A probabilistic analysis of the dynamics and predictability of tropical cyclogenesis', *J Atmos Sci* **65**: 3440-3459.

Skamarock WC, Klemp JB. (2008). 'A time-split nonhydrostatic atmospheric model for weather research and forecasting applications', *Journal of Computational Physics* **227**: 3465-3485.

Taljaard JJ. (1985). *Cut-off lows in the South African region*. Weather Bureau, Department of Transport.

Tian Y, Peters-Lidard CD, Choudhury BJ, Garcia M. (2007). 'Multitemporal analysis of TRMM-based satellite precipitation products for land data assimilation applications', *J Hydrometeorol* **8**: 1165-1183.

Tyson PD. (1981). 'Atmospheric circulation variations and the occurrence of extended wet and dry spells over southern Africa', *Journal of Climatology* **1**: 115-130.

Tyson PD, Dyer TG, Mametse MN. (1975). 'Secular changes in South African rainfall: 1880 to 1972', *Q J R Meteorol Soc* **101**: 817-833.

Usman MT, Reason C. (2004). 'Dry spell frequencies and their variability over southern Africa', *Climate research* **26**: 199-211.

Vitart F, Anderson D, Stockdale T. (2003). 'Seasonal forecasting of tropical cyclone landfall over Mozambique', *J Clim* **16**: 3932-3945.

Wada A, Usui N. (2007). 'Importance of tropical cyclone heat potential for tropical cyclone intensity and intensification in the western North Pacific', *J Oceanogr* **63**: 427-447.

Washington R, Preston A. (2006). 'Extreme wet years over southern Africa: Role of Indian Ocean sea surface temperatures', *Journal of Geophysical Research: Atmospheres* **111**.

Webster PJ, Holland GJ, Curry JA, Chang H. (2005). 'Changes in tropical cyclone number, duration, and intensity in a warming environment', *Science* **309**: 1844-1846.

Weldon D, Reason C. (2014). 'Variability of rainfall characteristics over the South Coast region of South Africa', *Theoretical and applied climatology* **115**: 177-185.

Wong ML, Chan JC, Zhou W. (2008). 'A simple empirical model for estimating the intensity change of tropical cyclones after landfall along the south China coast', *Journal of Applied Meteorology and Climatology* **47**: 326-338.

Zeng, Z., Y. Wang, and C. Wu, 2007: Environmental dynamical control of tropical cyclone intensity—An observational study. Mon. Weather Rev., 135, 38-59.